Published in final edited form as:

EnergyChem. 2019 July ; 1(1): . doi:10.1016/j.enchem.2019.100006.

Porous metal-organic frameworks for gas storage and separation: Status and challenges

Hao Li[a,b], **Libo Li**[b,c,d], **Rui-Biao Lin**[*,b], **Wei Zhou**[e], **Zhangjing Zhang**[a], **Shengchang Xiang**[*,a], **Banglin Chen**[*,b]

[a]Fujian Provincial Key Laboratory of Polymer Materials, College of Materials Science and Engineering, Fujian Normal University, Fuzhou 350007, Fujian, PR China

[b]Department of Chemistry, University of Texas at San Antonio, One UTSA Circle, San Antonio, TX 78249-0698, United States

[c]College of Chemistry and Chemical Engineering, Taiyuan University of Technology, Taiyuan 030024, Shanxi, PR China

[d]Shanxi Key Laboratory of Gas Energy Efficient and Clean Utilization, Taiyuan 030024, Shanxi, PR China

[e]NIST Center for Neutron Research, National Institute of Standards and Technology, Gaithersburg, MD 20899-6102, United States

Abstract

Gases are widely used as energy resources for industry and our daily life. Developing energy cost efficient porous materials for gas storage and separation is of fundamentally and industrially important, and is one of the most important aspects of energy chemistry and materials. Metal-organic frameworks (MOFs), representing a novel class of porous materials, feature unique pore structure, such as exceptional porosity, tunable pore structures, ready functionalization, which not only enables high density energy storage of clean fuel gas in MOF adsorbents, but also facilitates distinct host-guest interactions and/or sieving effects to differentiate different molecules for energy-efficient separation economy. In this review, we summarize and highlight the recent advances in the arena of gas storage and separation using MOFs as adsorbents, including progresses in MOF-based membranes for gas separation, which could afford broader concepts to the current status and challenges in this field.

Keywords

Metal-organic frameworks; Gas separation; Gas storage; Fuel gas; Membrane

[*]Correspondence: ruibiao.lin@utsa.edu (R.-B. L.), scxiang@fjnu.edu.cn (S. X.), banglin.chen@utsa.edu, banglin2010@gmail.com (B. C.).

■AUTHOR CONTRIBUTIONS

H.L., R.-B.L. and B. Chen co-wrote the manuscript. H.L. and L.L. contributed equally, R.-B.L., Z.Z., S.X., W.Z. and B. Chen discussed and commented on the manuscript.

■ **CONFLICT OF INTEREST**

The authors declare no conflict of interest.

INTRODUCTION

Modern civilization requires energy to function, giving a worldwide energy consumption about 575 quadrillion British thermal units (Btu, 1 Btu is about 1.055 kJ or 0.0003 kW-h) in 2015.[1] As important energy sources and energy carriers, gases (e.g., natural gas and biogas) make a major contribution to the energy production.[2] For example, natural gas (main component is methane) accounted for about 29% of the U.S. primary energy production in 2017.[3] In terms of energy production, the strongly growing worldwide demand on fossil fuels has brought significant environmental issues, especially the climate change caused by carbon emissions. Compared to liquid petroleum and solid coal, gases fuels are more environmentally friendly given to their lower carbon emissions and higher gravimetric energy densities. For hydrogen (H_2) and methane (CH_4), their gravimetric heats of combustion are 123 and 55.7 MJ/kg, respectively, comparing to that of 47.2 MJ/kg for gasoline.[4] The main challenge for gases fuels lies in their transportation, storage, and conversion that usually realize under require harsh conditions and consume massive amounts of energy, owing to their extremely low boiling point, low density, high critical pressure and high diffusivity. The current storage technologies for gas fuel involve liquefaction at low temperature (−253 °C for liquefied hydrogen) or compression under high pressure (hundreds of atmospheres) at ambient temperature, featuring high facility requirement. To realize cheap, safe and portable storage and transportation, an alternative approach is to employ porous materials for adsorbed storage systems that operate under moderate conditions.

Besides as energy sources, some gases (e.g. olefins gases and aromatic hydrocarbons vapors) are also important feedstocks in chemical industry. For instance, olefins (mainly ethylene, propylene and butadiene) are the cornerstone of many important manufacturing, with a worldwide production exceeding 200 million metric tons, equivalent to about 30 kg for each person on the planet.[5] The productions of these important industrial chemical are highly energy-intensive, e.g., the energy consumption in ethylene production is roughly estimated at 26 GJ per ton of ethylene.[6] Prior to the direct use of gas commodities, separation and purification processes are required, which conventionally accomplished by repeated distillation-compression cycling of the mixture. These heat-driven separation processes consume up to 10 times more energy than membrane-based and/or adsorptive separation technologies.[5] Given that the current energy use by separation and purification processes is more than 40% of total energy use in chemical industry,[5] tremendous energy savings can be expected by applying advanced adsorptive separation technologies based on porous materials. The key feature of these environmentally friendly, energy efficient separation technologies is the porous adsorbent or porous media (e.g. membrane).

Many common substances, such as charcoal, zeolites and ceramics, have long been used as porous media for adsorbents. To well handle gases, developing porous materials that show large storage capacity and high separation efficiency are urgent,[7] especially those with high porosity, and good modularity over different dimensions. In this context, many novel types of porous adsorbents have been developed over the last two decades, namely, metal-organic frameworks (MOFs),[8,9] covalent organic frameworks (COFs),[10–13] and hydrogen-bonded organic frameworks (HOFs).[14] Among different types of framework materials, MOFs are organic-inorganic hybrid solids that are self-assembled through the coordination of organic

linkers to metal ions/clusters. The moderate linkage strength (90–350 kJ/mol, comparing to 1–170 and 300–600 kJ/mol for those in HOFs and COFs, respectively)[14] and vast components variety in MOFs endow them with high crystallinity, exceptional porosity, high modularity and diverse functionality. Thus, MOFs represent the preeminent platform for developing novel multifunctional materials, referring to applications in gas storage and separation,[15–19] optical,[20,21] electric and magnetic materials,[22] chemical sensing,[23–27] catalysis,[28–38] biomedicine[39,40] and so on.[41–46]

MOFs are well recognized for gas storage and gas separation, owing to their ultrahigh porosity with surface area ranging from 100 to 10,000 m^2/g,[47,48] tunable pore size of 3 to 100 Å, high thermal stability (up to 500 °C) and even exceptional chemical stability.[9] The establishment of permanent porosity for MOFs was realized in late 1990s,[49,50] which initiated their applications as adsorbents. The rapidly refreshing records of pore surface area highlight this type of adsorbents very promising for gas processing. The initial efforts to utilize MOFs for fuel gas storage can be dated back to 1997 (for methane).[49] Similar adsorptive systems were subsequently applied for hydrogen storage started at 2003 and acetylene storage at 2005.[51,52] Since those pioneering attempts on MOFs for fuel gas storage, intensive research endeavors have been devoted to increase corresponding storage capacity, including enhancing binding affinity and optimization over porosity. Significant progresses have been made (Scheme 1),[53–56] affording superior performance to those of zeolites and porous carbon. Simultaneously, in MOFs, highly uniform pore size distribution, various functional sites and highly tunable pore size render them the most promising candidates for gas separation. Such potential has been well demonstrated by few selective gas adsorption examples based on single-component sorption isotherms for different gases. Structurally, the development of isoreticular principle[57,58] and framework interpenetration[59–62] enable the pore structures of MOFs to be controlled at very accurate level,[63] while the accessibility of functional sites especially open metal sites[64–66] and the implementation of post-synthetic modification[67–70] affording approaches to improve selective molecular recognition over different gases. Technically, the utilization of gas chromatography at 2006,[71] fixed-bed breakthrough at about 2006–2007 for separating gas mixtures,[72–75] and gas sorption site determination[52,76,77] by crystallography technologies dramatically facilitates MOFs in actual separation of gas mixtures. Since then, great efforts have been devoted to the field of MOFs for gas separation (Scheme 2)[15–17,78–82] resulting in lots of progresses especially for the industrially significant hydrocarbon separation.

To date, numerous MOFs have been applied for gas storage and separation. This active field represents one of the most important aspects of energy chemistry and materials. In this review, we focus on current status by selected MOFs examples to provide broad insight for new readers, especially highlight recent advances on addressing challenging storage and separation.

■ POROUS MOFS FOR GAS STORAGE

MOFs have been foreseen as prospective adsorbents for gas storage right after the discovery of their permanent porosities. Compared with the traditional porous materials, such as activated carbons and zeolites, MOFs are endowed with some advantageous structural

features like high porosity, high surface area, tunable pore size and geometry, and functionalizable pore surface. Thus, the emergence of MOFs provides great promise to store some important gases such as hydrogen (H_2), methane (CH_4), and acetylene (C_2H_2).[83] In this section, we will summarize the recent advances in these three aspects.

H_2 storage

With the increase in population and the development in economy, human society has a growing demand for energy resources. Exploitation of fossil fuels has incurred various environmental issues including climate change, which propels people to seek new energy carriers to minimize carbon footprint. H_2 has been regarded as one promising alternative because H_2 has the highest energy per mass of any fuel and emits zero carbon dioxide. However, the principal challenge lies in the comparatively low volumetric energy density at ambient conditions, especially for onboard vehicular applications. This prompts the development of advanced methods to store H_2 efficiently at near ambient conditions.

The U.S. Department of Energy (DOE) has released 2020 target capacities for H_2 storage in light-duty fuel cell vehicles.[9] The system gravimetric and volumetric H_2 capacities are required to be 4.5 wt% and 30 g/L, respectively, at an operating temperature of −40–60 °C. While pressure ranges are not given explicitly, operating under a maximum pressure of 100 bar is necessary to reduce the expenses of compression and storage vessel, while maintaining reasonable compacities.

The first example of H_2 storage in MOFs (MOF-5) was reported by Yaghi et al. in 2003 (although the uptake capacity was corrected until 2007).[51,84] After that, hundreds of MOF materials have been investigated for their potential in H_2 storage (Table 1).[85–90] Research has shown that the gravimetric H_2 storage capacities at 77 K and high pressure are mostly proportional to the pore volumes and/or surface areas of MOFs. For instance, NOTT-112, NU-111, and NU-100/PCN-610 are all rht-type MOFs with BET surface areas as 3800, 4930, and 6143 m^2/g respectively. Their total gravimetric H_2 uptakes at 77 K and 70 bar are 10.0, 13.6, and 16.4 wt%, which follows the same sequence as their surface areas.[91–94] The record total H_2 gravimetric uptake was achieved in MOF-210 reported by Furukawa et al. in 2010.[48] With a BET surface area of over 6200 m^2/g, MOF-210 exhibits a total gravimetric H_2 uptake of 17.6 wt% at 77 K and 80 bar.

For onboard applications of H_2 fuel cell, H_2 storage is required to be operated at near ambient temperatures. This task is extraordinarily challenging because the interactions between MOFs and H_2 are mainly weak van der Waals interactions. So far, no MOFs reported have met the DOE targets for gravimetric capacity. Though in some cases, the immobilization of open metal sites can enhance the interactions between MOF and H_2 and raise the isosteric heat of H_2 adsorption to about 12 kJ/mol.[4] Theoretical studies indicated that the minimum heat of H_2 adsorption is required to be 15 kJ/mol in order to realize high H_2 storage capacities at reasonable temperatures.[101]

Apart from gravimetric capacity, volumetric capacity is another important aspect to consider when evaluating MOFs for H_2 storage, because the available volume in light-duty vehicles for a tank containing H_2 adsorbent is very limited and is a critical factor in determining

the driving range of a vehicle. In 2017, Ahmed et al. employed empirical correlations and direct atomistic simulations to predict the H_2 capacities of 5309 MOFs drawn from databases of known compounds.[95] Despite the fact that MOFs with high gravimetric capacities usually have moderate volumetric capacities due to their large pore diameters and concomitant weak MOF-H_2 interactions, these predictions indicated that a simultaneous high gravimetric and volumetric H_2 densities can be achieved in MOFs. Several promising MOFs were thus synthesized with their usable H_2 capacities assessed. Among them, IRMOF-20 was experimentally demonstrated to exhibit both high usable volumetric and gravimetric capacities (51.0 g/L and 9.1 wt%, respectively, at a combined temperature and pressure swing from 77 K and 100 bar to 160 K and 5 bar), which represents the value of using computational screening to guide experimental efforts towards MOFs with desired storage performance.

Very recently, Kapelewski et al. evaluated the usable volumetric H_2 capacities of Ni_2(*m*-dobdc) (*m*-dobdc^{4-} = 4,6-dioxido-1,3-benzenedicarboxylate), which has a high density of coordinatively unsaturated metal sites that can interact with H_2 strongly.[96] Its adsorption isotherms were measured in the pressure range of 0–100 bar at near-ambient temperatures. Based on adsorption isotherm data, Ni_2(*m*-dobdc) was found to have a usable volumetric capacity between 100 and 5 bar of 11.0 g/L at 25 °C and 23.0 g/L with a temperature swing from −75 to 25 °C, making it the top-performing physisorptive storage material so far. Its high capacity is attributed to the presence of highly polarizing open Ni^{II} sites, which lead to strong binding interactions and a dense packing of H_2 within the MOF. This work may provide some guidance to develop new MOFs with high volumetric capacities for the ultimate purpose of realizing high gravimetric and volumetric H_2 storage capacities simultaneously.

CH_4 storage

Natural gas, whose main component is CH_4, is an abundant natural resource. The high research octane number (RON) of CH_4 and its low CO_2 emission make natural gas an appealing vehicular fuel. This motivates extensive efforts to study effective methods for CH_4 storage (Table 2).[54] Since the interactions between MOFs and CH_4 are moderate, storing CH_4 in MOFs can be realized at room temperature and reasonably high pressure, which is practically feasible and holds great promise.

To direct the research of ANG (adsorbed natural gas) technology, DOE in 2012 set the total CH_4 storage targets to be 700 cm^3 (STP)/g or 0.5 g/g gravimetrically and 350 cm^3 (STP)/cm^3 volumetrically at room temperature.[112] It is worth noting that a 25% adsorbent packing loss is considered. If the packing loss is neglected, the volumetric target corresponds to 263 cm^3 (STP)/cm^3, which is still ambitiously high.

High gravimetric CH_4 capacity—After Kitagawa and Yaghi independently realized the first two examples of MOFs for CH_4 storage,[49,57] considerable progress has been made in this field. Based on the abundant experimental data, it was found that the gravimetric CH_4 storage capacities of MOFs at high pressure are basically proportional to their pore volumes or surface areas.[113] This is straightforward to rationalize because larger porosities

indicate more space in MOFs to accommodate larger amounts of CH_4 molecules. Several empirical relationships between the CH_4 capacities of rigid MOFs and their pore volumes have been developed, which provide useful information to guide the discovery of promising MOF candidates for CH_4 storage.

In 2013, He et al. examined the gravimetric CH_4 capacities of a series of copper-tetracarboxylate frameworks having similar structures and topologies (NOTT-100, NOTT-101, NOTT-102, NOTT-103, and NOTT-109).[114] Their excess gravimetric CH_4 uptakes were found to rise progressively with the increasing porosities. An empirical equation was even derived through in-depth analysis to predict the CH_4 storage capacity of a specific MOF: $C_{excess} = -126.69 \times V_p^2 + 381.62 \times V_p - 12.57$, where C_{excess} is the excess gravimetric CH_4 capacity at 300 K and 35 bar in cm^3 (STP)/g, and V_p is the pore volume of a MOF in cm^3/g. By comparing the experimental and predicted excess gravimetric CH_4 uptakes of previously reported MOFs with V_p smaller than 1.5 cm^3/g, the established empirical equation was found to work reasonably well, which offers a convenient way to screen MOF materials for CH_4 storage.

Six reported MOFs with broad types of structure (HKUST-1, NiMOF-74, PCN-14, UTSA-20, NU-111, and NU-125) were also investigated for their CH_4 storage properties using a standardized measurement protocol by Peng et al. in 2013.[102] Their results revealed that the total gravimetric CH_4 uptake (at 298 K and 65 bar), pore volume, and inverse density of MOFs were linearly correlated with the BET surface area. Among the series, NU-111 with a measured BET surface area of 4930 m^2/g has a highest gravimetric uptake of 0.36 g/g. They also estimated that a hypothetical MOF with a surface area of 7500 m^2/g and a pore volume of 3.2 cm^3/g was able to reach the gravimetric target according to the linear correlation.

In 2016 Li et al. studied the gravimetric CH_4 capacities of MOFs at a slightly lower temperature of 270 K.[53] They found that slightly reducing the storage temperature to 270 K can considerably enhance the total gravimetric capacity at 65 bar. Moreover, an empirical equation ($C_{total} = -70.463 \times V_p^2 + 460.543 \times V_p - 2.709$, where C_{total} is the total gravimetric CH_4 capacity at 270 K and 65 bar, and V_p is the pore volume in cm^3/g) was also developed to predict CH_4 uptakes at 270 K.

These established empirical relationships are very useful because they can provide clues about the gravimetric CH_4 capacity of a specific MOF simply with information such as its pore volume and surface area. Evidently, MOFs with higher pore volumes and surface areas are more likely to have higher gravimetric CH_4 capacities. A viable strategy to improve the gravimetric CH_4 capacity in MOFs is to seek or develop MOFs with high porosities. In this regard, Alezi et al. reported a novel aluminum MOF (Al-soc-MOF-1) in 2015, which has an exceptionally high pore volume of 2.3 cm^3/g and a BET surface area of 5585 m^2/g (Fig. 1a).[105] This MOF thus exhibits the highest total gravimetric CH_4 uptake of ~580 cm^3 (STP)/g (0.42 g/g) reported so far at 298 K and 65 bar, and achieves 83% of the DOE gravimetric target (Fig. 1b).

High volumetric CH_4 capacity—Considering that the vehicles have limited space for CH_4 storage tanks, a high volumetric CH_4 capacities is even more important than gravimetric storage capacities. The highly porous feature of MOFs showing high gravimetric CH_4 uptakes usually leads to moderate or low volumetric capacities, because such materials tend to have large pores and weak MOF-CH_4 interactions. Studies have shown that the ideal MOFs for high volumetric CH_4 capacities should have balanced porosities and framework densities as well as high densities of suitable pore cages for the recognition of CH_4 molecules.[113] Accordingly, strategies like optimizing pore spaces and integrating functional sites into MOFs have been developed to target high total and working (deliverable amount between 5 and 65 bar) volumetric capacities.

HKUST-1 is one typical example illustrating the importance of optimal pore sizes for high volumetric CH_4 capacities. This MOF contains three types of cages with pore diameters as ~4, 10, and 11 Å, respectively, which are very suitable for CH_4 storage.[115] HKUST-1 was found to exhibit a remarkably high total volumetric CH_4 capacity of 267 cm^3 (STP)/cm^3 at 298 K and 65 bar by Peng et al. in 2013.[102] This value meets the volumetric target set by DOE on condition that the packing loss is ignored, and is still the highest reported so far. Wu et al. uncovered that the CH_4 adsorption primarily took place at the windows of the small octahedral cages and the open Cu^{II} sites.[116] Additionally, Hulvey et al. revealed that the small octahedral cages were even preferred over the OMSs as primary CH_4 adsorption sites, as evidenced by in situ neutron powder diffraction data.[117] These results demonstrate the beneficial role of suitable pore spaces in the high volumetric capacity of a MOF.

MAF-38, a MOF with no OMSs developed by Lin et al. in 2016, more evidently reveals the contribution from suitable pore sizes/shapes to the CH_4 storage in MOFs.[118] MAF-38 has two types of nanocages with internal free diameters of ~6.2 and 8.6 Å, respectively. These suitable pores give rise to an exceptionally high volumetric total CH_4 uptake of 263 cm^3 (STP)/cm^3 and a working capacity of 187 cm^3 (STP)/cm^3 in MAF-38 at 298 K and 65 bar, which are among the highest values in MOFs. Computational simulations confirmed that the suitable pore sizes/shapes and organic binding sites in MAF-38 synergistically reinforce the MOF-CH_4 and CH_4–CH_4 interactions, leading to a dense packing of CH_4 molecules.

Establishing MOFs with suitable pore sizes can also be realized by shrinking the organic linkers of known MOFs whose pore diameters are too large to confine CH_4 molecules. This is exemplified by Jiang et al. in 2016 who replaced the peripheral phenylene ring of benzene-1,3,5-tribenzoate (BTB) linker in MOF-205 with a shorter double-bond spacer, and constructed a series of new MOFs with acrylate links and different functional groups (MOF-905, MOF-905-Me_2, MOF-905-Naph, and MOF-905-NO_2).[108] With the same topology but smaller cages, the MOF-905 series show 11–21% increase on total volumetric CH_4 uptake over MOF-205. Among them, MOF-905 has the highest volumetric working capacity (desorption at 5 bar) of 203 cm^3 (STP)/cm^3 at 298 K and 80 bar, a value rivaling that of HKUST-1 (200 cm^3 (STP)/cm^3).

Besides developing MOFs with suitable pore sizes, incorporating functional groups/sites into MOFs is another approach to enhancing their volumetric CH_4 capacities. In 2014, Li et al. reported a new MOF UTSA-76 containing pyrimidine functional groups and having

exactly the same structure and comparable pore volume with respect to the isoreticular NOTT-101.[103] However, the total volumetric CH_4 capacity at 298 K and 65 bar was considerably increased from 237 cm^3 (STP)/cm^3 in NOTT-101 to 257 cm^3 (STP)/cm^3 in UTSA-76. Moreover, UTSA-76 achieved a record high volumetric working capacity of ~200 cm^3 (STP)/cm^3 between 5 bar and 65 bar. Computational studies and neutron scattering measurements revealed that the central "dynamic" pyrimidine groups within UTSA-76 may be responsible for its exceptionally high working capacity, because these pyrimidine groups were believed to adjust their orientations to optimize the CH_4 packing at high pressure. In 2015, Li et al. further expanded the idea and constructed a series of NOTT-101 isostructures containing Lewis basic nitrogen sites, which also exhibited enhanced volumetric total and working capacities at 298 K and 65 bar.[119]

In 2017 Yan et al. reported that the molecular dynamics within MOFs is a tunable factor to tailor their volumetric CH_4 capacities as well. In this work, three (3,24)-connected MOFs, MFM-112a, MFM-115a, and MFM-132a, with different linker backbone functionalization were synthesized.[110] Both MFM-112a and MFM-115a exhibit high total volumetric CH_4 uptakes of 236 and 256 cm^3 (STP)/cm^3 at 298 K and 80 bar. More importantly, MFM-115a also displays a remarkably high working capacity of 208 cm^3 (STP)/cm^3 at 298 K between 5 and 80 bar. Based on the solid-state ^{2} H NMR spectroscopy, these three MOFs contain molecular rotors exhibiting motion in fast, medium, and slow regimes, respectively. From in situ neutron powder diffraction data, the primary binding site in MFM-115a was located within the small pocket enclosed by the [$(Cu_2)_3$(isophthalate)$_3$] window and three phenyl panels. These experimental evidence reveals that the optimal molecular dynamics combined with suitable pore geometry/size accounted for the high volumetric CH_4 capacity in MFM-115a.

To realize high CH_4 working capacities in MOFs, it is essential to maximize the CH_4 uptake at the adsorption pressure of 65 bar in the isotherm and minimize the uptake at the desorption pressure of 5.0 or 5.8 bar. In this regard, Mason et al. in 2015 attempted to employ flexible MOFs to achieve the goal.[104] They noticed that flexible MOFs usually exhibit "gate-opening" behavior, which makes a non-porous structure expand to a porous framework as the gas pressure reaches a certain threshold.[120] Accordingly, a flexible MOF displays an "S-shaped" or "stepped" CH_4 adsorption isotherm. Thus, they proposed that if a responsive MOF can be designed to expand and store a large amount of CH_4 at 35–65 bar, and collapse to push out the adsorbed CH_4 molecules as the pressure is reduced to near 5.8 bar, it would possible to target an extraordinarily high CH_4 working capacity. The flexible MOF they chose was Co(bdp) (bdp^{2-} = 1,4-benzenedipyrazolate). *In situ* powder X-ray diffraction experiments confirmed its reversible structural phase transition, and a sharp step was observed at 16 bar in the CH_4 adsorption isotherm of Co(bdp) at 298 K with a very low CH_4 adsorbed amount of 0.2 mmol/g at 5.8 bar. Consequently, the working capacities of Co(bdp) at 298 K reach 155 cm^3 (STP)/cm^3 at 35 bar and 197 cm^3 (STP)/cm^3 at 65 bar, which are among the highest values at these conditions. In 2016, the same group further systematically controlled the pressure of the CH_4-induced framework expansion by ligand functionalization, which provides a tool to optimize the phase-change MOFs for better CH_4 storage performance.[121]

In 2018, Yang et al. report another new flexible MOF, NiL_2 (L = 4-(4-pyridyl)-biphenyl-4-carboxylic acid). NiL_2 is capable to switch between non-porous (closed) and porous (open) phases at a specific CH_4 pressure.[122] The material thus exhibited a total volumetric CH_4 uptake of 189 cm^3 (STP)/cm^3 at 298 K and 65 bar and a working capacity of 149 cm^3 (STP)/cm^3 (5–65 bar). These examples open another route to develop MOFs targeting high CH_4 volumetric working capacities.

Both high gravimetric and volumetric CH_4 capacity—Highly porous MOFs with large nanospaces are apparently favored for high gravimetric CH_4 capacities; however, their large pore diameters would lead to relatively weak CH_4-framework interactions and result in limited volumetric capacities.[113] On the other hand, MOFs with small nanospaces and moderate porosities would pack CH_4 molecules densely through strong CH_4-framework interactions for high volumetric capacities; however, their relatively low pore volumes would restrict the gravimetric CH_4 uptakes. The rationalization suggests the existence of an intrinsic trade-off and mutual compromise between gravimetric and volumetric CH_4 capacities in MOFs. In fact, most MOFs with the highest gravimetric (volumetric) uptakes generally exhibit moderate volumetric (gravimetric) capacities.[80] Though developing an ideal MOF with both high gravimetric and volumetric CH_4 capacities is very challenging, some progress has still been made in the past two years.

HKUST-1 exhibits an exceptionally high volumetric CH_4 capacity of 267 cm^3 (STP)/cm^3 at 298 K and 65 bar but modest gravimetric capacity due to the limited pore space. To overcome this trade-off, Spanopoulos et al. in 2016 implemented the strategy of reticular chemistry to construct an expanded HKUST-1-like tbo-MOF (Cu-tbo-MOF-5).[123] The gravimetric and volumetric BET surface areas of Cu-tbo-MOF-5 were enlarged to 3971 m^2/g and 2363 m^2/cm^3, which are 115% and 47% higher than the prototypical HKUST-1, respectively. As expected, Cu-tbo-MOF-5 was found to exhibit both high total gravimetric and volumetric CH_4 capacities at 298 K and 85 bar, which are 372 cm^3 (STP)/g and 221 cm^3 (STP)/cm^3, respectively. The gravimetric and volumetric working capacities between 5 and 80 bar are also as high as 294 cm^3 (STP)/g (0.217 g/g) and 175 cm^3 (STP)/cm^3, respectively, suggesting the conducive effect of judiciously enhanced surface areas on CH_4 capacities.

In 2017, Moreau et al. constructed a series of isoreticular octacarboxylate MOFs (MFM-180 to MFM-185) with linkers ranging from 19 to 30 Å in dimension for CH_4 storage.[124] The elongation of the linker in this series allows selective pore extension along one dimension, with BET surface areas systematically increased from 2610 to 4730 m^2/g. CH_4 adsorption studies showed that there is no uptake loss in the low-pressure region with increasing linker length, and both gravimetric and volumetric uptakes are enhanced at high pressure. This trend affords an impressively high CH_4 working capacity of 0.24 g/g and 163 cm^3 (STP)/cm^3 (298 K, 5–65 bar) for activated MFM-185a. The simultaneous high gravimetric and volumetric CH_4 capacities in MFM-185a are mainly ascribed to the selective elongation of the tubular cages with fixed diameter, which not only contributes to the enlarged pore volume but also guarantees the efficient packing of CH_4 molecules within the framework. Similarly, Zhang et al. in 2017 reported the fine-tuning of the pore space and chemistry in a family of isomorphic MOFs based on PCN-14 for CH_4 storage.[107] The resulting NJU-Bai

43 achieves both high volumetric and gravimetric working capacities of 198 cm^3 (STP)/cm^3 and 0.221 g/g, respectively, at 298 K and between 5 and 65 bar.

A combined strategy of elongating organic linker as well as introducing functional sites into MOFs was also found effective in increasing CH_4 capacities. In 2018, Wen et al. synthesized a new MOF named UTSA-110a, which was constructed by an extended linker containing a higher density of functional nitrogen sites with respect to UTSA-76 (Fig. 2a).[106] Consequently, UTSA-110a had a larger surface area and a higher content of functional *N* sites (3241 m^2/g and 3.94 mmol/cm^3, respectively) than UTSA-76 (2820 m^2/g and 2.64 mmol/cm^3, respectively). The enhanced porosity may improve the gravimetric total uptake while the high density of functional nitrogen sites may exert a positive influence in the CH_4-framework interactions for optimal volumetric uptake. As expected, UTSA-110a exhibited both high gravimetric (402 cm^3 (STP)/g) and volumetric (241 cm^3 (STP)/cm^3) total CH_4 capacities at 298 K and 65 bar. With a relatively low CH_4 uptake at 5.8 bar, UTSA-110a was also able to realize both high gravimetric and volumetric working capacities of 317 cm^3 (STP)/g and 190 cm^3 (STP)/cm^3, respectively, significantly outperforming those of HKUST-1 and UTSA-76 (Fig. 2b). Computational studies revealed that the synergistic effect of optimized porosity and favorable binding sites was the main reason for this excellent CH_4 storage performance in UTSA-110a.

C_2H_2 storage

C_2H_2 has been widely used for the manufacture of many chemical products and electric materials in modern industry. However, the safe storage of C_2H_2 still remains challenging due to its very explosiveness when compressed under pressures over 0.2 MPa. Currently, C_2H_2 in industry is stored in special cylinders filled with acetone and porous materials, which suffers from the acetone pollutant and high expenses. Therefore, developing new methods to safely store C_2H_2 is very necessary.

MOFs have been explored as C_2H_2 storage adsorbents.[56] Since the first example of C_2H_2 storage in MOF $Cu_2(pzdc)_2(pyz)$ (pzdc = pyrazine-2,3-dicarboxylate; pyz = pyrazine) was reported by Matsuda et al. in 2005,[52] a number of MOFs have been developed as C_2H_2 storage materials (Table 3). Some strategies have been found useful to enhance the C_2H_2-framework interactions so as to realize high C_2H_2 storage capacities in MOFs, which include (1) incorporation of open metal sites, (2) optimization of pore space/size, and (3) functionalization of organic linkers to provide specific binding sites for C_2H_2 molecule, detailed below.

The employment of open metal sites in MOFs for high C_2H_2 uptake was first reported by Xiang et al. in 2009.[125] They examined C_2H_2 storage properties of six MOF materials having different structures and porosities (HKUST-1, MOF-505, MOF-508, MIL-53, MOF-5, and ZIF-8). The results showed that HKUST-1 displays the highest C_2H_2 capacity of 201 cm^3/g at 295 K and 1 atm. The strong binding positions are located at open Cu^{II} sites, supported by neutron powder diffraction studies. These open Cu^{II} sites have strong preferred interactions with C_2H_2 molecules to result in a high C_2H_2 storage capacity. The same strategy was also utilized in the M-MOF-74 series (M = Co^{II}, Mn^{II}, Mg^{II}, and Zn^{II})

and showed high C_2H_2 uptakes as well, with Co-MOF-74 having 197 cm^3/g at 298 K and 1 bar.[127]

Introducing organic linkers containing functional sites/groups, such as basic pyridyl sites and amide groups, provides additional binding sites to interact with C_2H_2 molecules strongly, which is beneficial for high C_2H_2 storage capacities.[129,134] In 2013, Rao et al. reported the replacement of the central benzene spacer in the ligand of NOTT-101 with a pyridine ring having functional *N* sites, which resulted in an isoreticular NbO-type MOF ZJU-5.[129] ZJU-5 shows an extraordinarily high acetylene uptake of 193 cm^3/g at 298 K and 1 bar, higher than that of the prototypical NOTT-101 (184 cm^3/g). Following this work, Wen et al. in 2016 used the pyrazine ring to replace the central benzene to further increase the density of two Lewis basic nitrogen sites in the MOF and generate another isoreticular MOF ZJUT-40.[131] Consequently, ZJUT-40 exhibited a further enhanced C_2H_2 uptake of 216 cm^3/g (at 298 K and 1 bar) than those of NOTT-101 and ZJU-5. Since these isoreticular MOFs have almost the same structures, the increased C_2H_2 uptake in ZJUT-40 should be ascribed to its higher concentrations of Lewis basic nitrogen sites, which might have strong affinity with C_2H_2 molecule through the H–C≡C–H…N hydrogen bonding.

In addition to pyridyl sites, amide groups have also been found to strengthen the C_2H_2-framework interactions for higher C_2H_2 storage capacities. In 2017 Moreau et al. designed and synthesized a new copper (II) MOF MFM-188 using a judiciously designed tetra-amide octacarboxylate ligand >5,5′,5″,5″’-([1,1′-biphenyl] 3,3′,5,5″-tetracarbonyl)tetrakis (azanediyl)tetraisophthalic acid.[134] MFM-188 has moderate porosity but an extremely high C_2H_2 uptake of 232 cm^3/g at 295 K and 1 bar, which represents the highest value observed to date for porous materials. Neutron diffraction and inelastic neutron scattering studies provide cogent evidence of C_2D_2-amide binding interactions. Comprehensive investigation revealed that the high C_2H_2 uptake was attributed to a highly cooperative binding mechanism intrigued by the high density of free amide groups and open metal sites, as well as the appropriate pore geometry. Similarly, in 2016 Zhang et al. reported the construction of a MOF-505 analog with amide functional group in the linker. The resulting NJU-Bai 17 achieved an almost record high C_2H_2 uptake of 222.4 cm^3/g at 296 K and 1 bar.[132] Computational simulations also indicated the existence of H-bonding between C_2H_2 and amide group.

Suitable nanopore space/size is also an important factor in determining the C_2H_2 capacities of MOF materials. In 2015 Pang et al. developed a new MOF FJI-H8 with both suitable pore spaces (8, 12, and 15 Å in diameter, respectively) and open metal sites (3.59 mmol/g). FJI-H8 exhibits a record-high gravimetric C_2H_2 uptake of 224 cm^3 (STP)/g and a second-highest volumetric capacity of 196 cm^3 (STP)/cm^3 at 295 K and 1 atm.[133] Supposing each open Cu^{II} site binds one C_2H_2 molecule, the open Cu^{II} sites in FJI-H8 can only contribute 87 cm^3 of the total 224 cm^3 for the C_2H_2 storage capacity at 295 K and 1 atm. The remaining C_2H_2 uptake should be attributed to the suitable pore size in FJI-H8, which accounts for >60% of the total C_2H_2 uptake in FJI-H8. The contribution from suitable pore size was further confirmed by theoretical studies. This work represents as a good example to illustrate another structural feature that can be employed to design new MOF materials for high C_2H_2 storage capacities.

It should be noted that the operating pressure interval for rechargeable C_2H_2 delivery is strictly limited owing to its highly explosive nature. Therefore, the C_2H_2 working capacity of MOF adsorbents is very limited despite having very high total C_2H_2 uptake capacity. For practical application, the C_2H_2 working capacity or usable storage capacity has been proposed to be equivalent to the deliverable amount between 1.0–1.5 atm. In 2009, utilizing a unique MOF MAF-2 with kinetically controlled flexibility, Zhang et al. investigated the working capacity of MAF-2 in C_2H_2 storage.[135] This MOF exhibits a moderate C_2H_2 uptake of 70 cm^3 (STP)/g at 298 K and 1 atm, with a remarkable working capacity of 40-fold increase from gas cylinder between 1.0–1.5 atm. Single-crystal structure of gas-loaded MAF-2 reveals the formation of unprecedented C_2H_2 hexamers. Later, the record of C_2H_2 working capacity was promoted by the same group using a unique metal-organic zeolite MAF-7 that features uncoordinated functional *N* sites.[137] MAF-7 exhibits a C_2H_2 working capacity of 26.8 g/L at 298 K and between 1.0–1.5 atm, corresponding to about 50 times higher than that of a gas cylinder (0.532 g/L). Recently, based on comprehensive investigation of several isostructural ultramicroporous MOFs with pore size difference of hundredth-nanometer, He et al. discovered that MOF $[Cd_3(vtz)_6]$ shows a record-high C_2H_2 working capacity of 1.99 mmol/cm^3 (51.7 g/L), corresponding to about 98 times of that of a gas cylinder.[136]

■ PORE CHEMISTRY IN MOFS FOR GAS SEPARATION

Besides gas storage, MOFs have also shown great potential to perform gas separations as adsorbents based on their unique pore chemistry. The active field has experienced rapid developments over the past decade.[15,78,81,138–141] In this section, we will highlight some of the significant progresses made in recent years concerning several important gas separation scenarios (Table 4), including ethylene/ethane (C_2H_4/C_2H_6) separation, propylene/propane (C_3H_6/C_3H_8) separation, acetylene/ethylene (C_2H_2/C_2H_4) separation, acetylene/carbon dioxide (C_2H_2/CO_2) separation, propyne/propylene (C_3H_4/C_3H_6) separation, C_4 hydrocarbon separation, C_6 isomer separation, C_8 isomer separation, CO_2 capture and separation, and toxic gas removal.

C_2H_4/C_2H_6 separation

C_2H_4/C_2H_6 separation is an important aspect in olefin-paraffin separation, because C_2H_4 is a primary raw material in petrochemical industry. Traditional methods largely depend on energy-intensive cryogenic distillation. To separate C_2H_4/C_2H_6 mixtures efficiently, utilizing adsorbents such as MOFs to realize the separation has been perceived as a promising alternative. A number of MOFs have been studied to exhibit excellent separations mainly by one or more of the following mechanisms: (1) equilibrium-based mechanism; (2) kinetic-based mechanism; (3) gate-opening effect; and (4) molecular sieving effect. Depending on whether C_2H_4 or C_2H_6 is captured by adsorbents, MOF materials can be categorized into C_2H_4-or C_2H_6-selective adsorbents, detailed below.

C_2H_4-selective adsorbent—C_2H_4-selective adsorbents extract C_2H_4 from C_2H_4/C_2H_6 mixtures, primarily owing to the stronger framework-C_2H_4 interactions and smaller molecular size of C_2H_4.[173]

To achieve strong framework-C_2H_4 interactions, a high density of open metal sites in MOF adsorbents is a favorable feature. In 2012, Bloch et al. examined adsorption ability of light hydrocarbons in Fe_2(dobdc) (dobdc^{4-} = 2,5-dioxido-1,4-benzenedicarboxylate) and found that the material can achieve C_2H_4/C_2H_6 separation.[142] As evidenced by the steep rise in the isotherms, Fe_2(dobdc) exhibits a strong affinity towards the unsaturated hydrocarbons, including C_2H_2, C_2H_4, and C_3H_6. Neutron powder diffraction studies indicate that unsaturated hydrocarbons display side-on binding modes, with Fe-C distances in the range of 2.42(2) 2.60(2) Å (Fig. 3). While the interactions of C_2H_6 and CH_4 with the metal cations in Fe_2(dobdc) are weaker, as suggested by the elongated Fe-C distance of around 3 Å. The C_2H_4/C_2H_6 selectivity was calculated to be 13–18 for equimolar mixture at 318 K using ideal adsorbed solution theory (IAST). Breakthrough experiments further demonstrate that Fe_2(dobdc) is capable to separate equimolar mixture of C_2H_4 and C_2H_6 into pure component gases with a purity of 99% 99.5%. This work represents as a good example to illustrate the role of open metal sites in C_2H_4/C_2H_6 separation. The same group in 2018 reported the selective adsorption of C_2H_4 in Mn_2(*m*-dobdc)$_2$ (*m*-dobdc^{4-} = 4,6-dioxido-1,3-benzenedicarboxylate) also featuring a high density of open metal sites.[174]

In 2014, Yang et al. developed a hydroxyl–functionalized Al-MOF (NOTT-300) with high selectivity for C_2H_4/C_2H_6 separation.[18] The C_2H_4 and C_2H_6 adsorption amounts at 293 K and 1.0 bar in NOTT-300 were measured to be 4.28 and 0.85 mmol/g, respectively, giving rise to a notable uptake difference of 3.43 mmol/g as well as a very high C_2H_4/C_2H_6 selectivity of 48.7. This value is notably higher than that observed in Fe-MOF-74 (13.6), Co-MOF-74 (6), HKUST-1, and PAF-1-SO_3Ag (26.9).[175] *In situ* synchrotron X-ray and neutron powder diffraction experiments reveal that the M-OH groups, aromatic -CH groups, and phenyl rings in NOTT-300 can introduce weak additive, supramolecular interactions with the adsorbed C_2H_4 molecules, wherein the C···HO distance between C_2H_4 molecule and the hydroxyl group is about 4.62 Å. However, C_2H_6 is aligned at a very long distance to the OH group (C···O = 5.07 Å), thus resulting in weaker interactions with the NOTT-300 host. The stronger binding strengths toward C_2H_4 over C_2H_6 afforded the remarkable C_2H_4/C_2H_6 selectivity.

Precise tuning the pore size of MOFs to separate C_2H_4 from C_2H_6 based on molecular sieving effect is another powerful strategy for the targeted separation. In 2018, Lin et al. reported an ultramicroporous MOF [Ca(C_4O_4)(H_2O)] (termed as UTSA-280) synthesized from calcium nitrate and squaric acid.[143] UTSA-280 possesses rigid one-dimensional channels with the cross-sectional areas of ~14.4 Å 2 (Fig. 4), which falls right between the minimum cross-sectional area of C_2H_4 (13.7 Å 2) and C_2H_6 (15.5 Å 2). Thus, the pores of UTSA-280 serve as molecular sieves to impede the transport of C_2H_6, and allow the passage of C_2H_4, achieving an ideal separation of C_2H_4/C_2H_6 mixtures. Breakthrough experiments validates the efficacy of this molecular sieve to separate C_2H_4/C_2H_6 mixtures with high C_2H_4 productivity at 298 K and 1 bar. Very importantly, UTSA-280 is water-stable and can be readily prepared at the kilogram scale in an environmentally friendly method. These features are important for potential industrial implementation.

Subsequently, Bao et al. in 2018 reported a family of gallate-based MOF materials, M-gallate (M = Ni, Mg, Co), featuring three-dimensionally interconnected zigzag channels,

whose aperture sizes (3.47–3.69 Å) are highly suitable separate C_2H_4 (3.28 × 4.18 × 4.84 Å 3) from C_2H_6 (3.81 × 4.08 × 4.82 Å 3) through a partial sieving mechanism.[144] Particularly, Co-gallate shows a high C_2H_4/C_2H_6 IAST selectivity of 52 with a C_2H_4 uptake of 3.37 mmol/g at 298 K and 1 bar, and is confirmed by direct breakthrough experiments with equimolar C_2H_4/C_2H_6 mixtures.

C_2H_6 selective adsorbents—Typically, C_2H_4 is adsorbed preferentially over C_2H_6 in MOF materials, because unsaturated C_2H_4 often have stronger interactions with the framework due to its π-electron density and larger polarity. The desired high-purity C_2H_4 products are thus obtained by releasing the captured C_2H_4 from the adsorbents, which consumes considerable energy. To find an energy-economic approach, efforts have been devoted to seeking adsorbents that selectively extract C_2H_6 from the mixture, so that pure C_2H_4 can be produced directly from the outlet of the adsorbent fixed-bed.

In this regard, Liao et al. in 2015 reported the construction of a Zn-azolate MOF [Zn(batz)] (H_2batz = bis(5-amino-1*H*-1,2,4-triazol-3-yl)methane),denoted as MAF-49, for rarely selective adsorption of C_2H_6 over C_2H_4.[145] Based on single crystal X-ray diffraction analysis, MAF-49 is a three-dimensional framework with narrow one-dimensional zigzag channels (Fig. 5). Since there are only four out of eight nitrogen donors of $batz^{2-}$ participating in the coordination with Zn^{II}, the pore surface is rich with electronegative nitrogen atoms. Gas adsorption studies showed that MAF-49 had a higher C_2H_6 uptake than C_2H_4 under low pressure at 316 K, leading to an unusual inverse IAST C_2H_6/C_2H_4 selectivity of 9 (316 K and 1 bar). Computational simulations indicated that C_2H_6 molecule forms three strong C–H···N hydrogen bonds and three weak C–H···Nelectrostatic interactions with MAF-49. By contrast, for C_2H_4 molecule only two less strong C–H···N hydrogen bonds and two very weak C H···N electrostatic interactions were formed. The different binding strengths and numbers of interaction sites in the cases of C_2H_6 and C_2H_4 thus resulted in the selective adsorption of C_2H_6 over C_2H_4 in MAF-49, which was further confirmed by the single-crystal structures of MAF-49·C_2H_6 and MAF-49·C_2H_4.

Similarly, Hao et al. in 2018 reported a MOF TJT-100 that is capable to selectively adsorb C_2H_6 over C_2H_4.[176] Based on computational studies, the reversed C_2H_6/C_2H_4 selectivity stem from the formation of multiple C–H···O electrostatic interactions between C_2H_6 and the uncoordinated carboxylate oxygen atoms and coordinated water molecules towards the pore. While the corresponding "C_2H_4-framework" interaction is unfavorable.

Apart from hydrogen bonding and electrostatic interactions, van der Waals interactions can also be employed in the design and fabrication of MOFs for selective adsorption of C_2H_6 over C_2H_4. In 2018, Lin et al. discovered that controlling the pore structures in isoreticular ultramicroporous MOFs to enlarge the weakly polar interaction surface of MOFs can strengthen their binding affinities towards C_2H_6 and lead to higher C_2H_6/C_2H_4 selectivities.[146] It was found that compared with the prototypical $Cu(ina)_2$, the smaller-pore isoreticular analogue $Cu(Qc)_2$ exhibits an apparently larger C_2H_6/C_2H_4 uptake ratio of 237% (60.0/25.3 cm^3/cm^3) at ambient conditions, remarkably increasing the C_2H_6/C_2H_4 selectivity. Neutron powder diffraction studies clearly reveal that the $Cu(Qc)_2$ displays a self-adaptive sorption behavior towards C_2H_6, which enables its continuous maintenance of

the close van der Waals contacts with C_2H_6 molecules in its optimized pore structure, and thus the preferential binding of C_2H_6 over C_2H_4.

Similarly, Chen et al. in 2018 reported that PCN-250 can be utilized as a C_2H_6-selective adsorbent for efficient purification of C_2H_4 from C_2H_4/C_2H_6 mixtures.[147] Configurational-biased grand canonical Monte Carlo simulation reveal that both the pore effect and the van der Waals adsorption energy govern the separation of C_2H_6 over C_2H_4 for PCN-250, especially at low pressures.

Introducing peroxo sites into MOFs is another effective method to achieve C_2H_6/C_2H_4 separations. In 2018, Li et al. reported a microporous MOF, $[Fe_2(O_2)(dobdc)]$ ($dobdc^{4-}$ = 2,5-dioxido-1,4-benzenedicarboxylate) with Fe-peroxo sites for the preferential binding of C_2H_6 over C_2H_4 (Fig. 6), and thus achieved highly selective separation of C_2H_6/C_2H_4.[148] The C_2H_6 binding affinity was first exhibited in the single-component sorption isotherms of $Fe_2(O_2)(dobdc)$ at 298 K, in which C_2H_6 has a much higher adsorption capacity (74.3 cm^3/g) than C_2H_4 (around 57 cm^3/g) at 1 bar. To structurally elucidate how C_2H_6 and C_2H_4 are adsorbed in the framework to result in "reversed C_2H_6/C_2H_4 adsorption", high-resolution neutron powder diffraction experiments were conducted on C_2D_6-loaded and C_2D_4-loaded $Fe_2(O_2)(dobdc)$ sample. The preferential binding of C_2H_6 with peroxo sites were found to establish through C–D···O hydrogen bonding (D···O 2.17–2.22 Å), with D···O distance much shorter than the sum of van der Waals radii of oxygen (1.52 Å) and hydrogen (1.20 Å). Additionally, the nonplanar C_2D_6 molecule sterically match better with to the uneven pore surface in $Fe_2(O_2)(dobdc)$ than the planar C_2D_4 molecule, leading to stronger H bonds with the active site of Fe-peroxo and stronger van der Waals interactions with the ligand surface. $Fe_2(O_2)(dobdc)$ exhibits a IAST selectivity of 4.4 for C_2H_6/C_2H_4 (50/50) adsorption, which sets a new benchmark. The clean and sharp separation of C_2H_6/C_2H_4 in the column breakthrough experiments performed with a C_2H_6/C_2H_4 (50/50) mixture further demonstrates that $Fe_2(O_2)(dobdc)$ can readily produce high-purity C_2H_4 (≥99.99%) from C_2H_4/C_2H_6 mixtures.

Gate-opening effect can give rise to the preferential adsorption of C_2H_6 from C_2H_4/C_2H_6 mixtures as well. Gücüyener et al. in 2010 reported that C_2H_6 can be selectively adsorbed over C_2H_4 on ZIF-7.[177] This reversed adsorption mainly arises from a gate-opening effect in which specific threshold pressures control the uptake and release of adsorbates. Similar phenomenon was also observed in another flexible MOF, $Zn_2(bpdc)_2(bpee)$ (bpdc = 4,4′-biphenyldicarboxylate, bpee = 1,2-bipyriylethylene).[178]

C_3H_6/C_3H_8 separation

C_3H_6/C_3H_8 separation is a very challenging and industrially important process. Like C_2H_4/C_2H_6 separation, one or more of the four mechanisms (equilibrium-based mechanism, kinetic-based mechanism, gate-opening effect, and molecular sieving effect) account for the high C_3H_6/C_3H_8 selectivities achieved in MOFs. Much progress has been made in recent years based on distinct separation mechanisms.

Creating high densities of open metal sites in the pores of MOFs is a powerful general strategy to realize high C_3H_6/C_3H_8 selectivities. In 2012, Bae et al. examined the selective

adsorption of C_3H_6 over C_3H_8 in M-MOF-74 materials (M = Co, Mn, and Mg), which all bear high densities of open metal sites.[149] Among the series, Co-MOF-74 exhibits the highest thermodynamic C_3H_6/C_3H_8 selectivity. Similarly, Bachman et al. in 2017 evaluated the C_3H_6/C_3H_8 separation ability of several M_2(*m*-dobdc) (*M* = Mn, Fe, Co, Ni; *m*-dobdc^{4-} = 4,6-dioxido-1,3-benzenedicarboxylate).[19] These materials are structural isomers to the well-known M-MOF-74, but exhibit an increased affinity for C_3H_6 over C_3H_8 relative to their M-MOF-74 isomers, leading to the enhanced selectivities for C_3H_6/C_3H_8 separations. Among them, Fe_2(*m*-dobdc) displays the highest C_3H_6/C_3H_8 (>55) selectivity at ambient conditions, with C_3H_6 adsorption capacity higher than 7 mmol/g. Based on in situ single-crystal X-ray diffraction studies, the notable improvement in C_3H_6 affinity mainly results from the enhanced metal-C_3H_6 interactions induced by increased charge density at the metal site in M_2(*m*-dobdc). It should be noted that Fe_2(*m*-dobdc) also displays quite high C_2H_4/C_2H_6 selectivity (>25) as well.

While equilibrium-based separations are attained by the preferential equilibrated uptake of one component over the other, kinetic separation are accomplished by the diffusion rate difference of the adsorbates in and out of the adsorbents. In 2009, Li et al. realized the first the kinetic separation of C_3H_6 and C_3H_8 on three ZIFs.[179] Since then, a number of C_3H_6/C_3H_8 separation based on this mechanism were reported.

In 2011, Lee et al. synthesized a series of isostructural, noncatenated, zinc-pillared-paddlewheel MOFs from 1,2,4,5-tetrakis(carboxyphenyl)benzene and trans-1,2-dipyridylethene struts.[180] Substantial C_3H_6/C_3H_8 kinetic selectivity was observed in the adsorption. They discovered that the tuning of the pore apertures (via the introduction of Br atoms), the modulation of channel congestion (via the presence of the trimethylsilane group), the thin rectangular shape of the MOF crystals, as well as the fortuitous manner in which the modified channel is oriented perpendicular to the largest faces of the crystals are all responsible for the high C_3H_6/C_3H_8 kinetic selectivities achieved.

In 2017, Peng et al. reported an excellent performance for the kinetic separation of C_3H_6 and C_3H_8 realized in $Zn(ox)_{0.5}$(trz) at 323 K (ox = oxalate, trz = 1,2,4-triazole).[181] The considerable difference in diffusivity of C_3H_6 and C_3H_8 results in a kinetic separation factor of 1565, which is primarily ascribed to the appropriate pore apertures. Similarly, ELM-12 reported by Li et al. in 2018 with appropriate channels also achieved the desired kinetic separation performance.[182]

The size and shape of pore aperture is also tunable by adjusting the topology of the framework for kinetic separation purposes. In 2018, Xue et al. reported the adjustment the rectangular pore aperture size induced by the ftw topology using either the BPTC or ABTC ligand (H_4BPTC = biphenyl-3,3′,5,5′-tetracarboxylic acid; H_4ABTC = azobenzenetetracarboxylic acid).[183] The obtained ftw-MOF-ABTC, thus has the ability to kinetically separate C_3H_6 from C_3H_8.

Cadiau et al. in 2016 reported the fabrication of a fluorinated porous MOF (NbOFFIVE-1-Ni, denoted as KAUST-7) for the molecular exclusion of C_3H_6 from C_3H_8 at ambient conditions.[150] Buildt from Ni(II)-pyrazine square-grid layers and $NbOF_5^{2-}$ pillars,

NbOFFIVE-1-Ni is isostructural to SIFSIX-3-Ni. The rational use of $NbOF_5^{2-}$ rather SiF_6^{2-} gives rise to a longer metal-fluorine distance (1.95 Å) and a concomitant tilting of pyrazine molecules. Consequently, NbOFFIVE-1-Ni shows a smaller pore aperture size (3.0471 Å) than SI01FAFSIX-3-Ni (4.965 Å, Fig. 7a). The passing of C_3H_6 gas molecules suggests the plausible gate size associated with the extra tilting of the pyrazine under C_3H_6 gas stimuli. Single-component adsorption measurements indicate that NbOFFIVE-1-Ni adsorbs C_3H_6 but exclude C_3H_8 from entering the framework at 298 K and up to 1 bar (Fig. 7b). The molecular sieving based C_3H_6/C_3H_8 separation was further confirmed by breakthrough experiments with a 50/50 C_3H_6/C_3H_8 mixture (Fig. 7c), resulting in a C_3H_6 productivity of 0.6 mmol/g for a given cycle. The looked-for hindrance in NbOFFIVE-1-Ni dictates the pore size and its maximum opening, and facilitates the selective molecular exclusion of C_3H_8 from C_3H_6.

The molecular sieving of C_3H_6 from C_3H_8 was also well exemplified by Wang et al. in 2018 with a novel material $Y_6(OH)_8(abtc)_3(H_2O)_6(DMA)_2$ (denoted as Y-abtc, abtc = 3,3′,5,5-azobenzene-tetracarboxylates; DMA = dimethylammonium).[151] Y-abtc was synthesized through a topology-guided strategy to replacement of inorganic metal cluster (Fig. 8a). The resultant Y-abtc has optimal pore window size (4.72 Å), which falls right between the kinetic diameters of C_3H_6 (4.68 Å) and C_3H_8 (5.1 Å). This imparts Y-abtc with excellent ability to separate C_3H_8 from C_3H_6 based on the molecular sieving mechanism (Fig. 8b). Under ambient temperature and pressure, Y-abtc adsorbs C_3H_6 with fast kinetics but fully excludes C_3H_8. Multicomponent breakthrough experiments indicated that polymer-grade C_3H_6 (99.5%) can be obtained from a typical mixture concentration of cracking product (Fig. 8c). Considering the high thermal and hydrothermal stability of Y-abtc and its complete C_3H_6/C_3H_8 separation, this work demonstrates the true potential of Y-abtc as an alternative sorbent for efficient separation of C_3H_8/C_3H_6 mixtures.

C_2H_2/C_2H_4 separation

Separating C_2H_2 from C_2H_2/C_2H_4 mixtures is one of the crucial but challenging industrial-scale processes. Current commercial technologies entail partial hydrogenation and solvent extraction, which are highly costly and energy-consuming. Adsorption-based separation with porous materials offer an exceedingly efficient route to performing the targeted separation.

Since the first example for C_2H_2/C_2H_4 separation using MOFs was realized with M'MOF series by Xiang et al. in 2011,[152] a large number of MOF materials have been developed for this separation. However, most reported MOFs suffer from a trade-off between C_2H_2 adsorption capacity and C_2H_2/C_2H_4 selectivity. For instance, although the open metal sites in Fe-MOF-74 notably enhance its C_2H_2 uptake capacity, the large nanopores lead to a low selectivity of 2.08.[20,142] The same phenomenon was also observed in NOTT-300.[112] In contrast, the M'MOFs series have high selectivities up to 24, but very limited C_2H_2 uptakes owing to their narrow pore space.[184]

Great efforts have been devoted to dealing with the trade-off in C_2H_2/C_2H_4 separations in recent years. Hu et al. in 2015 synthesized a dual-functionalized MOF (UTSA-100) with narrow windows of 3.3 Å and suitable cages of 4.0 Å. These structural features enforce

its high adsorption selectivity (10.72). Moreover, the NH_2 groups within the framework have preferential interactions with C_2H_2 molecules to give rise to a moderately high C_2H_2 uptake.[153] UTSA-100 thus achieves a balanced high selectivity and high C_2H_2 uptake. Hazra et al. in 2017 reported a pillar-layered porous MOF bearing small windows of 5.5 × 4.0 $Å^2$. The MOF has a C_2H_2/C_2H_4 selectivity of 17 and moderate C_2H_2 capacity of 3.2 mmol/g at 283 K and 1 bar.[154]

In 2016, the trade-off was significantly reduced by Cui et al. in a series of SIFSIX materials. This work presented a comprehensive study on the C_2H_2 and C_2H_4 adsorption properties of SIFSIX-1-Cu, SIFSIX-2-Cu, SIFSIX-2-Cu-i, SIFSIX-3-Cu, SIFSIX-3-Zn, and SIFSIX-3-Ni.[128] All these SIFSIX materials display apparently higher C_2H_2 uptake than C_2H_4. Among them, SIFSIX-2-Cu-i exhibits a remarkably high C_2H_2 adsorption capacity of 2.1 mmol/g at 298 K and 0.025 bar, with a C_2H_2/C_2H_4 selectivity as high as 39.7–44.8 (Fig. 9). Density functional theory calculations and neutron powder diffraction studies indicate that each C_2H_2 molecule was simultaneously bound by two F atoms from different nets through hydrogen bonding to afford strong interactions between C_2H_2 and the framework, thus leading to the exceptionally high C_2H_2 uptake and selectivity. Column breakthrough experiments performed with 1/99 and 50/50 C_2H_2/C_2H_4 mixtures further confirm the excellent separation ability of SIFSIX-2-Cu-i.

To fully address the issue of trade-off in C_2H_2/C_2H_4 separation, Li et al. in 2018 constructed an ideal C_2H_2 molecular sieve SIFSIX-14-Cu-i (also termed as UTSA-200) using a shorter organic linker of 4,4′-azopyridine (9.0 Å) instead of 4,4′-dipyridylacetylene (9.6 Å) in SIFSIX-2-Cu-i.[155] UTSA-200 is isoreticular to the net of SIFSIX-2-Cu-i, but possesses contracted pore size (3.4 Å). Structural and modeling studies revealed that this smaller pore size in UTSA-200 can completely block the entrance of C_2H_4 molecules (Fig. 10a). Consequently, UTSA-200a exhibits a steep and high C_2H_2 uptake of 116 cm^3/cm^3 at 298 K and 1 bar in pure component adsorption isotherms (Fig. 10b). By contrast, the C_2H_4 uptake is about merely 0.25 mmol/g at 298 K and at a pressure up to 0.7 bar, which is dramatically lower than that of SIFSIX-2-Cu-i. Based on neutron powder diffraction studies, the ultrastrong C_2H_2 adsorption in UTSA-200 mainly originates from the stronger C-D···F hydrogen bonding (1.921 Å) compared to SIFSIX-2-Cu-i (2.015 Å). Due to the molecular exclusion of C_2H_4 and ultrastrong C_2H_2 capture ability, UTSA-200a exhibits the record selectivity of over 6000 at 298 K and 1 bar for 1/99 C_2H_2/C_2H_4 mixture, and also displays the highest C_2H_2 adsorption amount (1.74 mmol/g) from the gas mixture of this component. In breakthrough experiments, UTSA-200a achieves a record purification capacity for removal of trace C_2H_2 from C_2H_4 with a C_2H_2 uptake capacity of 1.18 mmol/g from 1/99 C_2H_2/C_2H_4 mixture to produce C_2H_4 with a purity of 99.9999% (Fig. 10c). UTSA-200a thus successfully overcomes the trade-off in C_2H_2/C_2H_4 separation and sets up new benchmarks in terms of both the capacity and selectivity.

C_2H_2/CO_2 separation

C_2H_2, as a critical feedstock chemical and fuel gas, is generally produced by partial combustion of CH_4 or cracking of hydrocarbons. Since CO_2 commonly exists in industrial processes, it is important to remove CO_2 from C_2H_2/CO_2 mixtures to generate C_2H_2 with

high-purity. Compared with the traditional method of cryogenic distillation or solvent extraction, separation realized by selective adsorption of one species over the other is eco-friendly and energy-economic. However, exploration of such adsorbents remains a great challenge, owing to their very similar physical properties like molecular size (C_2H_2, 3.32 × 3.34 × 5.70 $Å^3$; CO_2, 3.18 × 3.33 5.36 $Å^3$) and boiling point (C_2H_2, −84 °C; CO_2, −78.5 °C). Nevertheless, some MOFs still realized the desired C_2H_2/CO_2 separation in recent years.

The immobilization of functional sites in MOFs has been well documented as a promising strategy to enhance the recognition ability of MOFs for C_2H_2 over CO_2. In 2016, Luo et al. reported $Zn_2(H_2O)(dobdc)$ $0.5(H_2O)$ (termed as UTSA-74), a new isomeric Zn-MOF-74, for a highly selective C_2H_2/CO_2 separation.[156] Unlike the metal sites in Zn-MOF-74 that only bear the five-coordinate square pyramidal coordination geometry, the ones in UTSA-74 have two categories. Within the binuclear secondary building units in UTSA-74, one Zn^{II} (Zn1) is a tetrahedral while the other (Zn2) is an octahedral coordination geometry. After activation, the two axial water molecules on Zn2 sites can be removed to produce two binding sites per Zn2 ion. Accordingly, UTSA-74 adsorbs comparably amount of C_2H_2 (145 cm^3/cm^3) with respect to Zn-MOF-74. In terms of CO_2 adsorption, Zn2 sites in UTSA-74 are bridged by CO_2 molecules, as opposed to being terminally bound in Zn-MOF-74. This feature leads to its much lower CO_2 uptake (90 cm^3/cm^3) and a high C_2H_2/CO_2 selectivity of 9 at 100 kPa and 298 K.

In 2017, Lin et al. discovered a novel microporous SIFSIX-MOF, $[Zn(dps)_2(SiF_6)]$ (dps = 4,4′-dipyridylsulfide; termed as UTSA-300) for the optimized separation of C_2H_2 from CO_2 and C_2H_4.[157] UTSA-300 possesses two-dimensional channels of ~3.3 Å (Fig. 11), which transforms into its closed-pore phase after activation/desolvation. The shrinked structure is locked by strong C–H···F hydrogen bonds and **π**-**π** interactions. Interestingly, UTSA-300a adsorbs 76.4 cm^3/g C_2H_2 but negligible amounts of CO_2 and C_2H_4 under ambient conditions. High-resolution neutron powder diffraction studies and molecular modeling reveal that this phenomenon is attributed to the breaking of the original intranetwork hydrogen bond by C_2H_2 molecules. Specifically, one C_2H_2 molecules primarily bind to two hexafluorosilicate F atoms in a head-on orientation, and consequently expand the framework to its pore-open structure. Such pore-opening behavior was not observed in the cases of CO_2 and C_2H_4 due to the different binding modes and unfavorable pore size. Breakthrough Experiments further confirm the excellent separation ability of UTSA-300a for C_2H_2/CO_2 and C_2H_2/C_2H_4 mixtures.

While most MOFs preferentially adsorb C_2H_2 over CO_2. Pure C_2H_2 is produced from the release of the captured C_2H_2, which inevitably consumes considerable energy. In an ideal C_2H_2/CO_2 separation scenario, adsorbents are required to selectively adsorb CO_2 over C_2H_2, so that pure C_2H_2 can be generated directly during the “adsorption” process. In 2016, Foo et al. reported a new flexible MOF [Mn(bdc)(dpe)] (H_2bdc = 1,4-benzenedicarboxylic acid, dpe = 1,2-di(4-pyridyl)ethylene) with preferential adsorption of CO_2 over C_2H_2.[159] Interestingly, this MOF has a moderate CO_2 uptake of 48 cm^3/g at 273 K and 1 bar with no gate-opening effect. By contrast, a gate-opening effect was observed in the C_2H_2 adsorption isotherm at 273 K with a steep step occurring at over 1 bar. The low C_2H_2 uptake at 1

bar (10 cm^3/g) suggests that this MOF is capable to separate CO_2 from C_2H_2 at 273 K, as confirmed by simulated and experimental breakthrough experiments.

In 2016, Chen et al. reported two structurally close-related MOFs (SIFSIX-3-Ni and TIFSIX-2-Cu-i) that display distinct preferential adsorption behaviors of C_2H_2/CO_2 mixtures.[158] SIFSIX-3-Ni is a non-interpenetrated MOF with pore size of ~4.2 Å, while TIFSIX-2-Cu-i is a double-interpenetrated framework with a slightly large pore size of ~5.2 Å. Gas sorption analysis indicates that TIFSIX-2-Cu-i exhibits a preferential adsorption of C_2H_2 over CO_2, while SIFSIX-3-Ni has higher CO_2 uptake than C_2H_2 below 0.3 bar at 298 K. Such distinct adsorption behaviors are associated with the different pore sizes of the frameworks and the concomitant different binding sites, which are evidenced by molecular simulation experiments. Specifically, the pores in SIFSIX-3-Ni match well with CO_2 molecules to result in strong interactions between CO_2 and SiF_6^{2-} sites, whereas TIFSIX-2-Cu-i has more pore space to trap the slightly longer C_2H_2 molecules and thus exhibits preferential adsorption of C_2H_2 over CO_2.

C_3H_4/C_3H_6 separation

C_3H_6 is one prime raw materials for petrochemical production, and is primarily produced by steam cracking. The raw C_3H_6 product is unavoidably impurified by a trace amount of C_3H_4. To meet the criterion of polymer-grade C_3H_6, the C_3H_4 concentration is required to be less than 5 ppm. Compared with traditional cryogenic distillation, adsorptive separation of C_3H_4 from C_3H_6 with porous materials is deemed as a more economic and energy-efficient method. However, the removal of trace C_3H_4 (typically 1%) from C_3H_6 is very challenging because of their similar molecular sizes (C_3H_4 6.2 × 3.8 × 3.8 $Å^3$; C_3H_6, 6.5 × 4.0 × 4.2 $Å^3$) and other physical properties. So far, only several MOFs have been developed and show potential in this important but challenging separation.

In 2017, Li et al. reported the first example of using a flexible-robust MOF, $[Cu(bpy)_2(OTf)_2]$ (ELM-12, bpy = 4,4′-bipyridine, OTf^- = trifluoromethanesulfonate), to separate C_3H_4 from C_3H_4/C_3H_6 mixture (1/99, v/v).[160] ELM-12 is composed of a rigid square-grid copper bipyridine scaffold with dangling OTf^-groups. It has two types of cavities bearing a dumbbell-shape (Type I, pocket size 6.1 Å × 4.3 Å × 4.3 Å) and an ellipsoid-shaped (Type II, 6.8 Å × 4.0 Å × 4.2 Å), respectively (Fig. 12). These cavities match evidently better with the size and shape of C_3H_4 (6.2 Å × 3.8 Å × 3.8 Å) than those of C_3H_6 (6.5 Å × 4.0 Å × 3.8 Å), consequently ELM-12 exhibits notably a higher C_3H_4 uptake (1.83 mmol/g) than that of C_3H_6 (0.67 mmol/g) in gas sorption isotherms at 298 K and 0.01 bar, with adsorption selectivity reaching up to 84 for 1/99 mixture. Breakthrough experiments revealed that ELM-12 can effectively remove trace C_3H_4 from 1/99 C_3H_4/C_3H_6 mixtures at ambient conditions to produce C_3H_6 with a purity of 99.9998%. High-resolution neutron powder diffraction data indicated the existence of two C_3H_4 binding sites in ELM-12, in both of which C_3D_4 molecules interact with OTf^-groups through C–D···O hydrogen bonds. The strong binding affinity and suitable pore confinement for C_3H_4 in ELM-12 account for its high C_3H_4/C_3H_6 separation ability.

In 2018, Yang et al. investigated C_3H_4/C_3H_6 separation performance of a series of SIFSIX MOFs (SIFSIX-1-Cu, SIFSIX-2-Cu-i, and SIFSIX-3-Ni).[161] All three SIFSIX materials

displayed steep C_3H_4 uptakes in the low-pressure region of the adsorption isotherms at 298 K, and larger adsorption amounts of C_3H_4 than C_3H_6 at 1 bar. In particular, the pyrazine based ultra-microporous SIFSIX-3-Ni has a near-saturation C_3H_4 uptake of 2.65 mmol/g at an extremely low pressure (0.003 bar) with C_3H_4/C_3H_6 selectivity over 250, suggesting the existence of strong C_3H_4 interaction sites within SIFSIX-3-Ni. Based on the first-principle calculations and X-ray diffraction experiments, the pore space ($7.5 \times 4.6 \times 4.6$ Å^3) and the geometric disposition of SiF_6^{2-}anions in SIFSIX-3-Ni match well with the C_3H_4 molecule in terms of both molecular shape and hydrogen bonding sites, enabling the efficient single molecular trap of C_3H4 for C_3H_4/C_3H_6 separation. Breakthrough experiments further confirm that SIFSIX-3-Ni can remove trace C_3H_4 from C_3H_6 with a purification capacity of 1187 mL/g at ultralow concentration of 1000 ppm.

In 2018, Yang et al. further reported the one-step purification of C_3H_6 from multicomponent gases using a single material NbOFFIVE-2-Cu-i (also termed as ZU-62).[162] ZU-62 features asymmetric O/F node coordination, which leads to the formation of three types of nanopores bearing aperture sizes of 6.75 Å (Site I), 6.94 Å (Site II), 7.20 Å (Site III), respectively. These multiple binding sites enabled the simultaneously preferential adsorption of C_3H_4 (1.87 mmol/g) and propadiene (1.74 mmol/g) over C_3H_6 in gas sorption isotherms at 298 K and ultra-low pressure (5000 ppm) in ZU-62. The multisite capture mechanism was revealed by dispersion-corrected density functional theory calculations. This work provides some clues for the one-step purification from multicomponent mixtures.

In 2018, Li et al. conducted a comprehensive screening of a series of MOFs with broad types of structures, pore sizes, and functionalities (Fig. 13a).[185] Among them, the ultramicropous UTSA-200 ($[Cu(azpy)_2(SiF_6)]_n$, azpy = 4,4′-azopyridine) was identified as the best-performing material to remove trace amount of C_3H_4 from C_3H_4/C_3H_6 mixtures. UTSA-200 exhibits by far the highest C_3H_4 uptake (95 cm^3/cm^3 at 0.01 bar and 298 K) and record high C_3H_4/C_3H_6 selectivity (over 20,000) based on gas sorption isotherms (Fig. 13b), which set new benchmarks among all types of materials. Breakthrough experiments revealed that UTSA-200 can completely remove trace C_3H_4 from 1:99 and 0.1:99.9 (v/v) mixtures, thus producing 99.9999% pure C_3H_6 with productivities of 62.0 and 142.8 mmol/g, respectively. The strong C_3H_4/C_3H_6 separation ability mainly originates from the suitable dynamic pore size of UTSA-200 to block the passage of larger C_3H_6 molecules, as well as the strong binding sites and pore flexibility associated with the rotation of pyridine rings to effectively capture smaller-sized C_3H_4.

C_4 hydrocarbon separation

C_4 hydrocarbon separation is an important but challenging process in hydrocarbon purifications, because 1,3-butadiene (C_4H_6), 1-butene (n-C_4H_8), and isobutene (iso-C_4H_8) are essential raw materials for the production of a variety of synthetic rubbers and chemicals. However, their very similar structures bring considerable difficulty in efficient separation. Nevertheless, some MOFs still have been fabricated to address this challenging task.

In 2015, Assen et al. synthesized a novel rare-earth metal (RE) fcu-MOF with a suitable aperture size to achieve the practical steric adsorptive separation of branched paraffins from normal ones.[163] They judiciously chose a short linker fumarate (fum) to construct

RE-fum-fcu-MOF with a contracted triangular aperture size of about 4.7 Å. Because the optimal aperture is the sole access to the framework cages, they function as sorbate-size cutoffs, enabling a complete molecular sieving of branched paraffins from normal ones. Consequently, RE-fum-fcu-MOF displays a fully reversible Type-I gas sorption isotherm for *n*-C_4H_{10} at 293 K, while no iso-C_4H_{10} is adsorbed. The *n*-C_4H_{10}/iso-C_4H_{10} separation ability in RE-fum-fcu-MOF is further confirmed by breakthrough experiments using *n*-C_4H_{10}/iso-C_4H_{10}/N_2: 5/5/90 gas mixture performed at 298 K and 1 bar. As expected, iso-C_4H_{10} is not retained in the column, while *n*-C_4H_{10} is retained in the column for about 17 min with an adsorbed amount of 0.8 mmol/g.

In 2017, Zhang et al. reported a series of SIFSIX materials (GeFSIX-2-Cu-i (ZU-32), NbFSIX-2-Cu-i (ZU-52), GeFSIX-14-Cu-i (ZU-33)), which exhibit selective recognition of specific C_4 olefins.[164] They successfully fine-tuned the cavity size and functional site disposition with increments in 0.2 Å scale in the MOFs by rationally altering the anion pillars and organic linkers. GeFSIX-14-Cu-i, in particular, whose pores can have a size of 4.2 Å, if the plausible complete omission of the occurring steric hindrance of azpy (azpy = 4,4′-azopyridine) linker is considered. This pore is larger than the smallest cross sections of C_4H_6 and narrower than those of *n*-C_4H_8 and iso-C_4H_8, which makes the size exclusion of specific C_4 olefins in GeFSIX-14-Cu-i feasible. With the combined effect of molecular recognition via hydrogen bonding and size-sieving, these materials unexpectedly achieve the sieving separation of C_4H_6/*n*-C_4H_8, C_4H_6/iso-C_4H_8, and *n*-C_4H_8/iso-C_4H_8 with high capacities, as confirmed by breakthrough experiments.

MOFs with functional sites/groups commonly adsorb C_4H_6 preferentially over other C_4 hydrocarbons, because of its high degree of unsaturation and strong coordination ability. C_4H_6 is thus purified in a two-step process consisting of C_4H_6 capture and its subsequent release, which is energy-intensive and might induce undesired polymerization as well. To deal with this drawback, Liao et al. in 2017 fabricated a hydrophilic MOF [$Zn_2(btm)_2$] also termed as Zn-BTM, (H_2btm = bis(5-methyl-1*H*-1,2,4-triazol-3-yl)methane)) featuring flexible quasidiscrete pores and achieved the reversed preferential adsorption of *n*-C_4H_8, iso-C_4H_8 and C_4H_{10} over C_4H_6 with the MOF (Fig. 14a).[186] Zn-BTM display the C_4 hydrocarbon adsorption slopes in the sequence of C_4H_6 < C_4H_{10} < *n*-C_4H_8 < *i*- C_4H_8 at low pressure region in their single-component isotherms (Fig. 14b), which clearly indicates the preferential adsorption of C_4H_{10}, *n*-C_4H_8, and *i*-C_4H_8 over C_4H_6. Based on single crystal X-ray diffraction studies and computational simulations, the preferential adsorption derives from the conformational changes induced in the flexible C_4 molecules by quasi-discrete pores in Zn-BTM (Fig. 14c). While such a conformational change is difficult to occur in C_4H_6 due to a large bending energy penalty. In breakthrough experiments with Zn-BTM, C_4H_6 eluted first, followed by C_4H_{10}, *n*-C_4H_8, and *i*-C_4H_8, further demonstrating that Zn-BTM can efficiently purify C_4H_6 with a desired purity (≥99.5%).

Separation of C_6 isomers

Separating hexane isomers is regarded as a crucial process involved in petroleum industry, because it is closely related to the enhancement of octane ratings in gasoline. Hexane isomers include unreacted n-hexane (nHEX), monobranched isomers 2-methylpentane

(2MP), 3-methylpentane (3MP), dibranched isomers 2,2-dimethylbutane (22DMB) and 2,3-dimethylbutane (23DMB). At certain temperatures in ambient conditions, C_6 isomers exist in the form of gas vapor. In this scenario, employing MOFs to perform adsorption-based separation of these C_6 isomers are favorable.

The first example of using microporous MOF to separate alkane isomers was reported by Chen et al. in 2006.[71] They successfully separated C_6 hydrocarbons by means of gas chromatography with MOF-508 as the column filler. In the same year, Pan et al. realized the separation of C_4–C_6 hydrocarbons using a Cu-based microporous MOF.[187] After that, Bárcia et al. achieved a kinetic separation of hexane isomers using $Zn(bdc)(dabco)_{0.5}$ (bdc^{2-} = 1,4-benzenedicarboxylate; dabco = 1,4-diazabicyclo[2.2.2]octane) by fixed-bed adsorption.[73] Recently, a number of interesting works have been reported successively.

In 2013 Herm et al. reported utilizing a framework $Fe_2(BDP)_3$ (BDP^{2-} = 1,4-benzenedipyrazolate) featuring triangular channels to separate hexane isomers (Fig. 15).[188] Single-component adsorption isotherms and isosteric heat of adsorption of these isomers suggest that the higher degree of branching would lead to stronger adsorption strength. In breakthrough experiments conducted with a equimolar mixture of nHEX, 2MP, 3MP, 23DMB, and 22DMB, dibranched isomers eluted first, followed by monobranched isomer, and finally the linear isomer. Configurational-bias Monte Carlo simulations indicates that the origin of separation lies in the fact that the number of carbon atoms that can interact with the pore surface of $Fe_2(BDP)_3$ reduces with the increasing degree of branching. Thus, DMB isomers have the weakest interactions with MOF surface and wedge along the triangular channels most quickly.

In 2018, Wang et al. for the first time achieved a temperature- and adsorbate-dependent molecular sieving of linear, monobranched, and dibranched hexane isomers using a calcium-based MOF $Ca(H_2tcpb)$ (tcpb = 1,2,4,5-tetrakis(4-carboxyphenyl)-benzene) that exhibits.[189] $Ca(H_2tcpb)$ possesses one-dimensional channels bearing a size of 5.5–6 Å, which is close to the kinetic diameters of branched hexane isomers (5.0–6.2 Å). By screening the adsorption amounts of nHEX, 3MP, and 22DMB at various temperatures in $Ca(H_2tcpb)$, they found that the MOF is able to adsorb nHEX but exclude 3MP and 22DMB at 120 °C. Interestingly at 60 °C, $Ca(H_2tcpb)$ takes up nHEX and 3MP but blocks 22DMB. Taking advantage of the adsorption properties of $Ca(H_2tcpb)$, a successful separation of the ternary mixture into pure components was thus achieved through a two-column (120 °C and 60 °C respectively) breakthrough system. The same group further reported a topologically guided synthesis of a series of Zr-MOFs with rationally tuned pore structures for C_6 isomer separation. Among the series, $Zr_6O_4(OH)_4(bptc)_3$ ($bptc^{4-}$ = 3,3′,5,5′ -biphenyltetracarboxylate) adsorbs a large amount of nHEX but excludes branched isomers. While $Zr_6O_4(OH)_8(-H_2O)_4(abtc)_2$ ($abtc^{4-}$ = 3,3′5,5′ -azobenzene-tetracarboxylate) is able to discriminate all three C_6 isomers with a high 3MP/22DMB separation factor.[190]

CO_2 capture and separation

The atmospheric CO_2 concentration has risen sharply due to anthropogenic activities, with the primary emission coming from the combustion of fossil fuels. Considerable research efforts have been devoted to developing MOFs as adsorbents for CO_2 capture.[191]

Some thematic reviews have outlined the advances in this active field and summarized useful strategies to improve the CO_2 capture performance and separation capacities of MOFs.[79,192–198] In the following section, we provide a summary of the advancements achieved in recent years in this arena.

The SIFSIX MOFs have recently been demonstrated to be very promising physical CO_2 adsorbents. In 2013, Nugent et al. fabricated three SIFSIX MOFs (SIFSIX-2-Cu, SIFSIX-2-Cu-i, and SIFSIX-3-Zn) and studied their CO_2 capture abilities.[165] Although SIFSIX-2-Cu, SIFSIX-2-Cu-i, and SIFSIX-3-Zn all possess periodically arrayed functional SiF_6^{2-} moieties (Fig. 16), their pore sizes are different, which are 13.05 13.05 $Å^2$, 5.15 5.15 $Å^2$, and 3.84 3.84 $Å^2$, respectively. Gas sorption studies indicate that SIFSIX-3-Zn has the best CO_2 capture properties among the three MOFs, with not only a high volumetric CO_2 uptake of 84 cm^3/cm^3 at 298 K and 0.1 bar but also very high CO_2/N_2 (post-combustion separation), CO_2/CH_4 (natural gas upgrading) and CO_2/H_2 (pre-combustion separation) selectivities. Such adsorption performances are ascribed to a combined result of judiciously tailored pore size and functional fluorine moieties that significantly improve the interaction strength between CO_2 and SIFSIX-3-Zn, and was further validated by breakthrough experiments. Most importantly, these SIFSIX MOFs well maintain their selective adsorption CO_2 over N_2, H_2, and CH_4, even in the presence of moisture, which is very crucial in practical CO_2 capture scenarios. Subsequent endeavors have also been made by altering the metals species and/or anion pillars to further contract the pore size for better performance.[199,200] The resulting NbOFFIVE-1-Ni displays the highest CO_2 uptake (1.3 mmol/g and 51.4 cm^3 (STP)/cm^3 at 298 K and 400 ppm) as a physical adsorbent.

In 2017, Liang et al. constructed a new Cu-based MOF, FJI-H14, from 2,5-di(1H-1,2,4-triazol-1-yl)terephthalic acid (H_2BTTA).[166] FJI-H14 has a high density of open metal sites (3.07 mol/L) and Lewis basic sites (LBS, 6.15 mol/L), which is anticipated to have a high CO_2 uptake. Consequently, FJI-H14 displays an extraordinarily high volumetric CO_2 capacity of 171 cm^3/cm^3 at 298 K and 1 atm with CO_2/N_2 selectivity as high as 51 for a 15/85 CO_2/N_2 mixture. Based on simulation studies, the preferential CO_2 binding sites within FJI-H14 were further demonstrated to be open Cu^{II} sites and O atoms of carboxyl groups that function as Lewis bases. They can have strong Cu-O and C–O interactions with CO_2 molecules that give rise to high CO_2 capacity. Additionally, FJI-H14 is highly resistant to water and acid/base environments, making it a very promising material as a practical adsorbent for post-combustion CO_2 capture.

In 2015, Zhao et al. developed a strategy named pore space partition by regularly inserting symmetry-matching ligands into large pores to split them into smaller ones for enhanced CO_2 uptakes.[201] They introduced the *C*3-symmetric 2,4,6-tri(4-pyridyl) 1,3,5-triazine (TPT) ligand into large pores of the MIL-88-type structures. The obtained the CPM-33 series show apparently superior CO_2 uptake capacity in gas sorption studies. Among them, CPM-33b in particular, has a gravimetric CO_2 uptake of 126 cm^3/g at 298 K and 1 bar, which is among the highest in MOFs without open metal sites. In 2016, Zhai et al. applied this strategy to construct a series of homo- or heterometallic MIL-88-type MOFs, and that found that Mg_2V-DHBDC ($DHBDC^{2-}$ = 2,5-dihydroxy-1,4-benzenedicarboxylate) can achieve a CO_2 adsorption amount as high as 151.6 cm^3/g 298 K and 1 atm with good CO_2/CH_4

selectivity.[171] It should be noted that the high CO_2 capacity is accomplished with isosteric heat of adsorption as low as 20 kJ/mol, which would make the regeneration of the adsorbent consume less energy.

In 2016, Chen et al. realized the molecular sieving of CO_2 through a MOF [Cu(quinoline-5-carboxylate)$_2$]$_n$ named Qc-5-Cu-sql (sql = square lattice) with fine-tuned pore-sizes.[172] Qc-5-Cu-sql undergoes a phase transformation upon desolvation. The solvated (Qc-5-Cu-sql-α) and desolvated (Qc-5-Cu-sql-β) phase have pore size of around 3.8 and 3.3 Å, respectively. Since the kinetic diameters of CO_2, N_2 and CH_4 are 3.3, 3.64, and 3.8 Å, respectively, the narrower pore in Qc-5-Cu-sql-β is anticipated to exhibit a molecular sieving effect towards CO_2 over N_2 and CH_4. As expected, Qc-5-Cu-sql-β only adsorbs CO_2 with a moderate uptake of 48.4 cm^3/g but completely block N_2 (0.3 cm^3/g) and CH_4 (1.3 cm^3/g), thus achieving a remarkably high CO_2/N_2 (40,000) and CO_2/CH_4 (3300) selectivities at ambient conditions. Moreover, Qc-5-Cu-sql is stable in water vapor. Its separation ability was further validated by breakthrough experiments performed in dry and wet CO_2/N_2 gas mixtures.

Grafting alkylamine groups onto the pore surface of MOFs has been demonstrated to be an effective strategy to achieve highly selective adsorption of CO_2 over CH_4 or N_2 at low pressure.[169,202–205] Particularly, in 2015 McDonald et al. reported the observation of unusual step-shaped CO_2 adsorption isotherms in *N,N′*-dimethylethylenediamine (mmen) functionalized M_2(dobpdc) (*M* = Mg, Mn, Fe, Co, Zn; dobpdc^{4-} = 4,4′-dioxidobiphenyl-3,3′-dicarboxylate), which is indicative of "phase-change" during CO_2 adsorption.[168] Spectroscopic, diffraction, and computational studies suggested that the sharp adsorption step was associated with an unprecedented cooperative process in which CO_2 molecules insert into metal-amine bonds at a metal- and temperature-dependent pressure, triggering a reorganization of the amines into well-ordered chains of ammonium carbamate. Consequently, large CO_2 separation capacities can be achieved with small temperature swings and concomitant low regeneration energies. Then, an ultrahigh concentration of amine functional sites has been achieved in [Mg_2(dobdc)(N_2H_4)$_{1.8}$] by Liao et al. using hydrazine as the shortest diamine in amine grafting for low-concentration CO_2 capture.[169] Rely on the well-established carbamic acid formation, this new material has set a series of new records for CO_2 capture (Table 4), as demonstrated by gas sorption isotherms, NMR spectra, cycling sorption kinetic and breakthrough experiments.

Another state-of-the-art strategy for CO_2 capture is represented by biomimicking of carbonic anhydrase, which is an important and ubiquitous metalloenzyme that catalyzes the hydrolysis of carbon dioxide into bicarbonate species. The key structural fearure is the monodentate hydroxide at the metal nodes, which affords strong and reversible CO_2 binding. In 2015, Liao et al. firstly established the proof–of–concept of enzyme-like active site in MOFs for CO_2 capture, which is achieved in oxidized [M_2Cl_2(bbta)] (H_2bbta 1*H*,5*H*-benzo(1,2-*d*:4,5-*d*′)bistriazole; *M* Mn, MAF-X25; *M* Co, MAF-X27).[170] The post-synthetic immobilized M-OH sites afford chemisorption mechanism for CO_2 capture, resulting in very high CO_2 adsorption affinity and uptake capacity. These materials are also applicable under humidity condition as demonstrated by breakthrough studies. In 2018, the Wade group and Dincă group separately demonstrated a more specific biomimetic MOF model

of carbonic anhydrase for trace CO_2 capture, featuring terminal N_3Zn-OH units as the only active sites.[206,207] These resultant materials show remarkable CO_2 capture performance in the CO_2 mixture of 400 ppm concentration. These demonstrations of biomimetic behavior in MOF media afford an ideal platform at new dimension to understand the enzyme acivity and develop novel enzyme-inspired materials.

Simultaneously, in 2017, Lu et al. reported a redox-active MOF [MFM-300(V^{III})] which can be oxidized to its isostructural MFM-300(V^{IV}).[208] The bridging hydroxyl group V^{III}-(OH)-V^{III} in MFM-300(V^{III}) was deprotonated to V^{IV}-O-V^{IV} in MFM-300(V^{IV}). MFM-300(V^{III}) achieved a CO_2 adsorption amount of 6.0 mmol/g at 298 K and 1 bar based on gas adsorption analysis, while MFM-300(V^{IV}) only has CO_2 uptake of 3.54 mmol/g. Such pronounced difference in CO_2 capacities mainly derives from the different binding sites and subsequent packing modes of adsorbed CO_2 molecules in the two MOFs, which was revealed by neutron diffraction and inelastic scattering data. Specifically, MFM-300(V^{III}) forms hydrogen bonds with the guest via the OH group and the O-donor of CO_2 in an end-on manner. By contrast, CO_2-loaded MFM-300(V^{IV}) exhibits CO_2 bound side-on to the oxy group and sandwiched between two phenyl groups. This work well illustrates the conducive role the protons in hydroxyl groups in CO_2 adsorption in MOFs.

Toxic gas removal

The capture and separation of toxic gases with MOFs have attracted increasing attention in recent years. Commonly encountered toxic gases include sulfur dioxide (SO_2), hydrogen sulfide (H_2S), chlorine (Cl_2), nitric oxide (NO), nitrogen dioxide (NO_2), and ammonia (NH_3). Most of these gases are released as waste gases from industrial processes, which incur severe environment issues and cause great harm to human health. Some thematic reviews have summarized the advances in this field.[209–214] In this section, we will highlight several MOFs showing good potential to effectively remove these toxic gases.

In 2012, Yang et al. reported that NOTT-300 containing no amine groups can selectively bind SO_2 with the hydroxyl groups in pores.[215] Several characterization methods, including in situ powder X-ray diffraction, inelastic neutron scattering studies and modelling, indicate that the hydroxyl groups bind SO_2 via the formation of $O = S = O(\delta -)\cdots H(\delta +) - O$ hydrogen bonds. Such hydrogen bonds are reinforced by the weak supramolecular interactions with C–H atoms on the aromatic rings of the framework. Since the SO_2 binding strength is not as strong as $H_2N(\delta^-)\cdots C(\delta^+)O_2$ in carbamates (that result from the interaction between amine groups and CO_2), NOTT-300 has the potential to be utilized as an “easy-on/easy-off” SO_2 capture systems, which carry fewer economic and environmental penalties.

SO_2 capture can also be achieved in SIFSIX MOFs. In 2017, Cui et al. investigated the SO_2 capture ability of SIFSIX-1-Cu, SIFSIX-2-Cu, SIFSIX-2-Cu-i, SIFSIX-3-Zn, and SIFSIX-3-Ni.[216] SIFSIX-1-Cu and SIFSIX-2-Cu-i display higher SO_2 uptake than those of CO_2 and N_2 at ambient conditions. Especially the SO_2 uptake of SIFSIX-1-Cu (11.01 mmol/g at 298 K and 1 bar) is remarkably high, and ultrahigh low-pressure SO_2 uptakes (4.16 mmol/g at 298 K and 0.01 bar; 2.31 mmol/g at 298 K and 0.002 bar) can be achieved in SIFSIX-2-Cu-i. The SO_2/CO_2 selectivity on SIFSIX-2-Cu-i was calculated

to be 86–89. While SO_2/N_2 selectivities on SIFSIX-2-Cu-i and SIFSIX-1-Cu were 1285–3103 and 2510–3145, respectively. These excellent SO_2 separation performances result from strong host-guest interactions through $S^{\delta+}\ldots F^{\delta-}$ electrostatic interaction and multiple $O^{\delta-}\cdots H^{\delta+}$ dipole-dipole interactions, as elucidated by first principles density functional theory calculations and powder X-ray diffraction experiments. Breakthrough experiments further validate their ability to remove trace SO_2 from CO_2 or N_2.

The capture and separation of NH_3 is found to be associated with the open metal sites within MOFs. In 2016 Rieth et al. reported the high and reversible NH_3 uptake in mesoporous triazolate MOFs M_2Cl_2BTDD (M = Mn, Co, Ni; BTDD =bis(1*H*-1,2,3-triazole[4,5-*b*], [4′,5′-*i*])dibenzo[1,4]dioxin).[217] The same group in 2018 further studied a contracted series of triazolate MOFs, that is, microporous M_2Cl_2BBTA (M = Co, Ni, Cu; BBTA = 1*H*,5*H*-benzo(1,2-*d*),(4,5-*d*′)bistriazole) for NH_3 capture and separation.[218] Both M_2Cl_2BBTA and M_2Cl_2BTDD feature one dimensional hexagonal pores with regularly spaced open metal sites. The smaller pore diameter of M_2Cl_2BBTA (1.3 nm) than that of M_2Cl_2BTDD (2.3 nm) leads to the higher density of open metal sites in M_2Cl_2BBTA, which is beneficial for higher NH_3 capacities. Under equilibrium conditions at 298 K and 1 bar, Cu_2Cl_2BBTA displayed a record static NH_3 capacity of 19.79 mmol/g, which is more than twice the industry standard. In dynamic breakthrough experiments, dynamic NH_3 capacity of Co_2Cl_2BBTA can reach 8.56 mmol/g. They attributed the higher NH_3 capacity in smaller-pore Co_2Cl_2BBTA not only to the increase in open metal site density but also to the cooperative proximity effects that enhance the hydrogen bonding interactions between adsorbed NH_3 molecules. In terms of stability upon NH_3 adsorption, the trends are in line with the water substitution rates in simple metal-aquo complexes, which can act as an easy guide for designing future NH_3 capture adsorbents.

In 2018, Han et al. reported a reversible and selective adsorption of NO_2 in a robust MOF, MFM-300(Al).[148] MFM-300(Al) shows a NO_2 uptake as high as 14.1 mmol/g at 298 K and 1 bar. Moreover, the NO_2/SO_2, NO_2/CO_2, and NO_2/N_2 IAST selectivities at these conditions were calculated to be 18.1, 248, and >10,000, respectively. Based on the results from various characterization methods, they found that there exists five different types of soft supramolecular interaction that cooperatively bind both NO_2 and N_2O_4 molecules within MFM-300(Al), which take the main responsibility for the highly selective adsorption of NO_2 over other gas species. The captured NO_2 and N_2O_4 afford one-dimensional helical $(NO_2\ N_2O_4)_\infty$ chains that are stabilized by multiple weak intermolecular dipole interactions. Breakthrough experiments with several diluted NO_2 streams (5000 ppm diluted in He/N_2, 4000 ppm in He/CO_2, or 1666 ppm in He/SO_2) further confirmed that MFM-300(Al) is capable to efficiently separate the NO_2 in low concentration from these gas mixtures.

In 2010, Shimomura et al. reported the selective absorption of NO by a structurally and electronically dynamic MOF [Zn(TCNQ-TCNQ)bpy] (TCNQ = tetracyanoquinodimethane; bpy = 4,4′-bipyridyl). This unprecedented preference arises from the concerted effect of the charge-transfer interaction between TCNQ and NO molecules as well as the switchable gate opening and closing of the pores in the framework.[219]

In 2015, Bloch et al. reported the strong binding of NO at 298 K in Fe_2(dobdc) featuring redox-active open metal sites.[168] Fe_2(dobdc) displays an extraordinarily steep step at the low-pressure region in the NO adsorption isotherm, with adsorption capacity high higher than 16 wt% at 298 K and 1.2 bar (corresponding to one NO molecule per open Fe site). The fact that Fe_2(dobdc) approaches its saturation capacity (corresponding to 0.95 NO molecules per Fe site) near 0.007 bar indicates the strong binding of NO molecule in the framework. Characterized by infrared, UV–Vis, and Mössbauer spectroscopies, neutron powder diffraction, and magnetic susceptibility studies, the strong binding mainly results from the electron transfer from the Fe^{II} sites to form Fe^{III} NO^- adducts. Furthermore, it was found that $Fe_2(NO)_2$(dobdc) can release bound NO steadily under humid conditions over the course of more than 10 days, suggesting its potential to be applied for NO storage and release, such as in certain biomedical applications.

MOFs have also been investigated to capture fluorocarbons and chlorofluorocarbons (CFCs). In this aspect, Chen et al. in 2015 fabricated a mesoporous fluorinated MOFs, MOFF-5, from an extensively fluorinated tritopic tetrazolate-based ligand.[220] MOFF-5 has an accessible surface area of 2445 m^2/g, which translates into remarkably high adsorption capacities of fluorocarbons and CFCs. Their weight capacities can be up to 225%. Similarly, Lin et al. in 2015 studied the adsorption of a typical fluorocarbon R22 ($CHClF_2$) in a new series of isoreticular constructed from 3,3′,5,5′ -tetramethyl-4,4′-bipyrazolate and different linear dicarboxylate ligands.[221] It was found that the pore size and/ or porosity of the MOFs can affect the R22 adsorption performance, with a highest achieved uptake of 0.73–0.97 g/g (0.62–0.65 g/cm) at 298 K and 1 bar.

In 2018, Xie et al. constructed two Zr-MOFs named BUT-66 and BUT-67 from two long and angular lignds 4,4′ -(benzene-1,3-diyl)dibenzoate (BDB^{2-}) and 4,4′ -(naphthalene-2,7-diyl)dibenzoate (NDB^{2-}), respectively.[222] BUT-66 and BUT-67 possess two-fold interpenetrated pcu network structures and feature small hydrophobic pores that are suitable to capture aromatic volatile organic compounds (VOCs) from humid air (Fig. 17). BUT-66, in particular, displayed apparently higher benzene adsorption capacity (1.75 mmol/cm^3) at high temperature and low pressure than some benchmark materials, like MCM-41, MIL-101(Cr), ZIF-8, PAF-1, and Carboxen 1000. Additionally, BUT-66 is also capable to capture trace benzene (several parts per million) in humid air (relative humidity 50%) with a high capacity of ca. 0.28 mmol/cm^3. Single-crystal analyses of BUT-66 loaded with guest molecules suggest that its high performance originates from combined result of the small hydrophobic pores, mutually less interference between hydrophobic and hydrophilic adsorption sites, and the local rotatable phenyl rings within the rigid overall framework. This work demonstrates the promise of MOFs as advanced materials for practical application in air cleaning.

Carbon monoxide (CO) is an industrially important gas, either as valuable carbon products or as catalyst poisoning impurities during important chemical production. There are various needs to enrich/removal CO from the gaseous products before any further applications. The molecular size and properties of CO make it very challenging to separate from other small gas molecules such as N_2, CO_2, H_2, and CH_4. But by virtue of some unique structural features of MOFs, relevant separations can be still realized. For example, Sato

et al. reported a soft nanoporous MOF [Cu(aip)(H_2O)] (aip = 5-azidoisophthalate) for CO/N_2 separation.[223] This MOF can undergo a global structural transformation during the binding interaction of CO with open Cu2+ sites, which collaboratively enables the implementation of selective CO capture from N_2. Similar CO sorption behavior was also observed in Fe_2Cl_2(bbta) (H_2bbta = 1*H*,5*H*-benzo(1,2-*d*:4,5-*d*′)bistriazole) by Reed et al.[224] This MOF features coordinatively unsaturated Fe(II) sites, which can undergo a cooperative spin transition during CO adsorption, resulting in stepwise CO sorption with large separation capacity and selectivity over N_2 and H_2.

There are also needs for purification of CO during emerging chemical CO_2 conversion. In this context, the removal of easily polarized CO_2 from the mixture would be much more directly realized. Chen et al. demonstrated such purification can be readily achieved by using CO_2-selective MOFs as adsorbents,225 referring to SIFSIX-3-Ni and TIFSIX-2-Cu-i, which showing remarkable CO_2 uptake capacity and CO_2/CO selectivity. Thus high-purity CO can be readily obtained as demonstrated by breakthrough experiments.

Some other gas/vapor separations

Xenon/krypton (Xe/Kr) separation is of great industrial significance, affording important noble gases for applications in lighting, electronics, and the medical industry. Current industrial Xe production relies on cryogenic distillation of a by-product Xe/Kr mixture during air liquefaction, which is high energy-intensive and capital-intensive. In recent years, MOFs-based adsorptive separation technology shows great potential in energy-effective separation of Xe/Kr. There are more than 20 MOFs that have been carefully investigated for Xe/Kr separation. Comprehensive evaluation of these candidates has been performed by Banerjee and Thallapally et al.[226] Here we aim to briefly introduce this application by presenting selected examples.

The proof-of-concept of MOFs for Xe/Kr separation was established by Mueller et al. in 2006, as demonstrated by pressure–swing adsorption process on HKUST-1 in 6/94 Xe/Kr mixture at 55 °C and 40 bar.[72] The breakthrough results shows that the Xe can be capture from the mixture to a level of 50 ppm. Great progresses have been achieved under continuous efforts on this separation since 2012.[226] For example, in 2016, Banerjee et al. identified and affirmed a calcium 4,4′–sulfonyldibenzoate MOF SBMOF-1 as one of the most selective adsorbent for Xe/Kr separation after a high-throughput computational screening of large MOF database.[227] The microporous SBMOF-1 shows a pore size of about 4.2 Å, and well accommodation for Xe atoms with diameter of about 4.0 Å as revealed by crystallographic results of Xe-loaded SBMOF-1, affording a very high adsorption affinity of ~35 kJ/mol. Hence, SBMOF-1 shows remarkable capture capacity and Xe/Kr selectivity (~16) for trace Xe removal. Breakthrough analysis demonstrated the highest capture capacity of 13.2 mmol/kg for trace Xe from waste gas simulant processing. Further incorporation with functional sites into ultramicroporous MOFs can enhance the separation performance, as demonstrated by CROFOUR-1/2-Ni reported in 2016.[228] The optimal pore size and CrO_4^{2-} moiety enable CROFOUR-1-Ni to show a highest Q_{st} of 37.4 kJ/mol at zero loading and a Xe/Kr selectivity of 22.

The inert nature of noble gases appears to limit boosting of the binding affinity of MOFs for these gases, while the Kr-selective sorbents afford another approach for efficient Xe separation from Kr. Fernandez et al. reported a flexible MOF (FMOFCu, also [Cu(hfipbb)(H_2hfipbb)$_{0.5}$]) as a rare example for inverse Kr/Xe separation.[229] This MOF is described to exhibit temperature-dependent gating effect, referring to the shrinking of pore aperture size and simultaneous decreasing flexibility at lower temperature, which would restrict the diffusion of the larger Xe atoms (4.0 Å) and thus separate Xe/Kr mixture under kinetic nonequilibrium status. Accordingly, FMOFCu shows decreasing Xe uptake upon temperature drop below 273 K, and simultaneously keep continuous increasing uptake for Kr, resulting in inverse Kr/Xe separation. This inverse sorption behavior disappears at temperature above 273 K.

Purification of the C_8 alkylaromatics *o*-xylene (OX), *m*-xylene (MX), *p*-xylene (PX), and ethylbenzene (EB) is perceived as a very crucial task. However, the separation remains very challenging owing to the similar shapes, polarities and boiling points of the molecules. At relatively high ambient temperatures, C_8 alkylaromatics are in the form of gas vapor, which makes adsorption-based separation of C_8 isomers feasible. As a type of highly porous materials, MOFs are regarded as favorable adsorbents to realize the separation of xylene isomers in gas phase. Some progress has been made in recent years, which have been well summarized.15,16 Here we aim to update this application by selected examples.

In 2018, Gonzalez et al. investigated two MOFs, Co_2(dobdc) and Co_2(*m*-dobdc), for the separation of xylene isomers.[230] Based on the single component isotherms, Co_2(dobdc) is found to have different binding affinities of these C_8 alkylaromatics molecules, which follows the order of OX > EB > MX > PX. Multicomponent vapor-phase breakthrough experiments show that Co_2(dobdc) is able to distinguish these species. Single crystal X-ray diffraction measurement reveal that separation is mainly attributed to the nuanced differences in the interactions of OX, EB, and MX with two adjacent Co^{II} sites and the inability of PX to interact with a second Co^{II} center.

Deuterium is widely used in a number of commercial and scientific applications, especially shows great potential as an important energy source. Owing to its extremely low natural abundance of 0.0156%, the industrial deuterium production is currently based on enrichment from isotope mixtures through chemical exchange method (Girdler sulfide process) and cryogenic distillation (at 24 K), which are complicate and energy-intensive. In contrast, kinetic adsorptive separation based on kinetic quantum molecular sieving mechanism in porous materials at elevated temperatures (e.g. 77 K) is proposed to be more energy-efficient, which originates from different diffusion barriers related to the difference in the zero-point energy of the adsorbed H_2/D_2 isotopes. Accordingly, adsorbents with ultramicroporous structure showing a size difference of the de Broglie wavelength with the gas diameter are more favorable.[82] The first experimental example of MOFs for quantum sieving of D_2/H_2 is demonstrated by Chen et al. in 2008 using a metalloligand MOF (M'MOF-1) that integrates narrow confined pore structure with open metal sites.[140] The pore size of M'MOF-1 is about 5.6 Å. Although gas sorption study reveals that M'MOF-1 shows slightly higher adsorption enthalpy for D_2 over H_2, the D_2 still shows a significantly faster adsorption kinetic than H_2, resulting in potential D_2/H_2 separation. This is because the

heavier D_2 shows lower diffusion activation energy than that of H_2, which originate from its shorter de Broglie wavelength in confined pore channels at cryogenic temperature. In 2013, Teufel et al. reported abnormal hydrogen sorption phenomena in an ultramicroporous MOF [$Zn_5Cl_4(BBTA)_3$] (MFU-4) featuring temperature-triggered gate opening for D_2/H_2 separation.[231] The experimental D_2/H_2 selectivity under non-equilibrium condition was firstly realized in this work by using a thermal-desorption spectroscopy apparatus. Owing to extremely confined pore aperture, this MOF shows a non-equilibrium D_2/H_2 selectivity of 7.5 at 10 mbar and 60 K upon gas mixture exposure for 15 min before achieving equilibrium.

MOFs with open metal sites for enhanced hydrogen binding affinity have also been evaluated for selective quantum sieving of D_2 from H_2. For example, Fitz-Gerald et al. demonstrated that Ni-MOF-74 shows a largest adsorption heat difference of 1.4 kJ/mol for D_2/H_2, resulting in a selectivity of 5 at low pressure and 77 K.[232] In a recent work, Weinrauch et al. revealed that Cu(I)-MFU-4l with open Cu(I) sites shows remarkable adsorption enthalpy for D_2 (35 kJ/mol) with a difference of 2.5 kJ/mol with H_2,[233] which enables this MOF to capture D_2 with an experimental selectivity of 11.1 at 100 K for 1:1 D_2/H_2 mixture.

MOF-BASED MEMBRANES FOR GAS SEPARATION

To explore a highly efficient way to separate gas mixtures, membrane separation stands out as a promising strategy. Increasing research attention has been attracted worldwide to developing novel MOF-based membranes to accomplish the challenging separation tasks in an energy-economic manner. The separation performance of membranes is evaluated by two criteria, namely, permeability and selectivity. Some reviews have summarized the fabrication of MOF-based membranes,[234,235] and the advances in their separation performance over the years.[236–240] In this section, we will highlight some significant progress made in recent years in this active research field.

In 2014, Peng et al. reported the preparation of nanosheets from a layered MOF $Zn_2(bim)_4$ (bim^- = benzimidazolate) with maintenance of its morphological and structural integrity.[241] The exfoliation technique they employed was a soft-physical process in which the pristine layered MOF was wet-ball milled and exfoliated in volatile solvent subsequently. The resulting nanosheets thus possesses large lateral areas and high crystallinities, and were utilized as the building blocks for ultrathin molecular sieving membranes. They intentionally suppressed the lamellar stacking of nanosheets by a hot-drop coating process to minimize the blockage of gas molecule passways in restacking. Since the aperture size of a single-layered $Zn_2(bim)_4$ nanosheet is around 2.1 Å whose effective pore size might be larger due to structural flexibility, the generated membrane achieved an effective separation of H_2 (2.9 Å) and CO_2 (3.3 Å) through molecular sieving (Fig. 18). By optimizing the α-Al_2O_3 disk temperature to maximize the disordered stacking between $Zn_2(bim)_4$ nanosheet for higher H_2 permeance, the molecular sieving membrane eventually achieved a high H_2 permeance (2700 GPU) and a high H_2/CO_2 selectivity (291) simultaneously, which surpasses the Robeson's upper-bound for H_2/CO_2 gas pair.

Similarly, a membrane based on pure MOF nanosheets was also realized by Wang et al. in 2017. They fabricated nm-thick molecular sieving membranes derived from porous two-dimensional MAMS-1 nanosheets.[242] These membranes possess pore openings parallel to gas concentration gradient to allow high gas permeation flux and high selectivity for H_2/CO_2 separation. Furthermore, the membrane shows a reversed thermo-switchable H_2 permeation, which originate from the molecular flexibility of the building metal-organic nanosheets.

To guarantee the mechanical stability of the membranes, most MOF-based membranes are produced in the form of mixed matrix membrane as composite materials. Typically, the matrix is a type of polymer, such as 6FDA-DAM. In 2010, Bae et al. reported introducing ZIF-90 crystals with submicrometer into 6FDA-DAM polymer to fabricate ZIF-90/6FDA-DAM membranes with high performance for CO_2/CH_4 separation.[243]

In 2014, Rodenas et al. employed a bottom-up strategy to synthesize CuBDC MOF nanosheets with lamellae of micrometer lateral dimensions. By incorporating MOF nanosheets into polymer matrices, they fabricated a mixed matrix membrane possessing excellent ability to separate CO_2 from CO_2/CH_4 gas mixtures with an unusual increase in selectivity with pressure.[244] Compared with isotropic crystals, the superior occupation of the membrane cross-section by the MOF nanosheets endows the membrane with better molecular discriminating ability and eliminates unselective permeation pathways.

In 2016, Bachman et al. prepared some composite materials by dispersing Co_2(dobdc) and Ni_2(dobdc) MOF nanocrystals within 6FDA-DAM polyimide. These membranes display enhanced C_2H_4/C_2H_6 selectivity and greater C_2H_4 permeability and improved membrane stability than pure polymer membrane. Additionally, the framework-polymer interactions were found to reduce the chain mobility of the polymer and boost the separation performance of the membrane as well.[245]

In 2018, Liu et al. reported incorporation of submicrometersized RE-fcu-MOF crystals into 6FDA-DAM polymer matrix to generate hybrid membrane materials.[246] The hybrid membrane showed significantly enhanced performance in removing CO_2 and H_2S from CH_4 and separating butane isomers (nC_4 and iC_4). The property originates from precise control of the linker from 1,4-naphthalenedicarboxylate (naph) to fumarate (fum) to give rise to contracted MOF pore apertures and delimit the size of the triangular window (Fig. 19). As the sole entrance to the fcu-MOF pore, these triangular windows discriminate gas molecules and achieve separation purposes. This rational-design hybrid approach offers a toolbox for improving the transport properties of membranes containing hybridized MOF fillers with optimal apertures as molecular sieves. Notably, the Y-fum-fcu-MOF/6FDA-DAM membrane was also reported to exhibit good CO_2/CH_4 separation performance.[247]

In 2018, Liu et al. fabricated a new fluorinated MOF-based mixed-matrix membrane by incorporating the NbOFFIVE-1-Ni and AlFFIVE-1-Ni MOF crystals into 6FDA-DAM polymer.[248] The molecular transport in the channels was finely tuned through the MOF apertures, with the resulting fluorinated MOF-based membranes displaying excellent molecular sieving properties for the simultaneous removal of H_2S and CO_2 from CH_4.

While membranes in a dense film geometry achieve the gas separation purpose with good selectivity, fabricating the mixed matrix membranes into a hollow fiber geometry can further boost the performance of these materials. In 2012, Zhang et al. achieved significantly enhanced C_3H_6/C_3H_8 selectivity in mixed matrix membranes ZIF-8/6FDA-DAM.[249] In 2014, they further improved the C_3H_6/C_3H_8 separation performance by upgrading the material from the dense film geometry to the scalable hollow fiber geometry.[250] It is worth noting that this is the first example of the successful formation of high-loading mixed matrix hollow fiber membranes with significantly enhanced selectivity for C_3H_6/C_3H_8 separation.

In 2014, Brown et al. reported an approach named interfacial microfluidic membrane processing to fabricate MOF membranes in polymeric hollow fibers.[251] This method features the in situ synthesis of ZIF-8 film in the membrane module. In addition, the interface between two solvents was taken good advantage of to realize positional control over membrane formation. This scalable approach thus afford continuous molecular sieving ZIF-8 membranes in single and multiple poly(amide-imide) hollow fibers have good H_2/C_3H_8 and C_3H_6/C_3H_8 separation performance, with separation factors of 370 and 12, respectively.

In 2017, Kong et al. reported the fabrication of MOF/organosilica hybrid membrane on tubular ceramic substrates.[252] This is the first time that organosilica was utilized as the matrix to construct MOF/organosilica membrane. Because of its unique nature, organosilica networks enabled the preparation of ultrathin hybrid membrane, and optimized gas permeance and selectivity as well. MOF particles and organosilica match well with each other for their organic-inorganic hybrid feature. The generated thin and compact MOF/organosilica nanolayers displayed the collaborative advantages inherited from the two component such as high affinity towards ceramic substrate, tunable porous structure, and specific functional sites for the recognition and selective separation of gas molecules. It is worth noting that the as-prepared ZIF-8 and MIL-53-NH_2 incorporated organosilica nanocomposite membrane exhibited excellent H_2/CH_4 (H_2/CH_4 selectivity = 26.5; H_2 permeance = 1.06×10^{-6} mol m^{-2} s^{-1} Pa^{-1}) and CO_2/CH_4 (CO_2/CH_4 selectivity = 18.2; CO_2 = permeance 1.44×10^{-7} mol m^{-2} s^{-1} Pa^{-1}) separations, respectively, which are among the best-performing MOF-based membranes. This work provides a new synthetic strategy to develop MOF-based membranes for desired separation performance.

■ CHALLENGES AND PERSPECTIVES

The development of MOFs to satisfy the demands of gas storage and separation has captured the imagination of scientists and engineers, with significant progresses being made in this field. Compared with traditional porous adsorbents, referring to zeolites and activated carbons, MOFs are indeed promising for high-density fuel gas storage owing to their unique structural features including exceptional porosity and high modularity. The record uptake capacities of MOFs for H_2, CH_4, and C_2H_2 are far superior to those of traditional porous adsorbents. Although optimizing porosity, immobilizing functional sites and even gate-opening effect have been demonstrated to be feasible for increasing the total and working capacity of MOFs, there seem to be a ceiling for these capacity to further increase, and still no MOF material can meet the US Department of Energy ambitious targets set

to guide relevant applications. In this regard, unless disruptive mechanisms emerge, the feasible approach seem to be storing gas under slightly harsher operating conditions, either under higher pressures or at higher temperatures. It should be noted that it remains much to be addressed before MOF-gas onboard systems to be commercially affordable. To name a few, thermal management during gas charging and discharging should be taken into accounts considering corresponding exothermic and endothermic phenomenon; packing efficiency of bulk MOF adsorbents should be improved for compact concern. Therefore, an ideal adsorbent for gas storage would be those with both high gravimetric and volumetric storage capacities under mild conditions. If approved, great global benefits can be expected, considering the high energy density of these clean fuel gases.

In terms of gas separation, the emergence of energy-efficient adsorptive systems represented by MOFs has revolutionized this field. The unique pore features of MOFs render them as an ideal platform for exploring novel adsorbent materials. A rapid development of MOFs for gas separation has been witnessed in the last decade, especially during the last three years. The implementation of some important technologies such as gas chromatography, fixed-bed breakthrough experiments and crystallographic determination of gas adsorption sites has facilitated the development of this field. By virtue of precious control over the pore chemistry and size, significant progresses including molecular sieving for some important, challenging and highly energy-intensive gas separations have been achieved, referring to CO_2 capture, C_2H_2/C_2H_4, C_2H_4/C_2H_6, C_3H_4/C_3H_6, C_3H_6/C_3H_8, and C4 or C6 alkene or alkane isomers. In regards of high separation efficiency, MOFs simultaneously showing large uptake capacity and high selectivity hold the greatest promise. Therefore, the combination of functional binding sites and optimal pore size in single MOF, so called dual functionality, not only maximize interactions with goal gas molecules but also exclude other competing ones, which represents an exciting research directions. With continuous development in the field, the current focus of fundamental aspects is gradually shifting to practical considerations. In this context, there are still many challenges need to be overcome prior to further industrial application, including water resistance, purity tolerance, long-term durability, regeneration, adsorption kinetics, mechanical properties, large-scale deployment, processability and defect in membrane fabrication and so on. Under real conditions, the actual mixed gas streams can be humid under high pressure and/or high temperature, with various contaminants. Obviously, in this case, MOFs should be structurally stable while their separation performance keeps steady as expected. In fact, there are already many stable MOFs showing remarkable chemical stability. Another prerequisite is scale up MOFs production for large-scale deployment, in a low-cost way. Using simple precipitation reaction in water solution under ambient conditions or solvent-free reactions, certain MOFs have already been easily synthesized in large scale. For thin films and membranes fabrication, the key for practical application lies in addressing poor processability, membrane defects, low permeability and scaling up membranes to industrially large.

Overall, the spectrum of storage and separations technologies with energy efficient prospects has been significantly broadened. MOFs are taking their steps from laboratories to factories and from academia to industrial applications. Worldwide efforts from certain commercial companies have been dedicated to promote MOF adsorbents towards industrial applications.

It is expected that the close collaborations among scientists, engineers and industrial partners on this field will generate great energy benefits.

ACKNOWLEDGEMENTS

We gratefully acknowledge the financial support from National Natural Science Foundation of China (21673039, 21573042, 21606163, 21878205), Fujian Science and Technology Department (2018J07001), and the Welch Foundation (AX-1730).

AUTHOR BIOGRAPHIES

■

Hao Li was born in Wuhan, China. She received her Ph.D. (2017) from Texas A&M University under the supervision of Prof. Hong-Cai Zhou. She joined Prof. Banglin Chen's group as a joint postdoctoral researcher under the guidance of Prof. Shengchang Xiang from Fujian Normal University and Prof. Banglin Chen from the University of Texas at San Antonio in 2017. Her current research interest lies in metal-organic frameworks for light hydrocarbon separations.

Libo Li was born in Henan, China. He received his Ph.D. in 2015 from the Taiyuan University of Technology under the supervision of Prof. Jinping Li. After obtaining his Ph.D. degree, he worked at Prof. Banglin Chen's group at the University of Texas at San Antonio as a postdoctoral fellow from 2016 to 2018. His current research interest focuses on the metal-organic frameworks for gas adsorption and separation.

Rui-Biao Lin obtained his B.Sc. in Chemistry from Sun Yat-Sen University (SYSU) in 2009. After studying the synthesis and crystal engineering of functional coordination polymers under the supervision of professors Xiao-Ming Chen and Jie-Peng Zhang, he obtained his Ph.D. in 2014 (SYSU). He is currently in the lab of Prof. Banglin Chen at

the University of Texas at San Antonio as a post-doctoral fellow, where he is working on multifunctional porous materials.

Wei Zhou received his Ph.D. in 2005 from the University of Pennsylvania, under the supervision of Prof. John E. Fischer. From 2005 to 2007, he was a postdoctoral researcher at the NIST Center for Neutron Research (NCNR), working with Dr. Taner Yildirim. After that, he was appointed to his current position as a research scientist at NCNR. His research interests are in the areas of novel porous materials, computational materials design, and neutron diffraction/spectroscopy.

Shengchang Xiang received his Ph.D. degree in physical chemistry in 2003 from Fuzhou University. He joined Prof. XinTao Wu's Group at Fujian Institute of Research on the Structure of Matter, Chinese Academy of Sciences, as a postdoctoral Fellow and then associate professor (2003– 2007). He then worked with Prof. Banglin Chen at the University of Texas at San Antonio as a postdoctoral fellow (2007– 2012). He moved back to China in January 2012, and now he is the Professor of Chemistry at Fujian Normal University. His work is focused on multifunctional porous materials.

Banglin Chen was born in Zhejiang, China. He received B.S. (1985) and M.S. (1988) degrees in Chemistry from Zhejiang University in China, and his Ph.D. from National University of Singapore in 2000. He worked with professors Omar M. Yaghi at University of Michigan, Stephen Lee at Cornell University, and Andrew W. Maverick at Louisiana State University as a postdoctoral fellow during 2000–2003 before joining the University of Texas-Pan American in 2003. He moved to the University of Texas at San Antonio in August 2009, where he is a Dean's Distinguished Chair Professor of Chemistry.

REFERENCES

1. International Energy Outlook 2018 (US Energy Information Administration, 2018).

2. Chu S, Cui Y, Liu N. The path towards sustainable energy. Nat. Mater. 16, 16 (2016). [PubMed: 27994253]
3. https://www.eia.gov/energyexplained/?page=us_energy_home.
4. Suh MP, Park HJ, Prasad TK, Lim D-W. Hydrogen storage in metal–organic frameworks. Chem. Rev. 112, 782–835 (2012). [PubMed: 22191516]
5. Sholl DS, Lively RP. Seven chemical separations to change the world. Nature 532, 435–437 (2016). [PubMed: 27121824]
6. Worrell E, Phylipsen D, Einstein D, Martin N. Energy use and energy intensity of the U.S. chemical industry. LBNL-44314; Energy Analysis Department, Environmental Energy Technologies Division, 94720, Berkeley, California: Ernest Orlando Lawrence Berkeley National Laboratory. LBNL-44314.
7. Kitagawa S. Porous materials and the age of gas. Angew. Chem. Int. Ed. 54, 10686–10687 (2015).
8. Li B, Wen H-M, Cui Y, Zhou W, Qian G, Chen B. Emerging multifunctional metal–organic framework materials. Adv. Mater. 28, 8819–8860 (2016). [PubMed: 27454668]
9. Furukawa H, Cordova KE, O'Keeffe M, Yaghi OM. The chemistry and applications of metal-organic frameworks. Science 341, 1230444 (2013).
10. Ding S-Y, Wang W Covalent organic frameworks (COFs): from design to applications. Chem. Soc. Rev. 42, 548–568 (2013). [PubMed: 23060270]
11. Feng X, Ding X, Jiang D Covalent organic frameworks. Chem. Soc. Rev. 41, 6010–6022 (2012). [PubMed: 22821129]
12. Jiang J, Zhao Y, Yaghi OM. Covalent chemistry beyond molecules.. J. Am. Chem. Soc. 138, 3255–3265 (2016). [PubMed: 26863450]
13. Diercks CS, Yaghi OM. The atom, the molecule, and the covalent organic framework. Science 355 (2017).
14. Lin R-B, He Y, Li P, Wang H, Zhou W, Chen B. Multifunctional porous hydrogen-bonded organic framework materials. Chem. Soc. Rev. 48, 1362–1389 (2019). [PubMed: 30676603]
15. Bao Z, Chang G, Xing H, Krishna R, Ren Q, Chen B. Potential of microporous metal-organic frameworks for separation of hydrocarbon mixtures. Energy Environ. Sci. 9, 3612–3641 (2016).
16. Adil K, Belmabkhout Y, Pillai RS, Cadiau A, Bhatt PM, Assen AH, Maurin G, Eddaoudi M Gas/vapour separation using ultra-microporous metal–organic frameworks: insights into the structure/separation relationship. Chem. Soc. Rev. 46, 3402–3430 (2017). [PubMed: 28555216]
17. Wu H, Gong Q, Olson DH, Li J. Commensurate adsorption of hydrocarbons and alcohols in microporous metal organic frameworks. Chem. Rev. 112, 836–868 (2012). [PubMed: 22257090]
18. Yang S, Ramirez-Cuesta AJ, Newby R, Garcia-Sakai V, Manuel P, Callear SK, Campbell SI, Tang CC, Schröder M. Supramolecular binding and separation of hydrocarbons within a functionalized porous metal–organic framework. Nat. Chem. 7, 121 (2014). [PubMed: 25615665]
19. Bachma JE, Kapelewsk MT, Ree DA, Gonzale MI, Lon JRM(m-dobdc) (M Mn, Fe, Co, Ni) Metal–organic frameworks as highly selective, high-capacity adsorbents for olefin/paraffin separations. J. Am. Chem. Soc. 139, 15363–153l70 (2017). [PubMed: 28981259]
20. Cui Y, Yue Y, Qian G, Chen B. Luminescent functional metal–organic frameworks.. Chem. Rev. 112, 1126–1162 (2012). [PubMed: 21688849]
21. Sun C-Y, Wang X-L, Zhang X, Qin C, Li P, Su Z-M, Zhu D-X, Shan G-G, Shao K-Z, Wu H, et al. Efficient and tunable white-light emission of metal–organic frameworks by iridium-complex encapsulation. Nat. Commun. 4, 2717 (2013). [PubMed: 24212250]
22. Talin AA, Centrone A, Ford AC, Foster ME, Stavila V, Haney P, Kinney RA, Szalai V, El Gabaly F, Yoon HP, et al. Tunable electrical conductivity in metal-organic framework thin-film devices. Science 343, 66 (2014). [PubMed: 24310609]
23. Kreno LE, Leong K, Farha OK, Allendorf M, Van Duyne RP, Hupp JT. Metal–organic framework materials as chemical sensors. Chem. Rev. 112, 1105–1125 (2012). [PubMed: 22070233]
24. Hu Z, Deibert BJ, Li J. Luminescent metal–organic frameworks for chemical sensing and explosive detection. Chem. Soc. Rev. 43, 5815–5840 (2014). [PubMed: 24577142]

25. Campbell MG, Sheberla D, Liu SF, Swager TM, Dincă M. Cu(hexaiminotriphenylene)2: an electrically conductive 2D metal–organic framework for chemiresistive sensing. Angew. Chem. Int. Ed. 54, 4349–4352 (2015).
26. Lin R-B, Liu S-Y, Ye J-W, Li X-Y, Zhang J-P. Photoluminescent metal-organic frameworks for gas sensing. Adv. Sci. 3 (2016) 1500434–1500434.
27. Xu R, Wang Y, Duan X, Lu K, Micheroni D, Hu A, Lin W. Nanoscale metal–organic frameworks for ratiometric oxygen sensing in live cells. J. Am. Chem. Soc. 138, 2158–2161 (2016). [PubMed: 26864385]
28. Yang Q, Xu Q, Jiang H-L. Metal–organic frameworks meet metal nanoparticles: synergistic effect for enhanced catalysis. Chem. Soc. Rev. 46, 4774–4808 (2017). [PubMed: 28621344]
29. Zhao C, Dai X, Yao T, Chen W, Wang X, Wang J, Yang J, Wei S, Wu Y, Li Y. Ionic exchange of metal–organic frameworks to access single nickel sites for efficient electroreduction of CO2. J. Am. Chem. Soc. 139, 8078–8081 (2017). [PubMed: 28595012]
30. Lin R-G, Lin R-B, Chen B. A microporous metal–organic framework for selective C2H2 and CO2 separation. J. Solid State Chem. 252, 138–141 (2017).
31. Zhao M, Yuan K, Wang Y, Li G, Guo J, Gu L, Hu W, Zhao H, Tang Z. Metal–organic frameworks as selectivity regulators for hydrogenation reactions. Nature 539, 76 (2016). [PubMed: 27706142]
32. Xu H-Q, Hu J, Wang D, Li Z, Zhang Q, Luo Y, Yu S-H, Jiang H-L. Visible-light photoreduction of CO2 in a metal–organic framework: boosting electron–hole separation via electron trap states. J. Am. Chem. Soc. 137, 13440–13443 (2015). [PubMed: 26434687]
33. Li B, Leng K, Zhang Y, Dynes JJ, Wang J, Hu Y, Ma D, Shi Z, Zhu L, Zhang D, et al. Metal–organic framework based upon the synergy of a brønsted acid framework and lewis acid centers as a highly efficient heterogeneous catalyst for fixed-bed reactions. J. Am. Chem. Soc. 137, 4243–4248 (2015). [PubMed: 25773275]
34. Hod I, Deria P, Bury W, Mondloch JE, Kung C-W, So M, Sampson MD, Peters AW, Kubiak CP, Farha OK, et al. A porous proton-relaying metal-organic framework material that accelerates electrochemical hydrogen evolution. Nat. Commun. 6, 8304 (2015). [PubMed: 26365764]
35. Zhu Q-L, Li J, Xu Q. Immobilizing metal nanoparticles to metal–organic frameworks with size and location control for optimizing catalytic performance. J. Am. Chem. Soc. 135, 10210–10213 (2013). [PubMed: 23805877]
36. Feng D, Gu Z-Y, Li J-R, Jiang H-L, Wei Z, Zhou H-C. Zirconium-metalloporphyrin PCN-222: mesoporous metal–organic frameworks with ultrahigh stability as biomimetic catalysts. Angew. Chem. Int. Ed. 51, 10307–10310 (2012).
37. Zou R-Q, Sakurai H, Xu Q Preparation, adsorption properties, and catalytic activity of 3D porous metal–organic frameworks composed of cubic building blocks and alkali-metal ions. Angew. Chem. Int. Ed. 45, 2542–2546 (2006).
38. Zhu J, Usov PM, Xu W, Celis-Salazar PJ, Lin S, Kessinger MC, Landaverde-Alvarado C, Cai M, May AM, Slebodnick C, et al. A New class of metal-cyclam-based zirconium metal–organic frameworks for CO2 adsorption and chemical fixation. J. Am. Chem. Soc. 140, 993–1003 (2018). [PubMed: 29268601]
39. Lu K, Aung T, Guo N, Weichselbaum R, Lin W. Nanoscale metal–organic frameworks for therapeutic, imaging, and sensing applications. Adv. Mater. 30, 1707634 (2018).
40. Simon-Yarza T, Mielcarek A, Couvreur P, Serre C. Nanoparticles of metal-organic frameworks: on the road to in vivo efficacy in biomedicine. Adv. Mater. 30, 1707365 (2018).
41. Xia W, Mahmood A, Zou R, Xu Q. Metal–organic frameworks and their derived nanostructures for electrochemical energy storage and conversion. Energy Environ. Sci. 8, 1837–1866 (2015).
42. Zhu Q-L, Xu Q Metal–organic framework composites. Chem. Soc. Rev. 43, 5468–5512 (2014). [PubMed: 24638055]
43. Li S-L, Xu Q. Metal–organic frameworks as platforms for clean energy. Energy Environ. Sci. 6, 1656–1683 (2013).
44. Horike S, Umeyama D, Kitagawa S. Ion conductivity and transport by porous coordination polymers and metal–organic frameworks. Acc. Chem. Res. 46, 2376–2384 (2013). [PubMed: 23730917]

45. Che B, Xian S, Qia G. Metal organic frameworks with functional pores for recognition of small molecules. Acc. Chem. Res. 43, 1115–1124 (2010). [PubMed: 20450174]
46. Cui Y, Li B, He H, Zhou W, Chen B, Qian G. Metal–organic frameworks as platforms for functional materials. Acc. Chem. Res. 49, 483–493 (2016). [PubMed: 26878085]
47. Farha OK, Eryazici I, Jeong NC, Hauser BG, Wilmer CE, Sarjeant AA, Snurr RQ, Nguyen ST, Yazaydın AÖ, Hupp JT. Metal–organic framework materials with ultrahigh surface areas: is the sky the limit? J. Am. Chem. Soc. 134, 15016–15021 (2012). [PubMed: 22906112]
48. Furukawa H, Ko N, Go YB, Aratani N, Choi SB, Choi E, Yazaydin AÖ, Snurr RQ, O'Keeffe M, Kim J, et al. Ultrahigh porosity in metal-organic frameworks. Science 329, 424–428 (2010). [PubMed: 20595583]
49. Kondo ,M, Yoshitomi T, Matsuzaka H, Kitagawa S, Seki K. Three-dimensional framework with channeling cavities for small molecules: {[M2(4, 4′ -bpy)3(NO3)4] xH2O}n (M Co, Ni, Zn). Angew. Chem. Int. Ed. 36, 1725–1727 (1997). The first work demonstrating the porosity of MOF-type materials and relevant application on high-pressure methane storage.
50. Li H, Eddaoudi M, Groy TL, Yaghi OM. Establishing microporosity in open metal organic frameworks: gas sorption isotherms for Zn(BDC) (BDC 1,4-Benzenedicarboxylate). J. Am. Chem. Soc. 120, 8571–8572 (1998).
51. Rosi NL, Eckert J, Eddaoudi M, Vodak DT, Kim J, O'Keeffe M, Yaghi OM. Hydrogen storage in microporous metal-organic frameworks. Science 300, 1127–1129 (2003). [PubMed: 12750515] The first work reporting MOFs for high-pressure hydrogen storage, with uptake capacity correction in reference 84 (in 2007).
52. Matsuda R, Kitaura R, Kitagawa S, Kubota Y, Belosludov RV, Kobayashi TC, Sakamoto H, Chiba T, Takata M, Kawazoe Y, et al. Highly controlled acetylene accommodation in a metal–organic microporous material. Nature 436, 238 (2005). [PubMed: 16015325] The first work reporting MOFs for acetylene storage and selective acetylene adsorption over carbon dioxide.
53. Li B, Wen H-M, Zhou W, Xu, Jeff Q, Chen B. Porous metal-organic frameworks: promising materials for methane storage. Chem 1, 557–580 (2016).
54. He Y, Zhou W, Qian G, Chen B. Methane storage in metal–organic frameworks. Chem. Soc. Rev. 43, 5657–5678 (2014). [PubMed: 24658531]
55. He YB, Chen FL, Li B, Qian GD, Zhou W, Chen BL. Porous metal-organic frameworks for fuel storage. Coord. Chem. Rev. 373, 167–198 (2018).
56. Zhang Z, Xiang S, Chen B. Microporous metal-organic frameworks for acetylene storage and separation. CrystEngComm 13, 5983–5992 (2011).
57. Eddaoudi M, Kim J, Rosi N, Vodak D, Wachter J, O'Keeffe M, Yaghi OM. Systematic design of pore size and functionality in isoreticular MOFs and their application in methane storage. Science 295, 469–472 (2002). [PubMed: 11799235]
58. Delgado-Friedrichs O, Foster MD, O'Keeffe M, Proserpio DM, Treacy MMJ, Yaghi OM. What do we know about three-periodic nets? J. Solid State Chem. 178, 2533–2554 (2005).
59. Chen B, Eddaoudi M, Hyde ST, Keeffe M, Yaghi OM. Interwoven metal-organic framework on a periodic minimal surface with extra-large pores. Science 291, 1021–1023 (2001). [PubMed: 11161211]
60. Che B, M S, Hurtad EJ, Lobkovsk EB, Zho H-C. A triply interpenetrated microporous metal organic framework for selective sorption of gas molecules. Inorg. Chem. 46, 8490–8492 (2007). [PubMed: 17854181]
61. Chen B, Ji Y, Xue M, Fronczek FR, Hurtado EJ, Mondal JU, Liang C, Dai S. Metal organic framework with rationally tuned micropores for selective adsorption of water over methanol. Inorg. Chem. 47, 5543–5545 (2008). [PubMed: 18512902]
62. Xue M, Ma S, Jin Z, Schaffino RM, Zhu G-S, Lobkovsky EB, Qiu S-L, Chen B. Robust metal organic framework enforced by triple-framework interpenetration exhibiting high H2 storage density. Inorg. Chem. 47, 6825–6828 (2008). [PubMed: 18582032]
63. Zhai Q-G, Bu X, Zhao X, Li D-S, Feng P. Pore space partition in metal–organic frameworks. Acc. Chem. Res. 50, 407–417 (2017). [PubMed: 28106984]

64. Chen B, Eddaoudi M, Reineke ,TM, Kampf JW, O'Keeffe ,M, Yaghi OM. Cu(ATC) 6H2O: design of open metal sites in porous metal organic crystals (ATC: 1,3,5,7-adamantane tetracarboxylate). J. Am. Chem. Soc. 122, 11559–11560 (2000).

65. Chen B, Ockwig NW, Millward AR, Contreras DS, Yaghi OM. High H2 adsorption in a microporous metal–organic framework with open metal sites. Angew. Chem. Int. Ed. 44, 4745–4749 (2005).

66. Dincă M, Dailly A, Liu Y, Brown CM, Neumann DA, Long JR. Hydrogen storage in a microporous metal organic framework with exposed Mn2+ coordination sites. J. Am. Chem. Soc. 128, 16876–16883 (2006). [PubMed: 17177438]

67. Wang Z, Cohen SM. Postsynthetic covalent modification of a neutral metal organic framework. J. Am. Chem. Soc. 129, 12368–12369 (2007). [PubMed: 17880219]

68. Cohen SM. Postsynthetic methods for the functionalization of metal–organic frameworks. Chem. Rev. 112, 970–1000 (2012). [PubMed: 21916418]

69. Brozek CK, Dincă, M. Cation exchange at the secondary building units of metal-organic frameworks. Chem. Soc. Rev. 43, 5456–5467 (2014). [PubMed: 24831234]

70. We Y-S, Zhan M, Lia P-Q, Li R-B, L T-Y, Sha G, Zhan J-P, Che X-M. Coordination templated [2 2 2] cyclotrimerization in a porous coordination framework.. Nat. Commun. 6, 8348 (2015). [PubMed: 26384254]

71. Chen B, Liang C, Yang J, Contreras DS, Clancy YL, Lobkovsky EB, Yaghi OM, Dai S. A microporous metal–organic framework for gas-chromatographic separation of alkanes. Angew. Chem. Int. Ed. 45, 1390–1393 (2006). The first work reporting neat gas separation in MOFs by using gas chromatography to separate mixtures.

72. Mueller U, Schubert M, Teich F, Puetter H, Schierle-Arndt K, Pastré J. Metal–organic frameworks —prospective industrial applications. J. Mater. Chem. 16, 626–636 (2006).

73. Bárci PS, Zapat F, Silv JAC, Rodrigue AE, Che B. Kinetic separation of hexane isomers by fixed-bed adsorption with a microporous metal organic framework. J. Phys. Chem. B 111, 6101–6103 (2007).

74. Hayashi H, Côté AP, Furukawa H, O'Keeffe M, Yaghi O. M Zeolite A imidazolate frameworks. Nat. Mater. 6, 501 (2007). [PubMed: 17529969]

75. Banerjee R, Phan A, Wang B, Knobler C, Furukawa H, O'Keeffe M, Yaghi OM. High-throughput synthesis of zeolitic imidazolate frameworks and application to CO2 capture. Science 319, 939 (2008). [PubMed: 18276887]

76. Rowsell JLC, Spencer EC, Eckert J, Howard JAK, Yaghi OM. Gas adsorption sites in a large-pore metal-organic framework. Science 309, 1350–1354 (2005). [PubMed: 16123294]

77. Vaidhyanathan R, Iremonger SS, Shimizu GKH, Boyd PG, Alavi S, Woo TK. Direct observation and quantification of CO2 binding within an amine-functionalized nanoporous solid. Science 330, 650 (2010). [PubMed: 21030651]

78. Li J-R, Sculley J, Zhou H-C. Metal–organic frameworks for separations. Chem. Rev. 112, 869–932 (2012). [PubMed: 21978134]

79. Sumida K, Rogow DL, Mason JA, McDonald TM, Bloch ED, Herm ZR, Bae T-H, Long JR. Carbon dioxide capture in metal–organic frameworks. Chem. Rev. 112, 724–781 (2012). [PubMed: 22204561]

80. Li B, Wen HM, Yu Y, Cui Y, Zhou W, Chen B, Qian G. Nanospace within metal–organic frameworks for gas storage and separation. Mater. Today Nano 2, 21–49 (2018).

81. Zhao X, Wang Y, Li D-S, Bu X, Feng P. Metal–organic frameworks for separation. Adv. Mater. 30, 1705189 (2018).

82. Lin R-B, Xiang S, Xing H, Zhou W, Chen B. Exploration of porous metal–organic frameworks for gas separation and purification. Coord. Chem. Rev. 378, 87–103 (2019).

83. Getman RB, Bae Y-S, Wilmer CE, Snurr RQ. Review and analysis of molecular simulations of methane, hydrogen, and acetylene storage in metal–organic frameworks. Chem. Rev. 112, 703–723 (2012). [PubMed: 22188435]

84. Kaye SS, Dailly A, Yaghi OM, Long JR. Impact of preparation and handling on the hydrogen storage properties of Zn4O(1,4-benzenedicarboxylate)3 (MOF-5). J. Am. Chem. Soc. 129, 14176–14177 (2007). [PubMed: 17967030]

85. Allendorf MD, Hulvey Z, Gennett T, Ahmed A, Autrey T, Camp J, Seon Cho E, Furukawa H, Haranczyk M, Head-Gordon M, et al. An assessment of strategies for the development of solid-state adsorbents for vehicular hydrogen storage. Energy Environ. Sci. 11, 2784–2812 (2018).
86. Gómez-Gualdrón DA, Colón YJ, Zhang X, Wang TC, Chen Y-S, Hupp JT, Yildirim T, Farha OK, Zhang J, Snurr RQ. Evaluating topologically diverse metal–organic frameworks for cryo-adsorbed hydrogen storage. Energy Environ. Sci. 9, 3279–3289 (2016).
87. Yan Y, Yang S, Blake AJ, Schröder M. Studies on Metal–organic frameworks of Cu(II) with isophthalate linkers for hydrogen storage. Acc. Chem. Res. 47, 296–307 (2014). [PubMed: 24168725]
88. Dincă M, Long JR. Hydrogen storage in microporous metal–organic frameworks with exposed metal sites. Angew. Chem. Int. Ed. 47, 6766–6779 (2008).
89. Xiao B, Wheatley PS, Zhao XB, Fletcher AJ, Fox S, Rossi AG, Megson IL, Bordiga S, Regli L, Thomas KM, et al. High-capacity hydrogen and nitric oxide adsorption and storage in a metal-organic framework. J. Am. Chem. Soc. 129, 1203–1209 (2007). [PubMed: 17263402]
90. Murray LJ, Dinca M, Long JR. Hydrogen storage in metal-organic frameworks. Chem. Soc. Rev. 38, 1294–1314 (2009). [PubMed: 19384439]
91. Yan Y, Lin X, Yang S, Blake AJ, Dailly A, Champness NR, Hubberstey P, Schröder M. Exceptionally high H2 storage by a metal–organic polyhedral framework. Chem. Commun, 1025–1027 (2009).
92. Farha OK, Wilmer CE, Eryazici I, Hauser BG, Parilla PA, O'Neill K, Sarjeant AA, Nguyen ST, Snurr RQ, Hupp JT. Designing higher surface area metal–organic frameworks: are triple bonds better than phenyls? J. Am. Chem. Soc. 134, 9860–9863 (2012). [PubMed: 22670563]
93. Farha OK, Özgür Yazaydın A, Eryazici I, Malliakas CD, Hauser BG, Kanatzidis MG, Nguyen ST, Snurr RQ, Hupp JT. De novo synthesis of a metal–organic framework material featuring ultrahigh surface area and gas storage capacities. Nat. Chem. 2, 944 (2010). [PubMed: 20966950]
94. Yuan D, Zhao D, Sun D, Zhou H-C. An isoreticular series of metal–organic frameworks with dendritic hexacarboxylate ligands and exceptionally high gas-uptake capacity. Angew. Chem. Int. Ed. 49, 5357–5361 (2010).
95. Ahmed A, Liu Y, Purewal J, Tran LD, Wong-Foy AG, Veenstra M, Matzger AJ, Siegel DJ. Balancing gravimetric and volumetric hydrogen density in MOFs. Energy Environ. Sci. 10, 2459–2471 (2017).
96. Kapelewski MT, Runčevski T, Tarver JD, Jiang HZH, Hurst KE, Parilla PA, Ayala A, Gennett T, FitzGerald SA, Brown CM, et al. Record high hydrogen storage capacity in the metal–organic framework Ni2(m-dobdc) at near-ambient temperatures. Chem. Mater. 30, 8179–8189 (2018).
97. Park HJ, Suh MP. Mixed-ligand metal–organic frameworks with large pores: gas sorption properties and single-crystal-to-single-crystal transformation on guest exchange. Chem.–Eur. J. 14, 8812–8821 (2008). [PubMed: 18792044]
98. Sumida K, Brown CM, Herm ZR, Chavan S, Bordiga S, Long JR. Hydrogen storage properties and neutron scattering studies of Mg2(dobdc)—a metal–organic framework with open Mg2+ adsorption sites. Chem. Commun. 47, 1157–1159 (2011).
99. Zhao D, Yuan D, Yakovenko A, Zhou H-C. A NbO-type metal–organic framework derived from a polyyne-coupled di-isophthalate linker formed in situ. Chem. Commun. 46, 4196–4198 (2010).
100. Yan Y, Blake AJ, Lewis W, Barnett SA, Dailly A, Champness NR, Schröder M. Modifying cage structures in metal–organic polyhedral frameworks for H2 storage. Chem.–Eur. J. 17, 11162–11170 (2011). [PubMed: 21898615]
101. Bhatia SK, Myers AL. Optimum conditions for adsorptive storage. Langmuir 22, 1688–1700 (2006). [PubMed: 16460092]
102. Peng Y, Krungleviciute V, Eryazici I, Hupp JT, Farha OK, Yildirim T. Methane storage in metal–organic frameworks: current records, surprise findings, and challenges. J. Am. Chem. Soc. 135, 11887–11894 (2013). [PubMed: 23841800]
103. Li B, Wen H-M, Wang H, Wu H, Tyagi M, Yildirim T, Zhou W, Chen B. A porous metal–organic framework with dynamic pyrimidine groups exhibiting record high methane storage working capacity. J. Am. Chem. Soc. 136, 6207–6210 (2014). [PubMed: 24730649]

104. Mason JA, Oktawiec J, Taylor MK, Hudson MR, Rodriguez J, Bachman JE, Gonzalez MI, Cervellino A, Guagliardi A, Brown CM, et al. Methane storage in flexible metal–organic frameworks with intrinsic thermal management. Nature 527, 357 (2015). [PubMed: 26503057]

105. Alezi D, Belmabkhout Y, Suyetin M, Bhatt PM, Weseliński ŁJ, Solovyeva V, Adil K, Spanopoulos, Trikalitis PN, Emwas A-H, et al. MOF crystal chemistry paving the way to gas storage needs: aluminum-based soc-MOF for CH4, O2, and CO2 storage. J. Am. Chem. Soc. 137, 13308–13318 (2015). [PubMed: 26364990]

106. Wen H-M, Li B, Li L, Lin R-B, Zhou W, Qian G, Chen B. A metal–organic framework with optimized porosity and functional sites for high gravimetric and volumetric methane storage working capacities. Adv. Mater. 30, 1704792 (2018).

107. Zhang M, Zhou W, Pham T, Forrest KA, Liu W, He Y, Wu H, Yildirim T, Chen B, Space B, et al. Fine tuning of MOF-505 analogues to reduce low-pressure methane uptake and enhance methane working capacity. Angew. Chem. Int. Ed. 56, 11426–11430 (2017).

108. Jiang J, Furukawa H, Zhang Y-B, Yaghi OM. High methane storage working capacity in metal–organic frameworks with acrylate links. J. Am. Chem. Soc. 138, 10244–10251 (2016). [PubMed: 27442620]

109. Lin J-M, He C-T, Liu Y, Liao P-Q, Zhou D-D, Zhang J-P, Chen X-M. A metal–organic framework with a pore size/shape suitable for strong binding and close packing of methane. Angew. Chem. Int. Ed. 55, 4674–4678 (2016).

110. Yan Y, Kolokolov DI, da Silva I, Stepanov AG, Blake AJ, Dailly A, Manuel P, Tang CC, Yang S, Schröder M. Porous metal–organic polyhedral frameworks with optimal molecular dynamics and pore geometry for methane storage. J. Am. Chem. Soc. 139, 13349–13360 (2017). [PubMed: 28772068]

111. Chen C-X, Wei Z-W, Jiang J-J, Zheng S-P, Wang H-P, Qiu Q-F, Cao C-C, Fenske D, Su C-Y. Dynamic spacer installation for multirole metal–organic frameworks: a new direction toward multifunctional MOFs achieving ultrahigh methane storage working capacity. J. Am. Chem. Soc. 139, 6034–6037 (2017). [PubMed: 28388035]

112. Li P, Chen Q, Wang TC, Vermeulen NA, Mehdi BL, Dohnalkova A, Browning ND, Shen D, Anderson R, Gómez-Gualdrón DA, et al. Hierarchically engineered mesoporous metal-organic frameworks toward cell-free immobilized enzyme systems. Chem 4, 1022–1034 (2018).

113. Li B, Wen H-M, Zhou W, Chen B. Porous metal–organic frameworks for gas storage and separation: what, how, and why? J. Phys. Chem. Lett. 5, 3468–3479 (2014). [PubMed: 26278595]

114. He Y, Zhou W, Yildirim T, Chen B. A series of metal–organic frameworks with high methane uptake and an empirical equation for predicting methane storage capacity. Energy Environ. Sci. 6, 2735–2744 (2013).

115. Chui SS-Y, Lo SM-F, Charmant JPH, Orpen AG, Williams I. D A chemically functionalizable nanoporous material [Cu3(TMA)2(H2O)3]n. Science 283, 1148–1150 (1999). [PubMed: 10024237]

116. Wu H, Simmons JM, Liu Y, Brown CM, Wang X-S, Ma S, Peterson VK, Southon PD, Kepert CJ, Zhou H-C, et al. Metal–organic frameworks with exceptionally high methane uptake: where and how is methane stored? Chem. Eur. J. 16, 5205–5214 (2010). [PubMed: 20358553]

117. Hulvey Z, Vlaisavljevich B, Mason JA, Tsivion E, Dougherty TP, Bloch ED, Head-Gordon M, Smit B, Long JR, Brown CM. Critical factors driving the high volumetric uptake of methane in Cu3(btc)2. J. Am. Chem. Soc. 137, 10816–10825 (2015). [PubMed: 26263038]

118. Cui X, Chen K, Xing H, Yang Q, Krishna R, Bao Z, Wu H, Zhou W, Dong X, Han Y, et al. Pore chemistry and size control in hybrid porous materials for acetylene capture from ethylene. Science 353, 141–144 (2016). [PubMed: 27198674]

119. Li B, Wen H-M, Wang H, Wu H, Yildirim T, Zhou W, Chen B. Porous metal–organic frameworks with Lewis basic nitrogen sites for high-capacity methane storage. Energy Environ. Sci. 8, 2504–2511 (2015).

120. Kitaura R, Seki K, Akiyama G, Kitagawa S. Porous coordination-polymer crystals with gated channels specific for supercritical gases. Angew. Chem. Int. Ed. 42, 428–431 (2003).

121. Taylor MK, Runčevski T, Oktawiec J, Gonzalez MI, Siegelman RL, Mason JA, Ye J, Brown CM, Long JR. Tuning the adsorption-induced phase change in the flexible metal–organic framework Co(bdp). J. Am. Chem. Soc. 138, 15019–15026 (2016). [PubMed: 27804295]
122. Yang Q-Y, Lama P, Sen S, Lusi M, Chen K-J, Gao W-Y, Shivanna M, Pham T, Hosono N, Kusaka S, et al. Reversible switching between highly porous and nonporous phases of an interpenetrated diamondoid coordination network that exhibits gate-opening at methane storage pressures. Angew. Chem. Int. Ed. 57, 5684–5689 (2018).
123. Spanopoulos I, Tsangarakis C, Klontzas E, Tylianakis E, Froudakis G, Adil K, Belmabkhout Y, Eddaoudi M, Trikalitis PN. Reticular synthesis of HKUST-like tbo-MOFs with enhanced CH4 storage. J. Am. Chem. Soc. 138, 1568–1574 (2016). [PubMed: 26694977]
124. Moreau F, Kolokolov DI, Stepanov AG, Easun TL, Dailly A, Lewis W, Blake AJ, Nowell H, Lennox MJ, Besley E, et al. Tailoring porosity and rotational dynamics in a series of octacarboxylate metal-organic frameworks. Proc. Nat. Acad. Sci. 114, 3056–3061 (2017). [PubMed: 28280097]
125. Xian S, Zho W, Gallego JM, Li Y, Che B. Exceptionally high acetylene uptake in a microporous metal organic framework with open metal sites. J. Am. Chem. Soc. 131, 12415–12419 (2009). [PubMed: 19705919]
126. W H, Zho W, Yildiri T. High-capacity methane storage in metal organic frameworks M2(dhtp): the important role of open metal sites. J. Am. Chem. Soc. 131, 4995–5000 (2009). [PubMed: 19275154]
127. Xiang S, Zhou W, Zhang Z, Green MA, Liu Y, Chen B. Open metal sites within isostructural metal–organic frameworks for differential recognition of acetylene and extraordinarily high acetylene storage capacity at room temperature. Angew. Chem. Int. Ed. 49, 4615–4618 (2010).
128. Cui X, Chen K, Xing H, Yang Q, Krishna R, Bao Z, Wu H, Zhou W, Dong X, Han Y, et al. Pore chemistry and size control in hybrid porous materials for acetylene capture from ethylene. Science 353, 141–144 (2016). [PubMed: 27198674]
129. Rao X, Cai J, Yu J, He Y, Wu C, Zhou W, Yildirim T, Chen B, Qian G. A microporous metal–organic framework with both open metal and Lewis basic pyridyl sites for high C2H2 and CH4 storage at room temperature. Chem. Commun. 49, 6719–6721 (2013).
130. Cai J, Wang H, Wang H, Duan X, Wang Z, Cui Y, Yang Y, Chen B, Qian G. An amino-decorated NbO-type metal–organic framework for high C2H2 storage and selective CO2 capture. RSC Adv 5, 77417–77422 (2015).
131. Wen H-M, Wang H, Li B, Cui Y, Wang H, Qian G, Chen B. A microporous metal–organic framework with lewis basic nitrogen sites for high C2H2 storage and significantly enhanced C2H2/CO2 separation at ambient conditions. Inorg. Chem. 55, 7214–7218 (2016). [PubMed: 27176900]
132. Zhang M, Li B, Li Y, Wang Q, Zhang W, Chen B, Li S, Pan Y, You X, Bai J. Finely tuning MOFs towards high performance in C2H2 storage: synthesis and properties of a new MOF-505 analogue with an inserted amide functional group. Chem. Commun. 52, 7241–7244 (2016).
133. Pang J, Jiang F, Wu M, Liu C, Su K, Lu W, Yuan D, Hong M. A porous metal-organic framework with ultrahigh acetylene uptake capacity under ambient conditions. Nat. Commun. 6, 7575 (2015). [PubMed: 26123775]
134. Moreau F, da Silva I, Al Smail NH, Easun TL, Savage M, Godfrey HGW, Parker SF, Manuel P, Yang S, Schröder M. Unravelling exceptional acetylene and carbon dioxide adsorption within a tetra-amide functionalized metal-organic framework. Nat. Commun. 8, 14085 (2017). [PubMed: 28176793]
135. Zhang J-P, Chen X-M. Optimized acetylene/carbon dioxide sorption in a dynamic porous crystal. J. Am. Chem. Soc. 131, 5516–5521 (2009). [PubMed: 19323553]
136. He C-T, Ye Z-M, Xu Y-T, Zhou D-D, Zhou H-L, Chen D, Zhang J-P, Chen X-M. Hyperfine adjustment of flexible pore-surface pockets enables smart recognition of gas size and quadrupole moment. Chem. Sci. 8, 7560–7565 (2017). [PubMed: 29163911]
137. Zhang J-P, Zhu A-X, Lin R-B, Qi X-L, Chen X-M. Pore surface tailored SOD-type metal-organic zeolites. Adv. Mater. 23, 1268–1271 (2011). [PubMed: 21381128]

138. Herm ZR, Bloch ED, Long JR. Hydrocarbon separations in metal–organic frameworks. Chem. Mater. 26, 323–338 (2014).

139. Li J-R, Kuppler RJ, Zhou H-C. Selective gas adsorption and separation in metal-organic frameworks. Chem. Soc. Rev. 38, 1477–1504 (2009). [PubMed: 19384449]

140. Chen B, Zhao X, Putkham A, Hong K, Lobkovsky EB, Hurtado EJ, Fletcher AJ, Thomas KM. Surface interactions and quantum kinetic molecular sieving for h2 and d2 adsorption on a mixed metal organic framework material. J. Am. Chem. Soc. 130, 6411–6423 (2008). [PubMed: 18435535]

141. Yoon JW, Chang H, Lee SJ, Hwang YK, Hong DY, Lee SK, Lee JS, Jang S, Yoon TU, Kwac K, et al. Selective nitrogen capture by porous hybrid materials containing accessible transition metal ion sites. Nat. Mater. 16, 526–531 (2017). [PubMed: 27992421]

142. Bloch ED, Queen WL, Krishna R, Zadrozny JM, Brown CM, Long JR. Hydrocarbon separations in a metal-organic framework with open iron(II) coordination sites. Science 335, 1606–1610 (2012). [PubMed: 22461607]

143. Lin R-B, Li L, Zhou H-L, Wu H, He C, Li S, Krishna R, Li J, Zhou W, Chen B. Molecular sieving of ethylene from ethane using a rigid metal–organic framework. Nat. Mater. 17, 1128–1133 (2018). [PubMed: 30397312] A work descripting a cheap and stable MOF material for potential industial ethylene/ethane separation.

144. Bao Z, Wang J, Zhang Z, Xing H, Yang Q, Yang Y, Wu H, Krishna R, Zhou W, Chen B, et al. Molecular sieving of ethane from ethylene through the molecular cross-section size differentiation in gallate-based metal–organic frameworks. Angew. Chem. Int. Ed. 57, 16020–16025 (2018).

145. Liao P-Q, Zhang W-X, Zhang J-P, Chen X-M. Efficient purification of ethene by an ethane-trapping metal-organic framework. Nat. Commun. 6, 8697 (2015). [PubMed: 26510376]

146. Lin R-B, Wu H, Li L, Tang X-L, Li Z, Gao J, Cui H, Zhou W, Chen B Boosting ethane/ethylene separation within isoreticular ultramicroporous metal–organic frameworks. J. Am. Chem. Soc. 140, 12940–12946 (2018). [PubMed: 30216725]

147. Chen Y, Qiao Z, Wu H, Lv D, Shi R, Xia Q, Zhou J, Li Z. An ethane-trapping MOF PCN-250 for highly selective adsorption of ethane over ethylene. Chem. Eng. Sci. 175, 110–117 (2018).

148. Li L, Lin R-B, Krishna R, Li H, Xiang S, Wu H, Li J, Zhou W, Chen B. Ethane/ethylene separation in a metal-organic framework with iron-peroxo sites. Science 362, 443 (2018). [PubMed: 30361370] A work reporting ethane-selective MOF towards energy efficient separating adsorbent for the ethylene production.

149. Bae Y-S, Lee CY, Kim KC, Farha OK, Nickias P, Hupp JT, Nguyen ST, Snurr RQ. High propene/propane selectivity in isostructural metal–organic frameworks with high densities of open metal sites. Angew. Chem. Int. Ed. 51, 1857–1860 (2012).

150. Cadiau A, Adil K, Bhatt PM, Belmabkhout Y, Eddaoudi M. A metal-organic framework–based splitter for separating propylene from propane. Science 353, 137–140 (2016). [PubMed: 27387945] A work reporting a MOF sieve for potential industial propylene/propane separation.

151. Wang H, Dong X, Colombo V, Wang Q, Liu Y, Liu W, Wang X-L, Huang X-Y, Proserpio DM, Sironi A, et al. Tailor-made microporous metal–organic frameworks for the full separation of propane from propylene through selective size exclusion. Adv. Mater. 30, 1805088 (2018).

152. Xiang S-C, Zhang Z, Zhao C-G, Hong K, Zhao X, Ding D-R, Xie M-H, Wu C-D, Das MC, Gill R, et al. Rationally tuned micropores within enantiopure metal-organic frameworks for highly selective separation of acetylene and ethylene. Nat. Commun. 2, 204 (2011). [PubMed: 21343922]

153. Hu T-L, Wang H, Li B, Krishna R, Wu H, Zhou W, Zhao Y, Han Y, Wang X, Zhu W, et al. Microporous metal–organic framework with dual functionalities for highly efficient removal of acetylene from ethylene/acetylene mixtures. Nat. Commun. 6, 7328 (2015). [PubMed: 26041691]

154. Hazra A, Jana S, Bonakala S, Balasubramanian S, Maji TK. Separation/purification of ethylene from an acetylene/ethylene mixture in a pillared-layer porous metal–organic framework. Chem. Commun. 53, 4907–4910 (2017).

155. Li B, Cui X, O'Nolan D, Wen H-M, Jiang M, Krishna R, Wu H, Lin R-B, Chen Y-S, Yuan D, et al. An ideal molecular sieve for acetylene removal from ethylene with record selectivity and productivity. Adv. Mater. 29, 1704210 (2017).

156. Luo F, Yan C, Dang L, Krishna R, Zhou W, Wu H, Dong X, Han Y, Hu T-L, O'Keeffe M. UTSA-74: a MOF-74 isomer with two accessible binding sites per metal center for highly selective gas separation. J. Am. Chem. Soc. 138, 5678–5684 (2016). [PubMed: 27113684]

157. Lin R-B, Li L, Wu H, Arman H, Li B, Lin R-G, Zhou W, Chen B. Optimized separation of acetylene from carbon dioxide and ethylene in a microporous material. J. Am. Chem. Soc. 139, 8022–8028 (2017). [PubMed: 28574717]

158. Chen K-J, Scott HS, Madden DG, Pham T, Kumar A, Bajpai A, Lusi M, Forrest KA, Space B, Perry JJ IV, et al. Benchmark C2H2/CO2 and CO2/C2H2 separation by two closely related hybrid ultramicroporous materials. Chem 1, 753–765 (2016).

159. Foo ML, Matsuda R, Hijikata Y, Krishna R, Sato H, Horike S, Hori A, Duan J, Sato Y, Kubota Y, et al. An adsorbate discriminatory gate effect in a flexible porous coordination polymer for selective adsorption of CO2 over C2H2. J. Am. Chem. Soc. 138, 3022–3030 (2016). [PubMed: 26876504]

160. Li L, Lin R-B, Krishna R, Wang X, Li B, Wu H, Li J, Zhou W, Chen B. Flexible–robust metal–organic framework for efficient removal of propyne from propylene. J. Am. Chem. Soc. 139, 7733–7736 (2017). [PubMed: 28580788]

161. Yang L, Cui X, Yang Q, Qian S, Wu H, Bao Z, Zhang Z, Ren Q, Zhou W, Chen B. A single-molecule propyne trap: highly efficient removal of propyne from propylene with anion-pillared ultramicroporous materials. Adv. Mater. 30, 1705374 (2018).

162. Yang L, Cui X, Zhang Z, Yang Q, Bao Z, Ren Q, Xing H. An asymmetric anion-pillared metal–organic framework as a multisite adsorbent enables simultaneous removal of propyne and propadiene from propylene. Angew. Chem. Int. Ed. 57, 13145–13149 (2018).

163. Assen AH, Belmabkhout Y, Adil K, Bhatt PM, Xue D-X, Jiang H, Eddaoudi M. Ultra-tuning of the rare-earth fcu-MOF aperture size for selective molecular exclusion of branched paraffins. Angew. Chem. Int. Ed. 54, 14353–14358 (2015).

164. Zhang Z, Yang Q, Cui X, Yang L, Bao Z, Ren Q, Xing H. Sorting of C4 olefins with interpenetrated hybrid ultramicroporous materials by combining molecular recognition and size-sieving. Angew. Chem. Int. Ed. 56, 16282–16287 (2017).

165. Nugent P, Belmabkhout Y, Burd SD, Cairns AJ, Luebke R, Forrest K, Pham T, Ma S, Space B, Wojtas L, et al. Porous materials with optimal adsorption thermodynamics and kinetics for CO2 separation. Nature 495, 80 (2013). [PubMed: 23446349]

166. Liang L, Liu C, Jiang F, Chen Q, Zhang L, Xue H, Jiang H-L, Qian J, Yuan D, Hong M. Carbon dioxide capture and conversion by an acid-base resistant metal-organic framework. Nat. Commun. 8, 1233 (2017). [PubMed: 29089480]

167. Chen K-J, Madden DG, Pham T, Forrest KA, Kumar A, Yang Q-Y, Xue W, Space B, Perry Iv JJ, Zhang J-P, et al. Tuning pore size in square-lattice coordination networks for size-selective sieving of CO2. Angew. Chem. Int. Ed. 55, 10268–10272 (2016).

168. McDonald TM, Mason JA, Kong X, Bloch ED, Gygi D, Dani A, Crocellà V, Giordanino F, Odoh SO, Drisdell WS, et al. Cooperative insertion of CO2 in diamine-appended metal-organic frameworks. Nature 519, 303 (2015). [PubMed: 25762144]

169. Liao P-Q, Chen X-W, Liu S-Y, Li X-Y, Xu Y-T, Tang M, Rui Z, Ji H, Zhang J-P, Chen X-M. Putting an ultrahigh concentration of amine groups into a metal–organic framework for CO2 capture at low pressures. Chem. Sci. 7, 6528–6533 (2016). [PubMed: 27928493]

170. Liao P-Q, Chen H, Zhou D-D, Liu S-Y, He C-T, Rui Z, Ji H, Zhang J-P, Chen X-M. Monodentate hydroxide as a super strong yet reversible active site for CO2 capture from high-humidity flue gas. Energy Environ. Sci. 8, 1011–1016 (2015).

171. Zhai Q-G, Bu X, Mao C, Zhao X, Daemen L, Cheng Y, Ramirez-Cuesta AJ, Feng P. An ultra-tunable platform for molecular engineering of high-performance crystalline porous materials. Nat. Commun. 7, 13645 (2016). [PubMed: 27924818]

172. Cui X, Chen K, Xing H, Yang Q, Krishna R, Bao Z, Wu H, Zhou W, Dong X, Han Y, et al. Pore chemistry and size control in hybrid porous materials for acetylene capture from ethylene. Science 353, 141 (2016). [PubMed: 27198674]

173. Min Wang Q, Shen D, Bülow M, Ling Lau M, Deng S, Fitch FR, Lemcoff NO, Semanscin J. Metallo-organic molecular sieve for gas separation and purification. Microporous Mesoporous Mater 55, 217–230 (2002).

174. Bachman JE, Reed DA, Kapelewski MT, Chachra G, Jonnavittula D, Radaelli G, Long JR. Enabling alternative ethylene production through its selective adsorption in the metal–organic framework Mn2(m-dobdc). Energy Environ. Sci. 11, 2423–2431 (2018).

175. Li B, Zhang Y, Krishna R, Yao K, Han Y, Wu Z, Ma D, Shi Z, Pham T, Space B, et al. Introduction of π -complexation into porous aromatic framework for highly selective adsorption of ethylene over ethane. J. Am. Chem. Soc. 136, 8654–8660 (2014). [PubMed: 24901372]

176. Hao H-G, Zhao Y-F, Chen D-M, Yu J-M, Tan K, Ma S-Q, Chabal Y, Zhang Z-M, Dou J-M, Xiao Z-H, et al. Simultaneously trapping C2H2 and C2H6 into a robust metal-organic framework from a ternary mixture of C2H2/C2H4/C2H6 for purification of C2H4. Angew. Chem. Int. Ed. 57, 16067–16071 (2018).

177. Gücüyener C, van den Berg J, Gascon J, Kapteijn F. Ethane/ethene separation turned on its head: selective ethane adsorption on the metal organic framework zif-7 through a gate-opening mechanism. J. Am. Chem. Soc. 132, 17704–17706 (2010). [PubMed: 21114318]

178. Nijem N, Wu H, Canepa P, Marti A, Balkus KJ, Thonhauser T, Li J, Chabal YJ. Tuning the gate opening pressure of metal–organic frameworks (MOFs) for the selective separation of hydrocarbons. J. Am. Chem. Soc. 134, 15201–15204 (2012). [PubMed: 22946693]

179. Li K, Olson DH, Seidel J, Emge TJ, Gong H, Zeng H, Li J. Zeolitic imidazolate frameworks for kinetic separation of propane and propene. J. Am. Chem. Soc. 131, 10368–10369 (2009). [PubMed: 19722614]

180. Le CY, Ba Y-S, Jeon NC, Farh OK, Sarjean AA, Ster CL, Nickia P, Snur RQ, Hup JT, Nguye ST. Kinetic separation of propene and propane in metal organic frameworks: controlling diffusion rates in plate-shaped crystals via tuning of pore apertures and crystallite aspect ratios. J. Am. Chem. Soc. 133, 5228–5231 (2011). [PubMed: 21417272]

181. Peng J, Wang H, Olson DH, Li Z, Li J. Efficient kinetic separation of propene and propane using two microporous metal organic frameworks. Chem. Commun. 53, 9332–9335 (2017).

182. Li L, Lin R-B, Wang X, Zhou W, Jia L, Li J, Chen B. Kinetic separation of propylene over propane in a microporous metal-organic framework. Chem. Eng. J. 354, 977–982 (2018).

183. Xue D-X, Cadiau A, Weselin ŁJ, Jiang H, Bhatt PM, Shkurenko A, Wojtas L, Zhijie C, Belmabkhout Y, Adil K, et al. Topology meets MOF chemistry for pore-aperture fine tuning: ftw-MOF platform for energy-efficient separations via adsorption kinetics or molecular sieving. Chem. Commun. 54, 6404–6407 (2018).

184. Das MC, Guo Q, He Y, Kim J, Zhao C-G, Hong K, Xiang S, Zhang Z, Thomas KM, Krishna R, et al. Interplay of metalloligand and organic ligand to tune micropores within isostructural mixed-metal organic frameworks (Mr MOFs) for their highly selective separation of chiral and achiral small molecules. J. Am. Chem. Soc. 134, 8703–8710 (2012). [PubMed: 22545712]

185. Li L, Wen H-M, He C, Lin R-B, Krishna R, Wu H, Zhou W, Li J, Li B, Chen B. A Metal–Organic Framework with Suitable Pore Size and Specific Functional Sites for the Removal of Trace Propyne from Propylene. Angew. Chem. Int. Ed. 57, 15183–15188 (2018).

186. Liao P-Q, Huang N-Y, Zhang W-X, Zhang J-P, Chen X-M. Controlling guest conformation for efficient purification of butadiene. Science 356, 1193–1196 (2017). [PubMed: 28619946] A work reporting a fiexible MOF for inverse separation of butane and butene over butadiene.

187. Pan L, Olson DH, Ciemnolonski LR, Heddy R, Li J. Separation of hydrocarbons with a microporous metal–organic framework. Angew. Chem. Int. Ed. 45, 616–619 (2006).

188. Herm ZR, Wiers BM, Mason JA, van Baten JM, Hudson MR, Zajdel P, Brown CM, Masciocchi N, Krishna R, Long JR. Separation of hexane isomers in a metal-organic framework with triangular channels. Science 340, 960 (2013). [PubMed: 23704568]

189. Wang H, Dong X, Velasco E, Olson DH, Han Y, Li J. One-of-a-kind: a microporous metal–organic framework capable of adsorptive separation of linear, mono- and di-branched alkane

isomers via temperature- and adsorbate-dependent molecular sieving. Energy Environ. Sci. 11, 1226–1231 (2018).

190. Wang H, Dong X, Lin J, Teat SJ, Jensen S, Cure J, Alexandrov EV, Xia Q, Tan K, Wang Q, et al. Topologically guided tuning of Zr-MOF pore structures for highly selective separation of C6 alkane isomers. Nat. Commun. 9, 1745 (2018). [PubMed: 29717138]
191. Bastin L, Bárcia PS, Hurtado EJ, Silva JAC, Rodrigues AE, Chen B. A microporous metal organic framework for separation of CO2/N2 and CO2/CH4 by fixed-bed adsorption. J. Phys. Chem. C 112, 1575–1581 (2008).
192. Kumar A, Madden DG, Lusi M, Chen K-J, Daniels EA, Curtin T, Perry JJ, Zaworotko MJ. Direct air capture of CO2 by physisorbent materials. Angew. Chem. Int. Ed. 54, 14372–14377 (2015).
193. Wilmer CE, Farha OK, Bae Y-S, Hupp JT, Snurr RQ. Structure–property relationships of porous materials for carbon dioxide separation and capture. Energy Environ. Sci. 5, 9849–9856 (2012).
194. Burd SD, Ma S, Perman JA, Sikora BJ, Snurr RQ, Thallapally PK, Tian J, Wojtas L, Zaworotko MJ. Highly selective carbon dioxide uptake by [Cu(bpy-n)2(SiF6)] (bpy-1 4,4r -bipyridine; bpy-2 1,2-bis(4-pyridyl)ethene). J. Am. Chem. Soc. 134, 3663–3666 (2012). [PubMed: 22316279]
195. Yanai N, Kitayama K, Hijikata Y, Sato H, Matsuda R, Kubota Y, Takata M, Mizuno M, Uemura T, Kitagawa S. Gas detection by structural variations of fluorescent guest molecules in a flexible porous coordination polymer. Nat. Mater. 10, 787 (2011). [PubMed: 21892178]
196. Hamon L, Llewellyn PL, Devic T, Ghoufi A, Clet G, Guillerm V, Pirngruber GD, Maurin G, Serre C, Driver G, et al. . Co-adsorption and separation of CO2 CH4 mixtures in the highly flexible MIL-53(Cr) MOF. J. Am. Chem. Soc. 131, 17490–17499 (2009). [PubMed: 19904944]
197. Lan Y-Q, Jiang H-L, Li S-L, Xu Q. Mesoporous metal-organic frameworks with size-tunable cages: selective CO2 uptake, encapsulation of Ln3+ cations for luminescence, and column-chromatographic dye separation. Adv. Mater. 23, 5015–5020 (2011). [PubMed: 21989794]
198. Caskey SR, Wong-Foy AG, Matzger AJ. Dramatic tuning of carbon dioxide uptake via metal substitution in a coordination polymer with cylindrical pores. J. Am. Chem. Soc. 130, 10870–10871 (2008). [PubMed: 18661979]
199. Shekhah O, Belmabkhout Y, Chen Z, Guillerm V, Cairns A, Adil K, Eddaoudi M. Made-to-order metal-organic frameworks for trace carbon dioxide removal and air capture. Nat. Commun. 5, 4228 (2014). [PubMed: 24964404]
200. Bhatt PM, Belmabkhout Y, Cadiau A, Adil K, Shekhah O, Shkurenko A, Barbour LJ, Eddaoudi M. A fine-tuned fluorinated MOF addresses the needs for trace CO2 removal and air capture using physisorption. J. Am. Chem. Soc. 138, 9301–9307 (2016). [PubMed: 27388208]
201. Zhao X, Bu X, Zhai Q-G, Tran H, Feng P. Pore space partition by symmetry-matching regulated ligand insertion and dramatic tuning on carbon dioxide uptake. J. Am. Chem. Soc. 137, 1396–1399 (2015). [PubMed: 25621414]
202. McDonald TM, Lee WR, Mason JA, Wiers BM, Hong CS, Long JR. Capture of carbon dioxide from air and flue gas in the alkylamine-appended metal–organic framework mmen-Mg2(dobpdc). J. Am. Chem. Soc. 134, 7056–7065 (2012). [PubMed: 22475173]
203. Demessence A, D'Alessandro DM, Foo ML, Long JR. Strong CO2 binding in a water-stable, triazolate-bridged metal organic framework functionalized with ethylenediamine. J. Am. Chem. Soc. 131, 8784–8786 (2009). [PubMed: 19505094]
204. Milner PJ, Siegelman RL, Forse AC, Gonzalez MI, Runčevski T, Martell JD, Reimer JA, Long JR. A diaminopropane-appended metal–organic framework enabling efficient CO2 capture from coal flue gas via a mixed adsorption mechanism. J. Am. Chem. Soc. 139, 13541–13553 (2017). [PubMed: 28906108]
205. Siegelman RL, McDonald TM, Gonzalez MI, Martell JD, Milner PJ, Mason JA, Berger AH, Bhown AS, Long JR. Controlling cooperative CO2 adsorption in diamine-appended Mg2(dobpdc) metal–organic frameworks. J. Am. Chem. Soc. 139, 10526–10538 (2017). [PubMed: 28669181]
206. Bien CE, Chen KK, Chien S-C, Reiner BR, Lin L-C, Wade CR, Ho WSW. Bioinspired metal–organic framework for trace CO2 capture. J. Am. Chem. Soc. 140, 12662–12666 (2018). [PubMed: 30256632]

207. Wright AM, Wu Z, Zhang G, Mancuso JL, Comito RJ, Day RW, Hendon CH, Miller JT, Dincă MA structural mimic of carbonic anhydrase in a metal-organic framework. Chem 4, 2894–2901 (2018).

208. Lu Z, Godfrey HGW, da Silva I, Cheng Y, Savage M, Tuna F, McInnes EJL, Teat SJ, Gagnon KJ, Frogley MD, et al. Modulating supramolecular binding of carbon dioxide in a redox-active porous metal-organic framework. Nat. Commun. 8, 14212 (2017). [PubMed: 28194014]

209. Shah MS, Tsapatsis M, Siepmann JI. Hydrogen sulfide capture: from absorption in polar liquids to oxide, zeolite, and metal-organic framework adsorbents and membranes. Chem. Rev. 117, 9755–9803 (2017). [PubMed: 28678483]

210. Woellner M, Hausdorf S, Klein N, Mueller P, Smith MW, Kaskel S. Adsorption and detection of hazardous trace gases by metal–organic frameworks. Adv. Mater. 30, 1704679 (2018).

211. Wang H, Lustig WP, Li J. Sensing and capture of toxic and hazardous gases and vapors by metal–organic frameworks. Chem. Soc. Rev. 47, 4729–4756 (2018). [PubMed: 29532822]

212. DeCoste JB, Peterson GW. Metal–organic frameworks for air purification of toxic chemicals. Chem. Rev. 114, 5695–5727 (2014). [PubMed: 24750116]

213. Barea E, Montoro C, Navarro JAR. Toxic gas removal – metal–organic frameworks for the capture and degradation of toxic gases and vapours. Chem. Soc. Rev. 43, 5419–5430 (2014). [PubMed: 24705539]

214. Bobbitt NS, Mendonca ML, Howarth AJ, Islamoglu T, Hupp JT, Farha OK, Snurr RQ. Metal–organic frameworks for the removal of toxic industrial chemicals and chemical warfare agents. Chem. Soc. Rev. 46, 3357–3385 (2017). [PubMed: 28345694]

215. Yang S, Sun J, Ramirez-Cuesta AJ, Callear SK, David WIF, Anderson DP, Newby R, Blake AJ, Parker JE, Tang CC, et al. Selectivity and direct visualization of carbon dioxide and sulfur dioxide in a decorated porous host. Nat. Chem. 4, 887 (2012). [PubMed: 23089862]

216. Cui X, Yang Q, Yang L, Krishna R, Zhang Z, Bao Z, Wu H, Ren Q, Zhou W, Chen B, et al. Ultrahigh and selective SO2 uptake in inorganic anion-pillared hybrid porous materials. Adv. Mater. 29, 1606929 (2017).

217. Rieth AJ, Tulchinsky Y, Dincă, M. High and reversible ammonia uptake in mesoporous azolate metal–organic frameworks with open Mn, Co, and Ni sites. J. Am. Chem. Soc. 138, 9401–9404 (2016). [PubMed: 27420652]

218. Rieth AJ, Dincă, M. Controlled gas uptake in metal–organic frameworks with record ammonia sorption. J. Am. Chem. Soc. 140, 3461–3466 (2018). [PubMed: 29425040]

219. Shimomura S, Higuchi M, Matsuda R, Yoneda K, Hijikata Y, Kubota Y, Mita Y, Kim J, Takata M, Kitagawa S. Selective sorption of oxygen and nitric oxide by an electron-donating flexible porous coordination polymer. Nat. Chem. 2, 633–637 (2010). [PubMed: 20651724]

220. Li B, Wen H-M, Wang H, Wu H, Yildirim T, Zhou W, Chen B. Porous metal-organic frameworks with Lewis basic nitrogen sites for high-capacity methane storage. Energy Environ. Sci. 8, 2504–2511 (2015).

221. Lin R-B, Li T-Y, Zhou H-L, He C-T, Zhang J-P, Chen X-M. Tuning fluorocarbon adsorption in new isoreticular porous coordination frameworks for heat transformation applications. Chem. Sci. 6, 2516–2521 (2015). [PubMed: 29308161]

222. Xie L-H, Liu X-M, He T, Li J-R. Metal-organic frameworks for the capture of trace aromatic volatile organic compounds. Chem 4, 1911–1927 (2018).

223. Sato H, Kosaka W, Matsuda R, Hori A, Hijikata Y, Belosludov RV, Sakaki S, Takata M, Kitagawa S. Self-accelerating CO sorption in a soft nanoporous crystal. Science 343, 167 (2014). [PubMed: 24336572]

224. Reed DA, Keitz BK, Oktawiec J, Mason JA, Runčevski T, Xiao DJ, Darago LE, Crocellà V, Bordiga S, Long JR. A spin transition mechanism for cooperative adsorption in metal–organic frameworks. Nature 550, 96 (2017). [PubMed: 28892810]

225. Chen K-J, Yang Q-Y, Sen S, Madden DG, Kumar A, Pham T, Forrest KA, Hosono N, Space B, Kitagawa S, et al. Efficient CO2 removal for ultra-pure CO production by two hybrid ultramicroporous materials. Angew. Chem. Int. Ed. 57, 3332–3336 (2018).

226. Banerjee D, Simon CM, Elsaidi SK, Haranczyk M, Thallapally P. K Xenon gas separation and storage using metal-organic frameworks. Chem 4, 466–494 (2018).

227. Banerjee D, Simon CM, Plonka AM, Motkuri RK, Liu J, Chen X, Smit B, Parise JB, Haranczyk M, Thallapally PK. Metal–organic framework with optimally selective xenon adsorption and separation. Nat. Commun. 7, 11831 (2016).

228. Mohamed MH, Elsaidi SK, Pham T, Forrest KA, Schaef HT, Hogan A, Wojtas L, Xu W, Space B, Zaworotko MJ, et al. Hybrid ultra-microporous materials for selective xenon adsorption and separation. Angew. Chem. Int. Ed. 55, 8285–8289 (2016).

229. Fernandez CA, Liu J, Thallapally PK, Strachan DM. Switching Kr/Xe selectivity with temperature in a metal–organic framework. J. Am. Chem. Soc. 134, 9046–9049 (2012). [PubMed: 22591325]

230. Gonzalez MI, Kapelewski MT, Bloch ED, Milner PJ, Reed DA, Hudson MR, Mason JA, Barin G, Brown CM, Long JR. Separation of xylene isomers through multiple metal site interactions in metal–organic frameworks. J. Am. Chem. Soc. 140, 3412–3422 (2018). [PubMed: 29446932]

231. Teufel J, Oh H, Hirscher M, Wahiduzzaman M, Zhechkov L, Kuc A, Heine T, Denysenko D, Volkmer D. MFU-4 – a metal-organic framework for highly effective H2/D2 separation. Adv. Mater. 25, 635–639 (2013). [PubMed: 23135873]

232. FitzGerald SA, Pierce CJ, Rowsell JLC, Bloch ED, Mason JA. Highly selective quantum sieving of D2 from H2 by a metal–organic framework as determined by gas manometry and infrared spectroscopy. J. Am. Chem. Soc. 135, 9458–9464 (2013). [PubMed: 23711176]

233. Weinrauch I, Savchenko I, Denysenko D, Souliou SM, Kim HH, Le Tacon M, Daemen LL, Cheng Y, Mavrandonakis A, Ramirez-Cuesta AJ, et al. Capture of heavy hydrogen isotopes in a metal-organic framework with active Cu(I) sites. Nat. Commun. 8, 14496 (2017). [PubMed: 28262794]

234. Zhang Y, Feng X, Li H, Chen Y, Zhao J, Wang S, Wang L, Wang B. Photoinduced postsynthetic polymerization of a metal–organic framework toward a flexible stand-alone membrane. Angew. Chem. Int. Ed. 54, 4259–4263 (2015).

235. Al-Maythalony BA, Shekhah O, Swaidan R, Belmabkhout Y, Pinnau I, Eddaoudi M. Quest for anionic MOF membranes: continuous sod-ZMOF membrane with CO2 adsorption-driven selectivity. J. Am. Chem. Soc. 137, 1754–1757 (2015). [PubMed: 25580818]

236. Seoane B, Coronas J, Gascon I, Benavides ME, Karvan O, Caro J, Kapteijn F, Gascon J Metal–organic framework based mixed matrix membranes: a solution for highly efficient CO2 capture? Chem. Soc. Rev. 44, 2421–2454 (2015). [PubMed: 25692487]

237. Park HB, Kamcev J, Robeson LM, Elimelech M, Freeman BD. Maximizing the right stuff: the trade-off between membrane permeability and selectivity. Science 356 (2017).

238. Koros WJ, Zhang C. Materials for next-generation molecularly selective synthetic membranes. Nat. Mater. 16, 289 (2017). [PubMed: 28114297]

239. Qiu S, Xue M, Zhu G Metal–organic framework membranes: from synthesis to separation application. Chem. Soc. Rev. 43, 6116–6140 (2014). [PubMed: 24967810]

240. Knebel A, Geppert B, Volgmann K, Kolokolov DI, Stepanov AG, Twiefel J, Heitjans P, Volkmer D, Caro J. Defibrillation of soft porous metal-organic frameworks with electric fields. Science 358, 347–351 (2017). [PubMed: 29051376]

241. Peng Y, Li Y, Ban Y, Jin H, Jiao W, Liu X, Yang W. Metal-organic framework nanosheets as building blocks for molecular sieving membranes. Science 346, 1356–1359 (2014). [PubMed: 25504718]

242. Wang X, Chi C, Zhang K, Qian Y, Gupta KM, Kang Z, Jiang J, Zhao D. Reversed thermo-switchable molecular sieving membranes composed of two-dimensional metal-organic nanosheets for gas separation. Nat. Commun. 8, 14460 (2017). [PubMed: 28205528]

243. Bae T-H, Lee JS, Qiu W, Koros WJ, Jones CW, Nair S A high-performance gas-separation membrane containing submicrometer-sized metal–organic framework crystals. Angew. Chem. Int. Ed. 49, 9863–9866 (2010).

244. Rodenas T, Luz I, Prieto G, Seoane B, Miro H, Corma A, Kapteijn F, Llabrés i Xamena FX, Gascon J. Metal–organic framework nanosheets in polymer composite materials for gas separation. Nat. Mater. 14, 48 (2014). [PubMed: 25362353]

245. Bachman JE, Smith ZP, Li T, Xu T, Long JR. Enhanced ethylene separation and plasticization resistance in polymer membranes incorporating metal–organic framework nanocrystals. Nat. Mater. 15, 845 (2016). [PubMed: 27064528]

246. Liu G, Chernikova V, Liu Y, Zhang K, Belmabkhout Y, Shekhah O, Zhang C, Yi S, Eddaoudi M, Koros WJ. Mixed matrix formulations with MOF molecular sieving for key energy-intensive separations. Nat. Mater. 17, 283–289 (2018). [PubMed: 29434309]

247. Liu Y, Liu G, Zhang C, Qiu W, Yi S, Chernikova V, Chen Z, Belmabkhout Y, Shekhah O, Eddaoudi M, et al. Enhanced CO2/CH4 separation performance of a mixed matrix membrane based on tailored MOF-polymer formulations. Adv. Sci. 5, 1800982 (2018).

248. Liu G, Cadiau A, Liu Y, Adil K, Chernikova V, Carja I-D, Belmabkhout Y, Karunakaran M, Shekhah O, Zhang C, et al. Enabling fluorinated MOF-based membranes for simultaneous removal of H2S and CO2 from natural gas. Angew. Chem. Int. Ed. 57, 14811–14816 (2018).

249. Zhang C, Dai Y, Johnson JR, Karvan O, Koros WJ. High performance ZIF-8/6FDA-DAM mixed matrix membrane for propylene/propane separations. J. Membrane Sci. 389, 34–42 (2012).

250. Zhang C, Zhang K, Xu L, Labreche Y, Kraftschik B, Koros WJ. Highly scalable ZIF-based mixed-matrix hollow fiber membranes for advanced hydrocarbon separations. AIChE J 60, 2625–2635 (2014).

251. Brown AJ, Brunelli NA, Eum K, Rashidi F, Johnson JR, Koros WJ, Jones CW, Nair S. Interfacial microfluidic processing of metal-organic framework hollow fiber membranes. Science 345, 72–75 (2014). [PubMed: 24994649]

252. Kong C, Du H, Chen L, Chen B. Nanoscale MOF/organosilica membranes on tubular ceramic substrates for highly selective gas separation. Energy Environ. Sci. 10, 1812–1819 (2017).

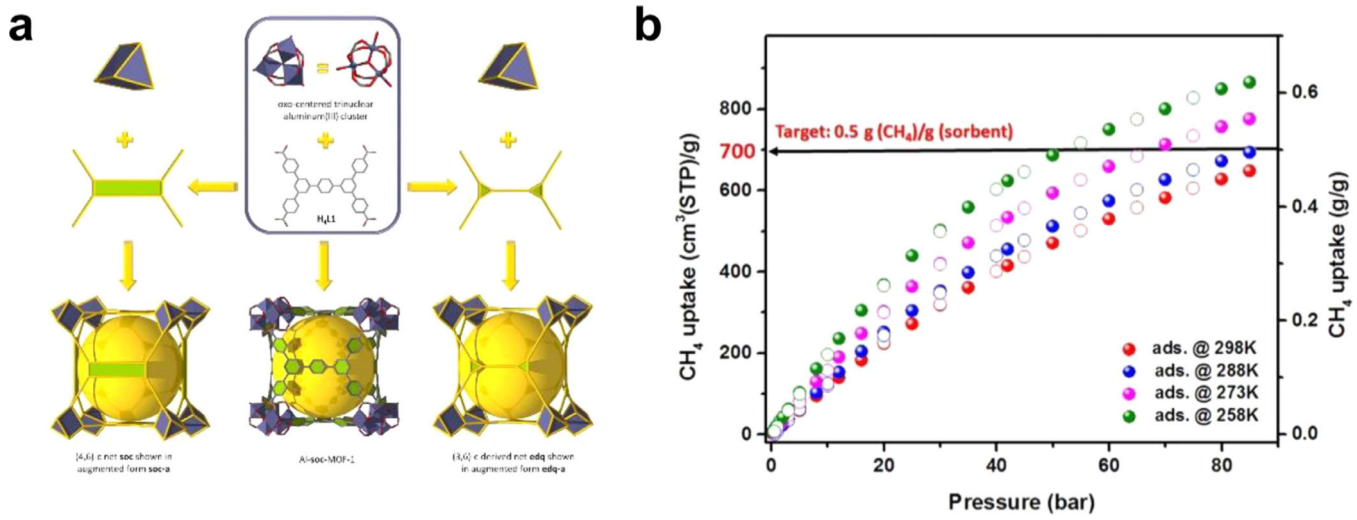

Fig. 1.

(a) Structure of Al-soc-MOF-1. (b) Single-component CH_4 sorption isotherms at different temperatures for Al-soc-MOF-1. Reprinted with permission from Alezi et al.[105] Copyright 2015, ACS Publications.

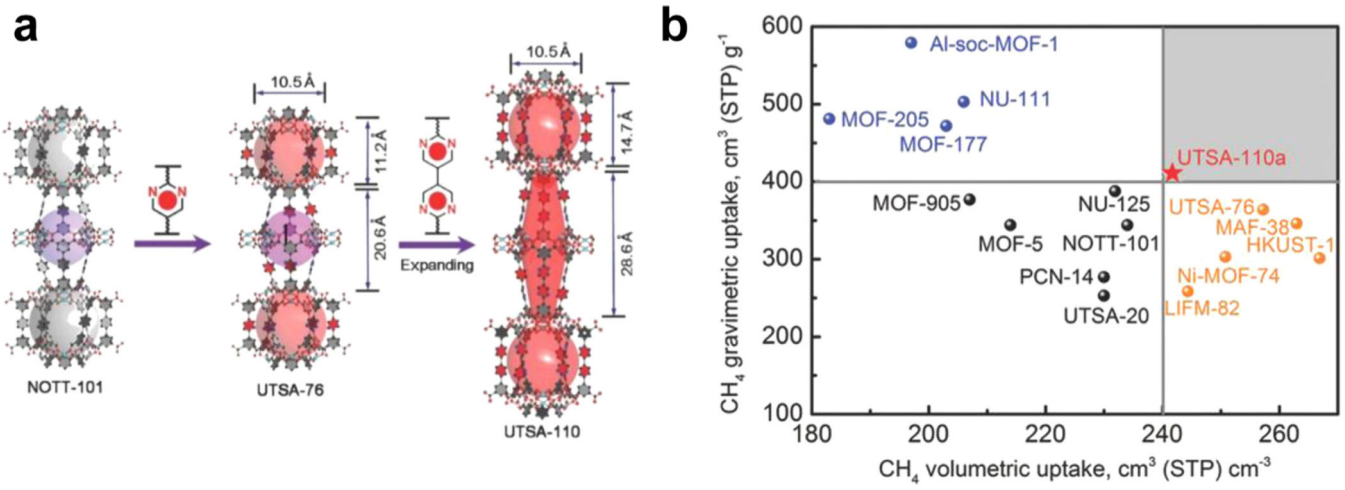

Fig. 2.

(a) Comparison of the crystal structures of NOTT-101, UTSA-76, and UTSA-110. (b) Total CH_4 gravimetric and volumetric capacities at 298 K and 65 bar for UTSA-110a in comparison with those of some benchmark MOFs. Reprinted with permission from Wen et al.[106] Copyright 2018, John Wiley and Sons.

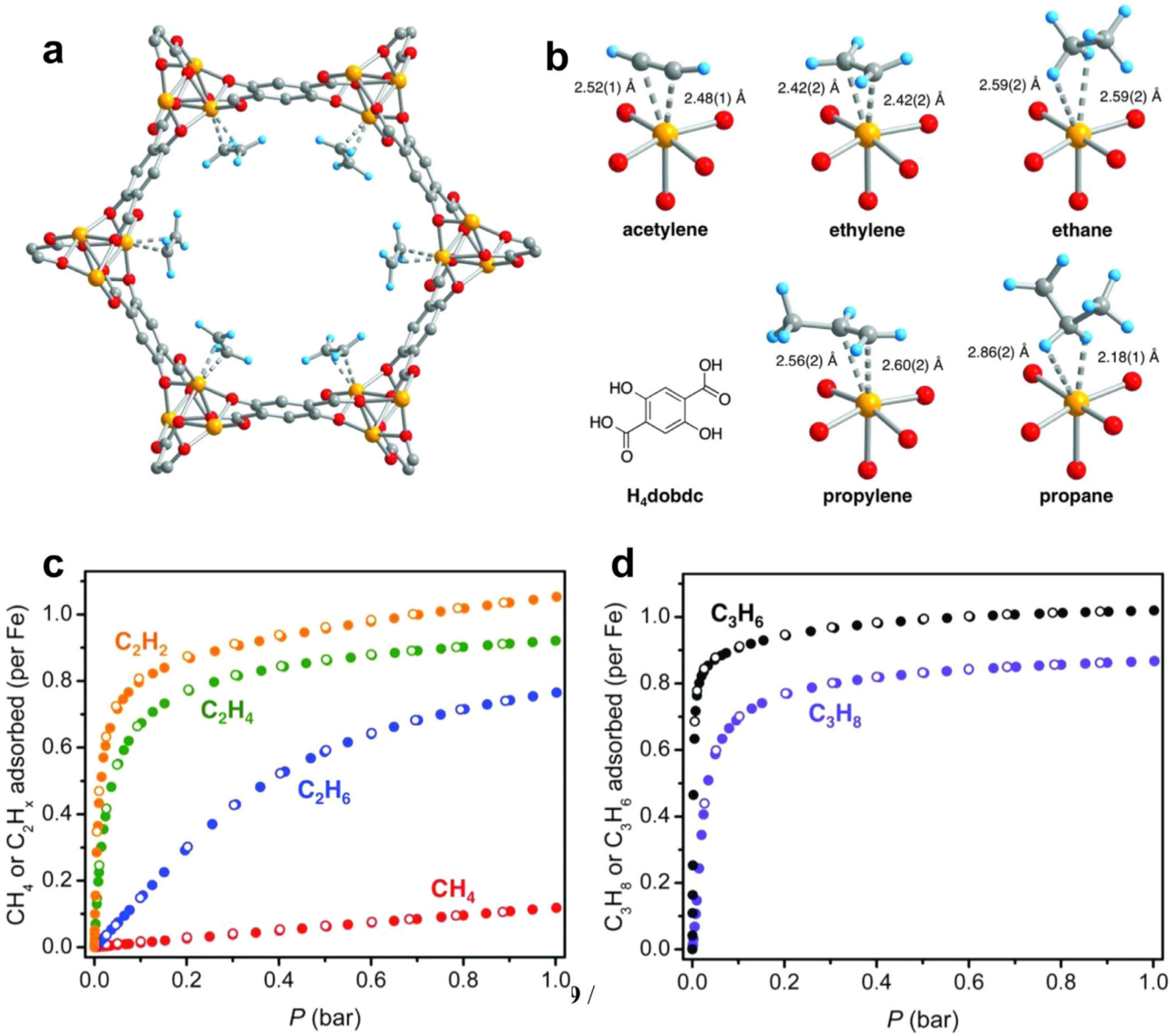

Fig. 3.

(a) A portion of the solid-state structure of $Fe_2(dobdc)•2C_2D_4$, determined from neutron powder diffraction analysis. Orange, red, grey, and blue spheres represent Fe, O, C, D atoms, respectively. (b) $H_4(dobdc)$ ligand and the first coordination spheres for Fe center upon dosing $Fe_2(dobdc)$ with C_2H_2, C_2H_4, C_2H_6, C_3H_6, and C_3H_8. Gas sorption isotherms for (c) CH_4, C_2H_6, C_2H_4, and C_2H_2 (d) C_3H_8 and C_3H_6 in $Fe_2(dobdc)$ at 318 K. Reprinted with permission from Bloch et al.[142] Copyright 2012, the American Association for the Advancement of Science. (For interpretation of the references to color in this figure legend, the reader is referred to the web version of this article.)

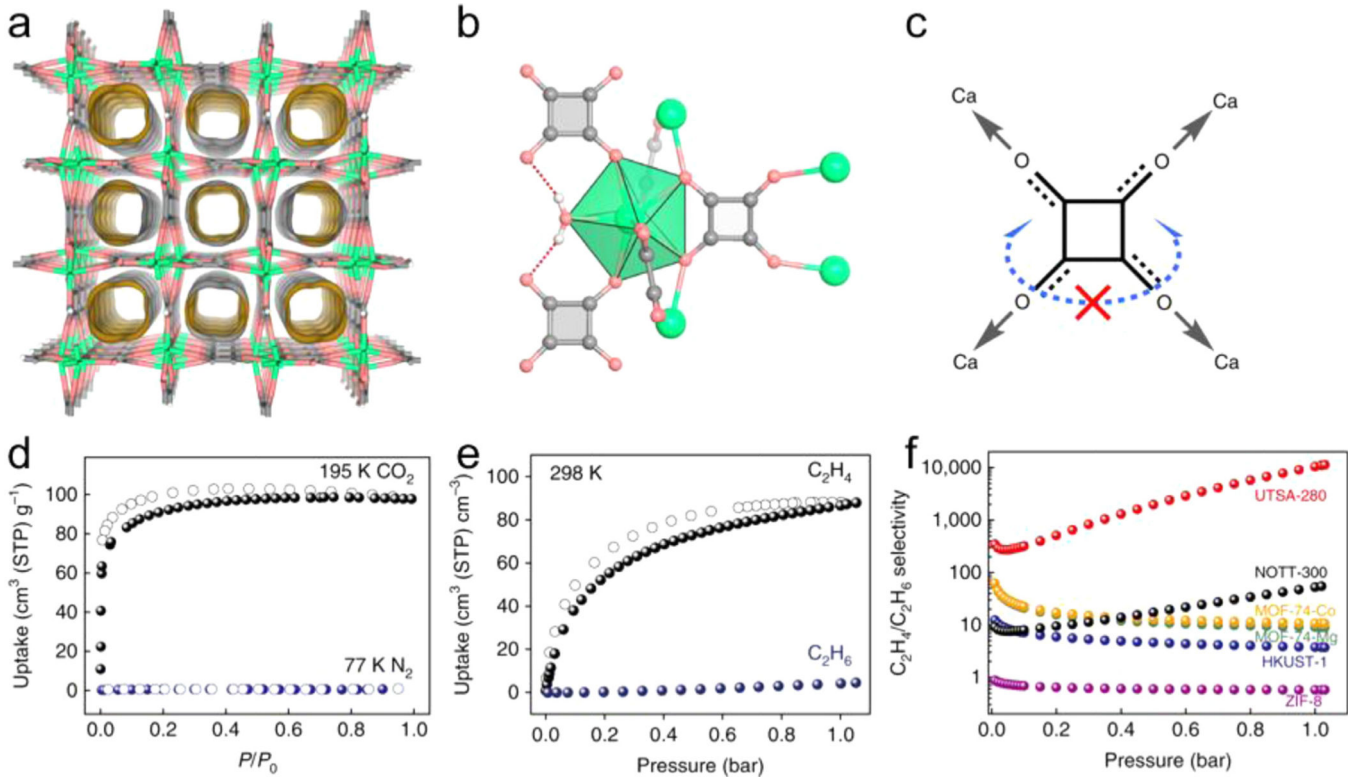

Fig. 4.

(a) The crystal structure of guest-free UTSA-280 determined from single-crystal X-ray diffraction, showing one-dimensional channels viewed along the [001] direction. Green, light coral and grey nodes represent Ca, O and C atoms, respectively. (b) The local coordination environments of the squarate linker and calcium atoms. (c) A schematic diagram showing the coordination constraints applied on the $C_4O_4^{2-}$ linker. (d) Single-component sorption isotherms of CO_2 at 195 K and N_2 at 77 K for UTSA-280. (e) Single-component sorption isotherms of C_2H_4 and C_2H_6 at 298 K for UTSA-280. (f) Qualitative comparison of IAST adsorption selectivities of different MOFs for an equimolar C_2H_4/C_2H_6 mixture at 298 K. Reprinted with permission from Lin et al.[143] Copyright 2018, Springer Nature. (For interpretation of the references to color in this figure legend, the reader is referred to the web version of this article.)

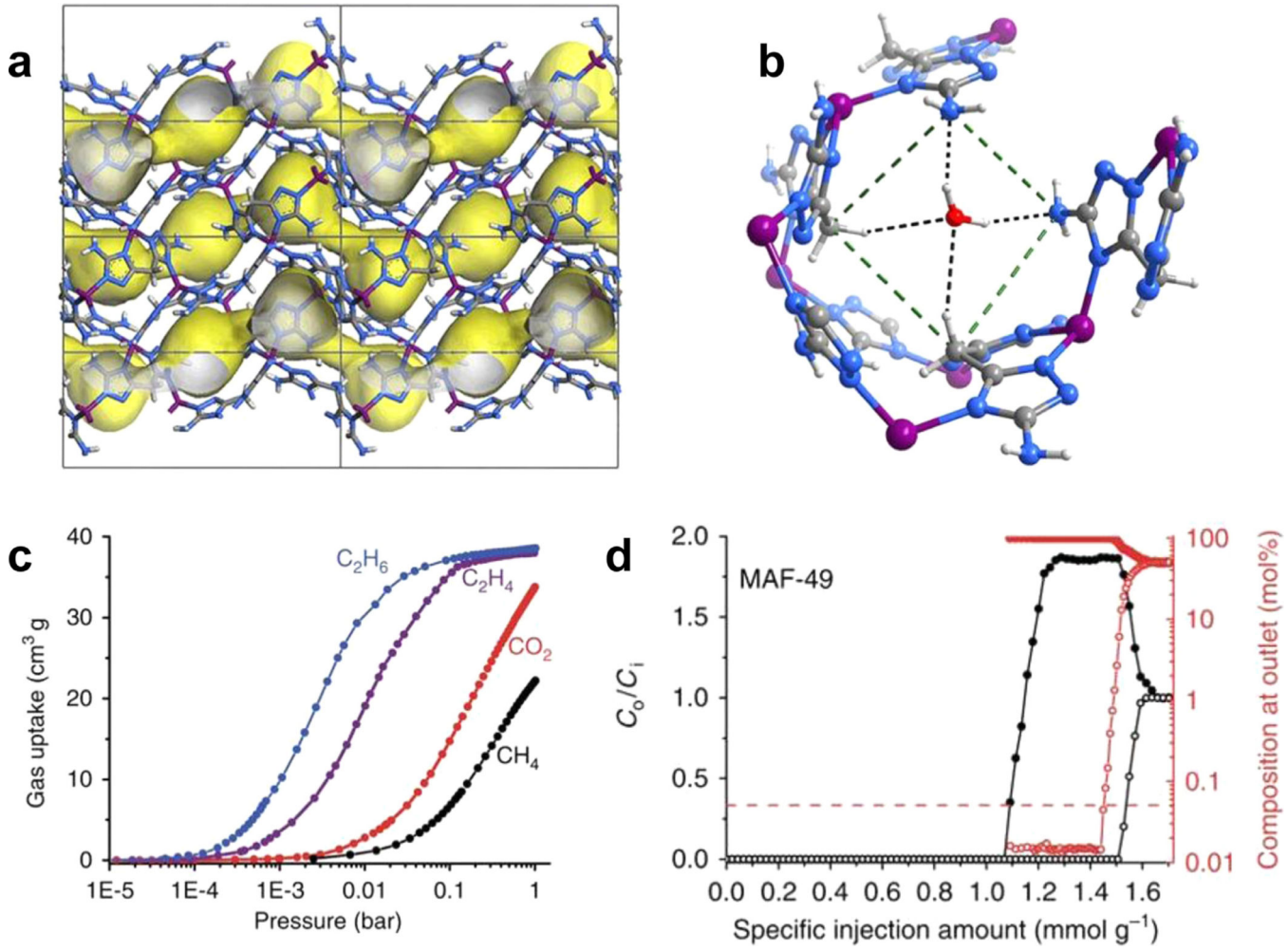

Fig. 5.

(a) X-ray crystal structure of MAF-49·H_2O. Zn purple, C dark grey, H light grey, N blue; and yellow/grey curved surface represents pore surface. Guest molecules are omitted for clarity. (b) Local environment and hydrogen-bonding interactions of the narrowest channel neck (highlighted by green dashed lines). (c) Gas adsorption isotherms for C_2H_6, C_2H_4, CO_2 and CH_4 in MAF-49 at 316 K. (d) C_2H_4/C_2H_6 (1:1) mixture breakthrough curves of MAF-49 measured at 313 K and 1 bar. Solid symbols: C_2H_4, Open symbols: C_2H_6. Reprinted with permission fromLiao et al.[145] Copyright 2015, Springer Nature. (For interpretation of the references to color in this figure legend, the reader is referred to the web version of this article.)

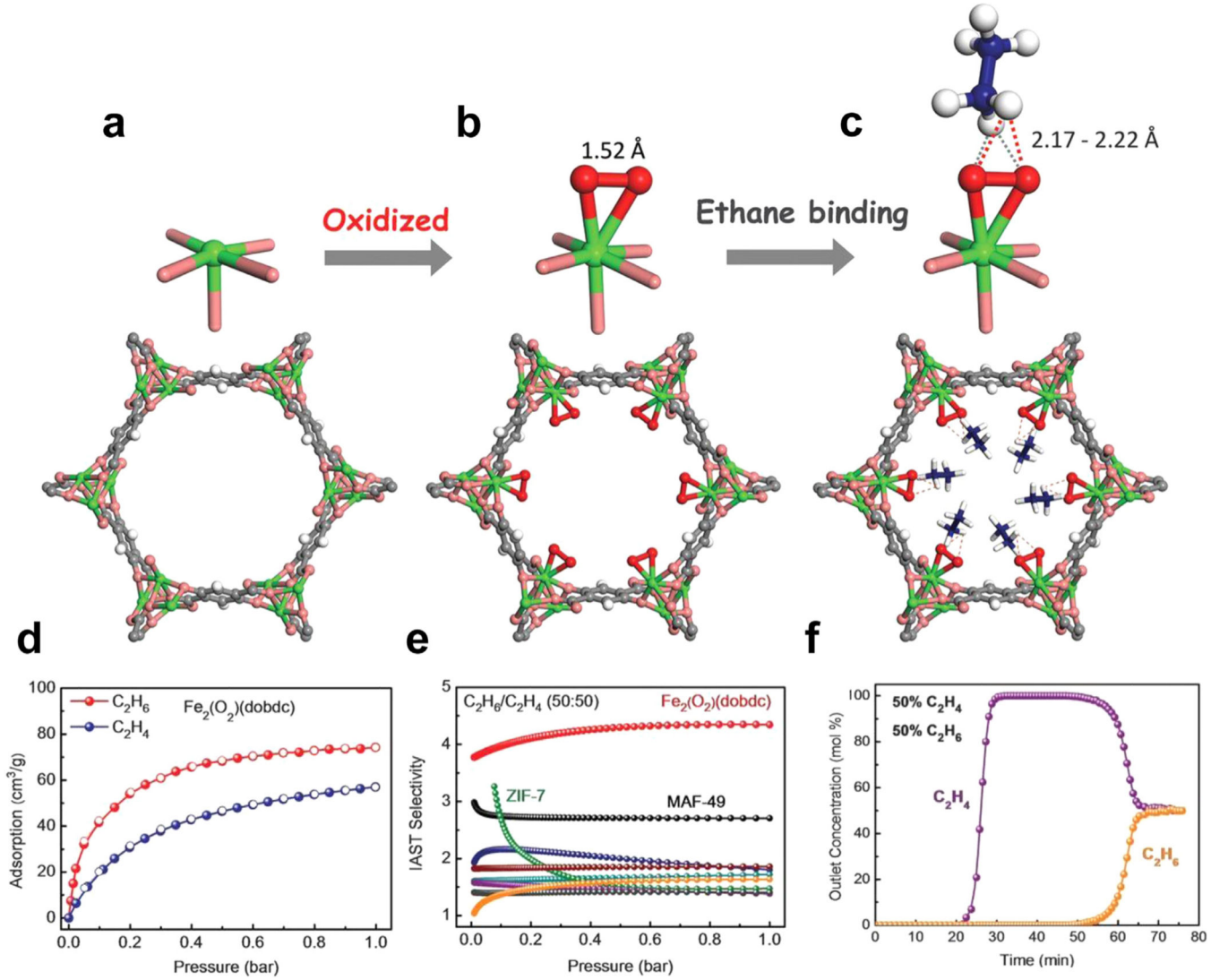

Fig. 6.

Structures of (a) Fe_2(dobdc), (b) $Fe_2(O_2)$(dobdc) and (c) $Fe_2(O_2)$(dobdc) C_2D_6 at 7 K. Note the change from the open Fe^{II} site to the Fe^{III} -peroxo site for the preferential binding of C_2H_6. Fe, green; C, dark gray; O, pink; O_2^{2-}, red; H or D, white; C in C_2D_6, blue. (d) Adsorption (solid) and desorption (open) isotherms of C_2H_6 (red circles) and C_2H_4 (blue circles) in $Fe_2(O_2)$(dobdc) at 298 K. (e) Comparison of the IAST selectivities of $Fe_2(O_2)$(dobdc) with those of previously reported best-performing materials for C_2H_6/C_2H_4 (50/50) mixtures. (f) Experimental column breakthrough curves for a C_2H_6/C_2H_4 (50/50) mixture in an absorber bed packed with $Fe_2(O_2)$(dobdc) at 298 K and 1.01 bar. Reprinted with permission from Li et al.[148] Copyright 2018, the American Association for the Advancement of Science. (For interpretation of the references to color in this figure legend, the reader is referred to the web version of this article.)

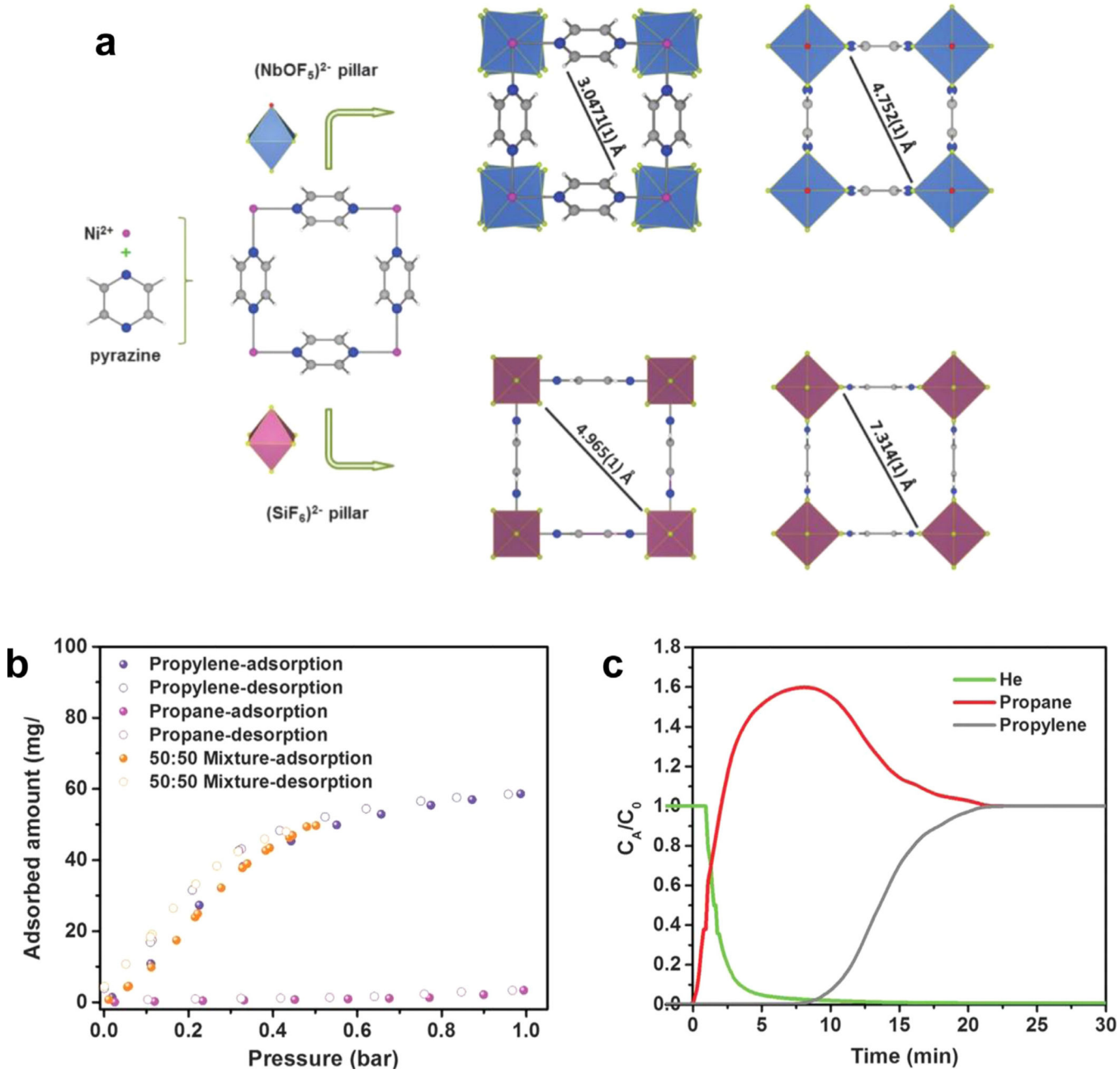

Fig. 7.

(a) Structure description of NbOFFIVE-1-Ni highlighting the building blocks arrangement and its comparison with the parent SIFSIX-3-Ni. (b) The pure C_3H_8 (pink), pure C_3H_6 (purple), and equimolar mixture of C_3H_6/C_3H_8 50/50 (orange) isotherms of NbOFFIVE-1-Ni have been collected at 298 K, demonstrating the full C_3H_6 from C_3H_8 sieving ability of this adsorbent at 1 bar. (c) $C_3H_6/C3H_8$ 50/50 mixed-gas experiment using a packed column bed at 298 K and a 1 bar total pressure and 4 cm^3/min total flow, confirming the infinite C_3H_6/C_3H_8 separation factor. Reprinted with permission from Cadiau et al.[150] Copyright 2016, the American Association for the Advancement of Science. (For interpretation of the

references to color in this figure lege nd, the reade r is refe rred to the web version of this article.)

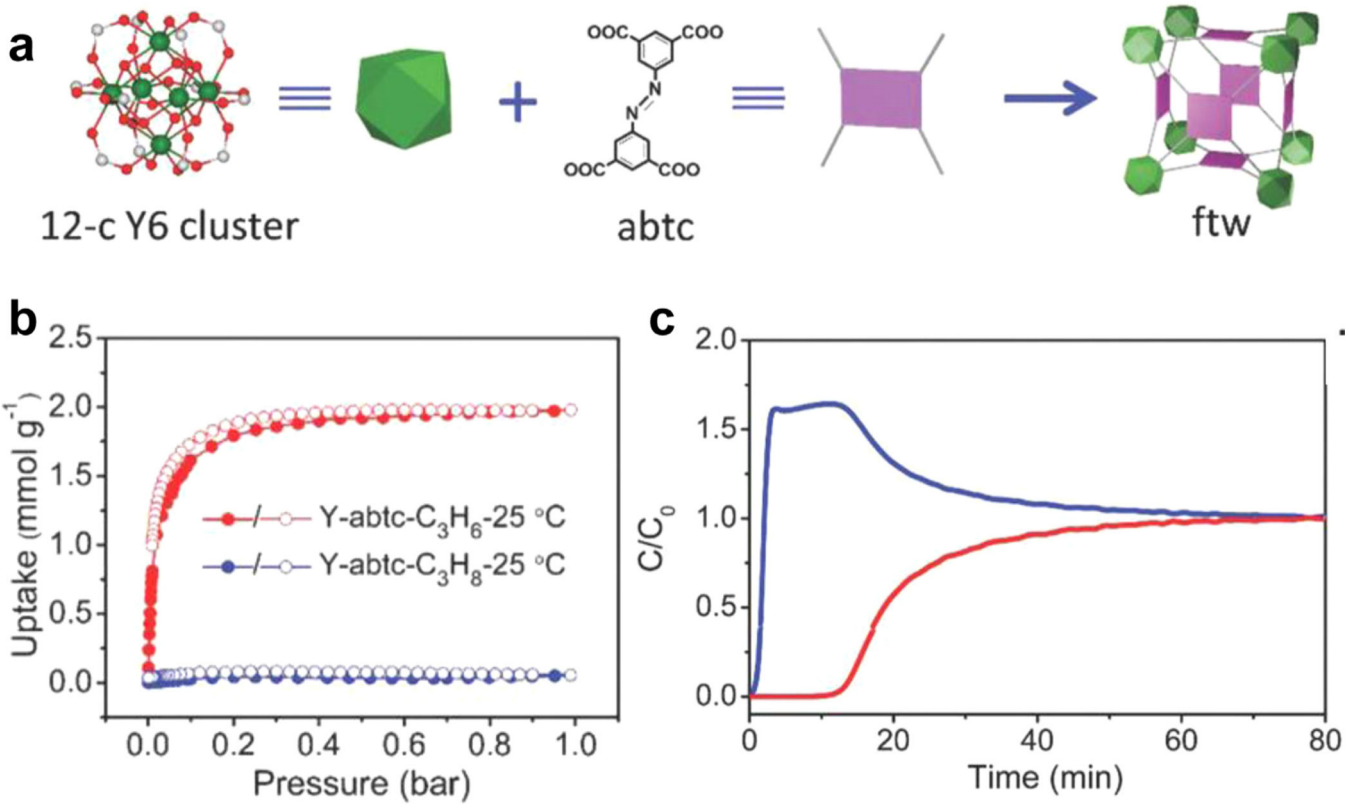

Fig. 8.

(a) Building units and structure of Y-abtc. (b) Adsorption-desorption isotherms of C_3H_8 and C_3H_6 at 25 °C for Y-abtc. (c) Multicomponent column breakthrough results for Y-abtc at 25 °C for an equimolar mixture of C_3H_8 and C_3H_6. Reprinted with permission from Wang et al.[151] Copyright 2018, John Wiley and Sons.

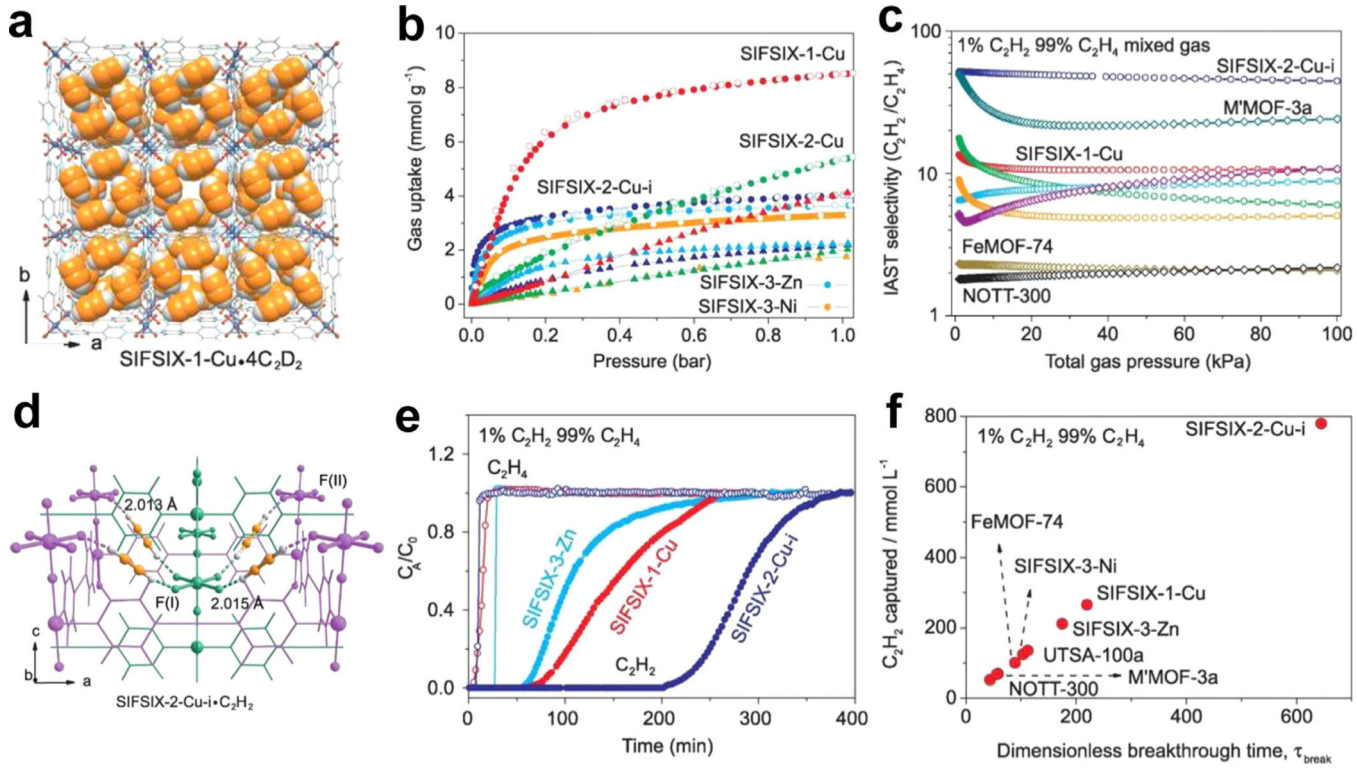

Fig. 9.

(a) Neutron crystal structure of SIFSIX-1-Cu•$4C_2D_2$ at 200 K, determined from Rietveld analysis. (b) Adsorption isotherms of C_2H_2 (filled circles) and C_2H_4 (triangles) in SIFSIX-1-Cu (red), SIFSIX-2-Cu (green), SIFSIX-2-Cu-i (blue), SIFSIX-3-Zn (light blue), and SIFSIX-3-Ni (orange) at 298 K in a range of 0–1.0 bar (c) Comparison of the IAST selectivities at varying pressures for a 1% C_2H_2 mixture of SIFSIX materials versus those of previously reported best-performing materials for C_2H_2/C_2H_4 mixtures. (d) C_2H_2 adsorption binding sites in SIFSIX-2-Cu-i calculated by dispersion-corrected density functional theory (the different nets are highlighted in magenta and green for clarity). (e) Experimental column breakthrough curves for C_2H_2/C_2H_4 (1/99) separations with SIFSIX-1-Cu, SIFSIX-2-Cu, and SIFSIX-3-Zn at 298 K and 1.01 bar. (f) Plots of the amount of C_2H_2 captured from C_2H_2/C_2H_4 1/99 mixture as a function of τ_{break} in the simulated column breakthrough. Reprinted with permission from Cui et al. [128] Copyright 2016, the American Association for the Advancement of Science. (For interpretation of the references to color in this figure legend, the reader is referred to the web version of this article.)

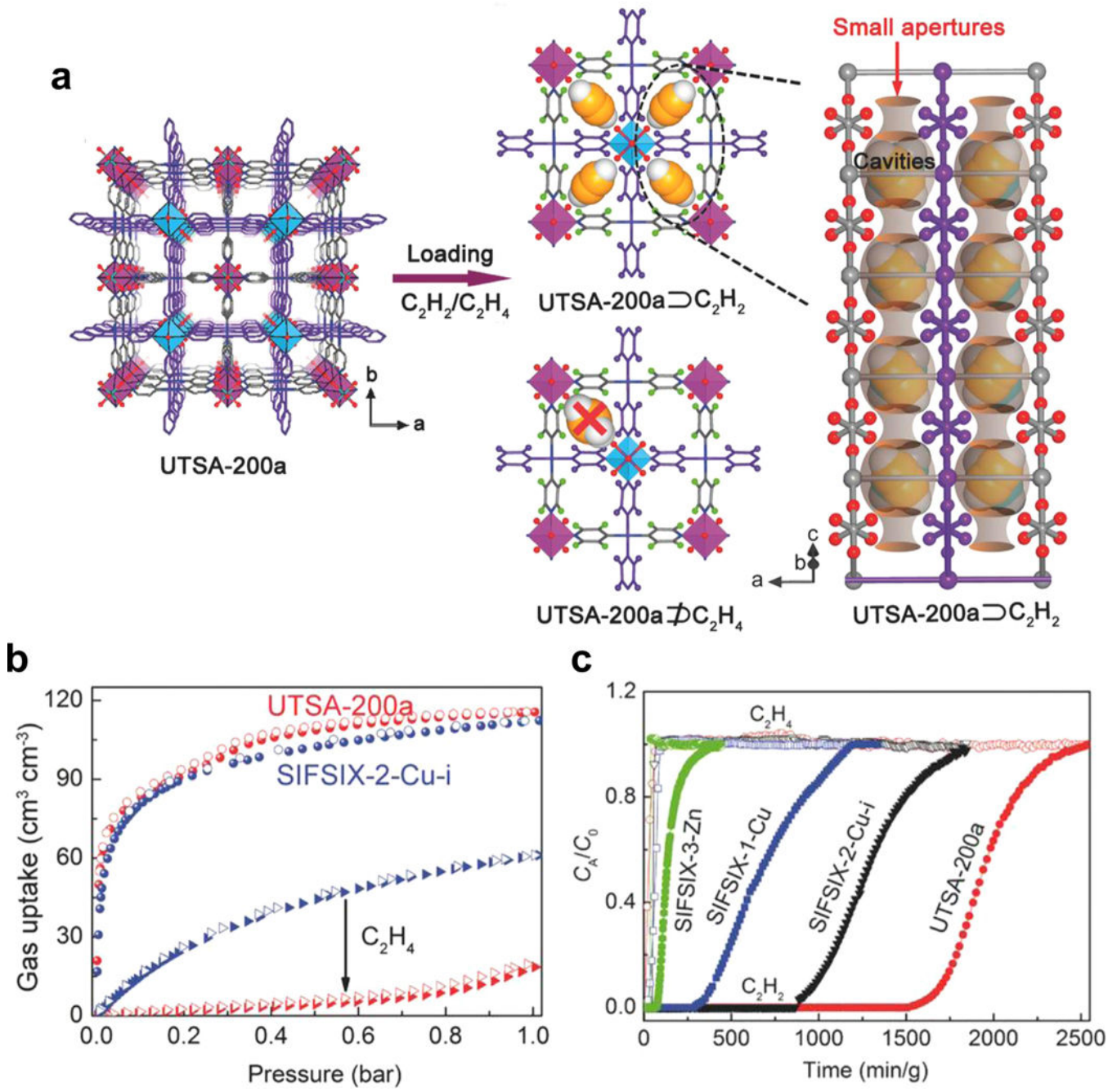

Fig. 10.

(a) Structure description of UTSA-200a. (b) Adsorption isotherms of C_2H_2 (circles) and C_2H_4 (triangles) for UTSA-200a and SIFSIX-2-Cu-i at 298 K in 0–1.0 bar. (c) Experimental column breakthrough curves for C_2H_2/C_2H_4 separations with UTSA-200a, SIFSIX-2-Cu-i, SIFSIX-1-Cu, and SIFSIX-3-Zn at 298 K and 1.01 bar. Reprinted with permission from Li et al.[155] Copyright 2017, John Wiley and Sons.

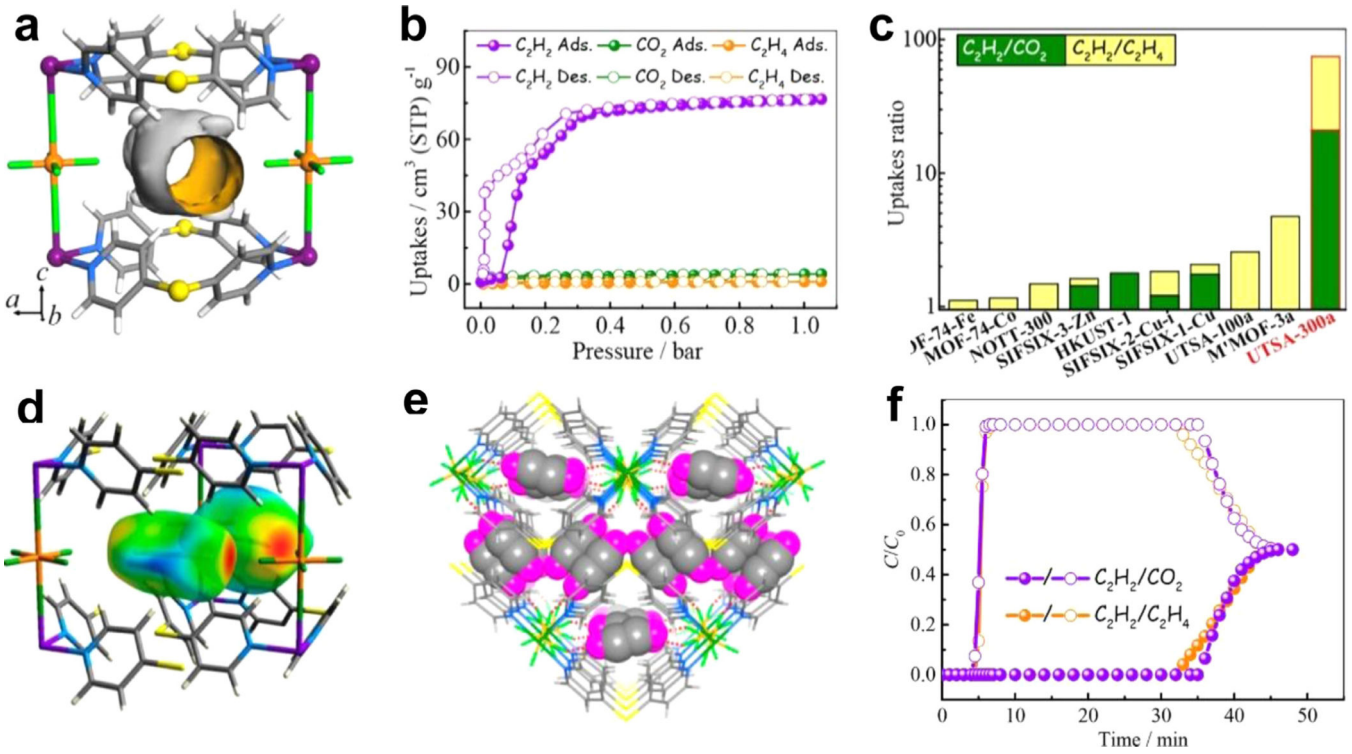

Fig. 11.

(a) Perspective views of cage unit in UTSA-300 showing aperture size of 3.3 Å (Zn, Si, F, S, N, and C are represented by purple, orange, green, bright yellow, light blue, and gray, respectively, and solvent molecules are omitted for clarity). (b) C_2H_2, CO_2, and C_2H_4 single-component sorption isotherms for UTSA-300a at 273 K. (c) Comparison of uptakes ratio among UTSA-300a and representative MOFs at ambient conditions. (d) Preferential binding sites in UTSA-300 for C_2D_2 molecules shown with Hirshfeld surface (d_i) displaying C–D···F interactions (red area). (e) Packing diagram of UTSA- 300 ⊃ C_2D_2 from neutron powder diffraction data. C_2D_2 molecules are shown in a CPK model. (f) Experimental column breakthrough curves for equimolar C_2H_2/CO_2 (purple) and C_2H_2/C_2H_4 (orange) mixtures (298 K, 1 bar) in an adsorber bed packed with UTSA-300a. Reprinted with permission from Lin et al.[157] Copyright 2017, American Chemical Society. (For interpretation of the references to color in this figure legend, the reader is referred to the web version of this article.)

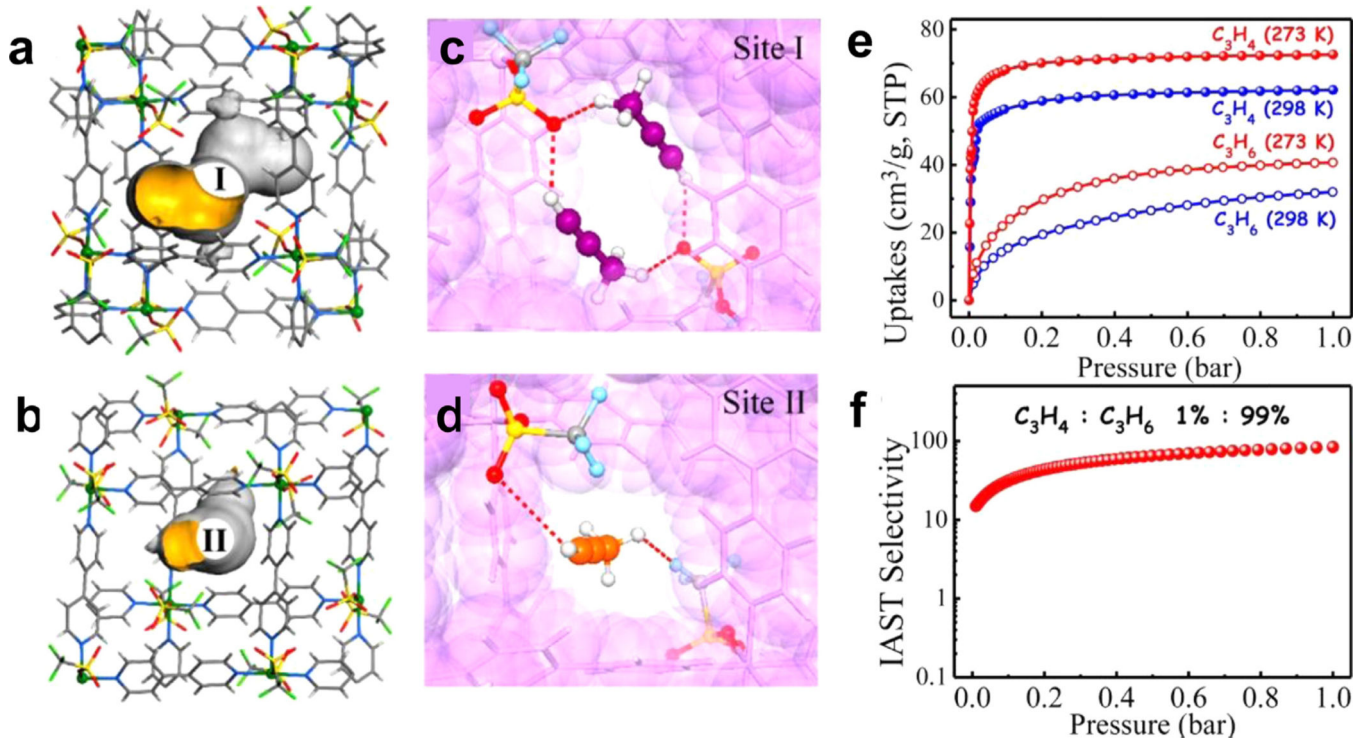

Fig. 12.

Schematic diagrams of (a) Type I and (b) Type II cavities in ELM-12 (Cu, green; C, gray; O, red; S, yellow; F, light green). Preferential binding sites for C_3D_4 molecules in (c) site I and (d) site II, as determined by neutron powder diffraction data. (e) C_3H_4 and C_3H_6 adsorption isotherms of ELM-12. (f) Predicted selectivity of ELM-12 for C_3H_4/C_3H_6 (1/99) at 298 K. Reprinted with permission from Li et al.[160] Copyright 2017, American Chemical Society. (For interpretation of the references to color in this figure legend, the reader is referred to the web version of this article.)

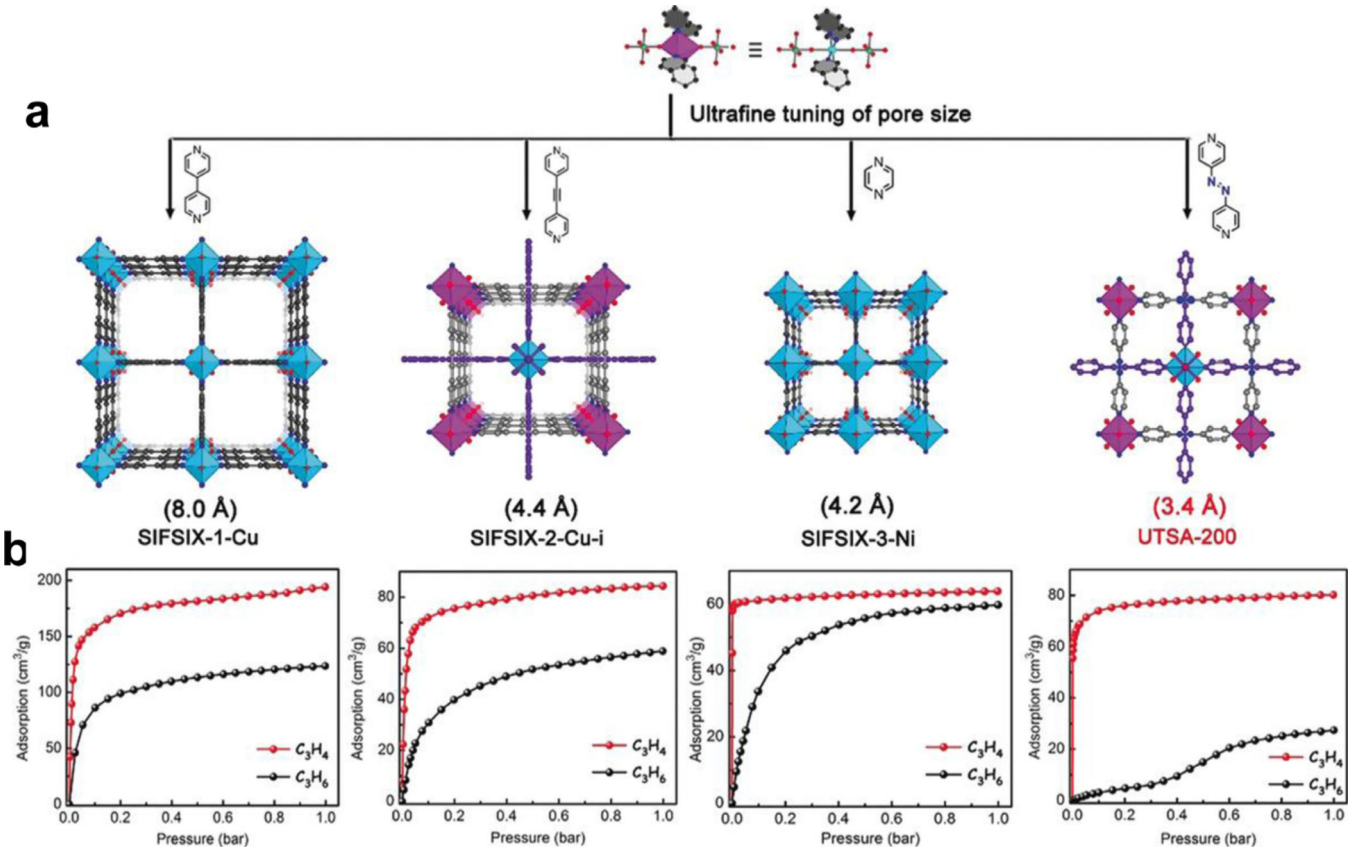

Fig. 13.

(a) The pore aperture and pore chemistry of a series of SIFSIX materials. (b) C_3H_4 and C_3H_6 adsorption isotherms of the corresponding SIFSIX material at 298 K. Reprinted with permission from Li et al.[185] Copyright 2018, John Wiley and Sons.

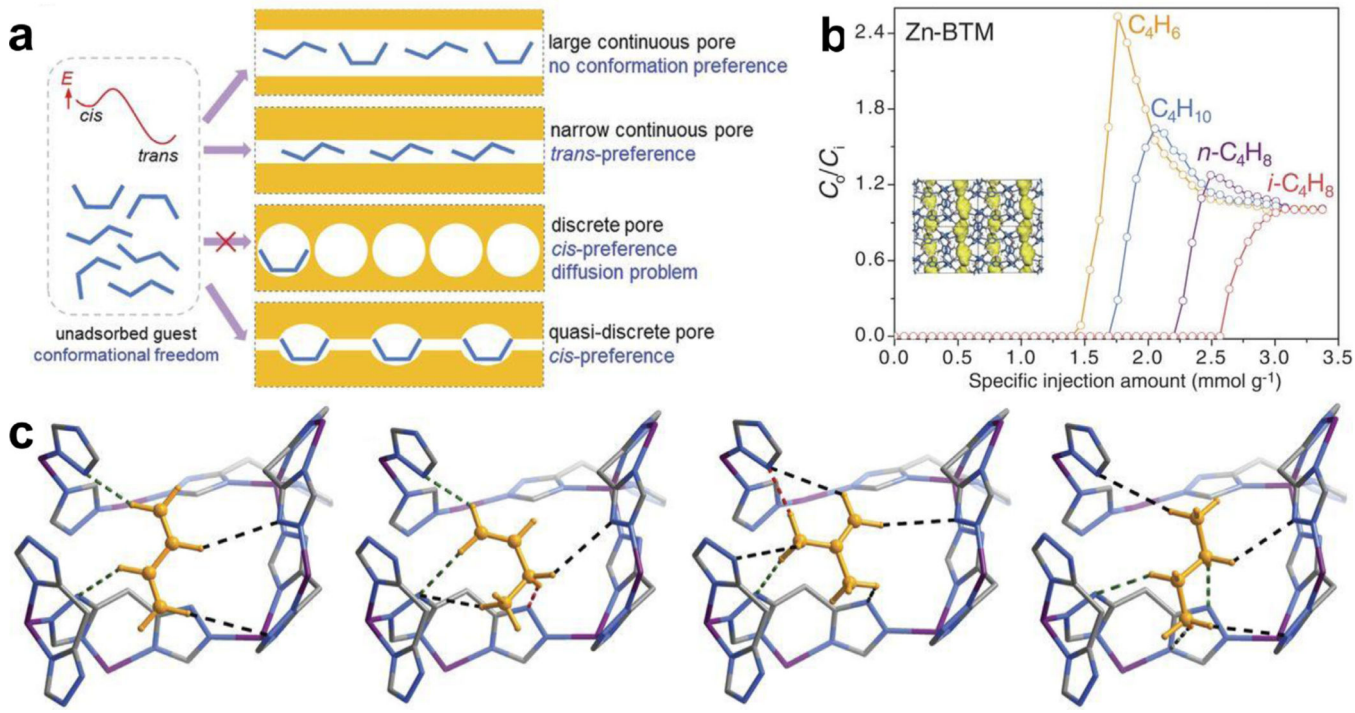

Fig. 14.

(a) Controlling the guest conformations by variation of the pore size, shape, and dimensionality. (b) Breakthrough curve of Zn-BTM for a 5:2:2:1 C_4H_6/n-C_4H_8/i-C_4H_8/C_4H_{10} mixture. (c) Single crystal X-ray host-guest structures of C_4H_6, n-C_4H_8, i-C_4H_8, and C_4H_{10}. Reprinted with permission from Liao et al.[186] Copyright 2017, the American Association for the Advancement of Science.

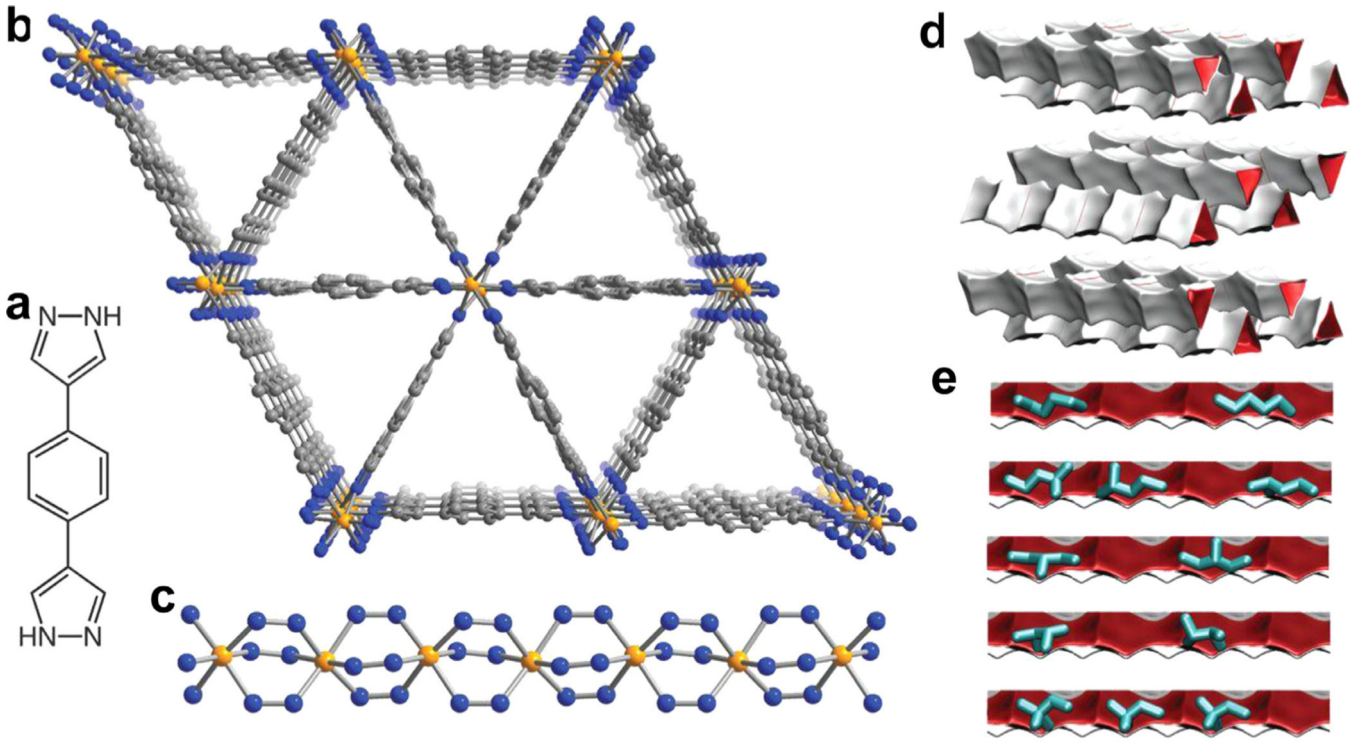

Fig. 15.

(a) Structure of H_2BDP ligand. (b) A portion of $Fe_2(BDP)_3$ structure, as determined by analysis of powder x-ray diffraction data. Orange, blue, and gray spheres represent Fe, N, and C atoms, respectively; H atoms are omitted for clarity. (c) A perpendicular view of the one-dimensional chains of pyrazolate-bridged Fe3+ octahedra, excluding C and H atoms. (d) The van der Waals surfaces associated with the corrugated triangular channels running through the structure. (e) Snapshots of the hexane isomers within the channels of $Fe_2(BDP)_3$ for a loading of four molecules per unit cell at 160 °C, as observed in Configurational-bias Monte Carlo simulations. Reprinted with permission from Herm et al.[188] Copyright 2013, the American Association for the Advancement of Science. (For interpretation of the references to color in this figure legend, the reader is referred to the web version of this article.)

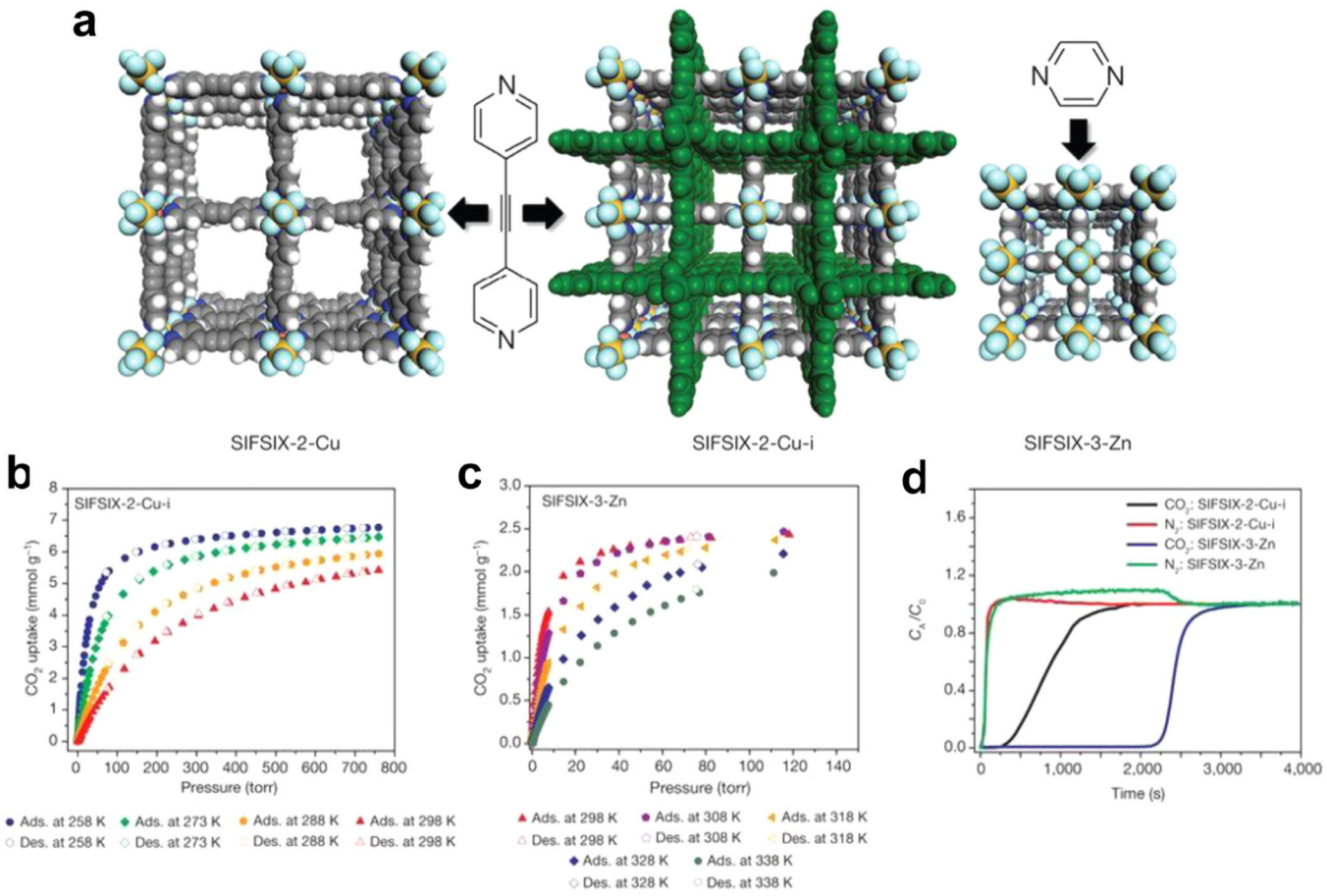

Fig. 16.

(a) Structures and organic linkers of SIFSIX-2-Cu, SIFSIX-2-Cu-i and SIFSIX-3-Zn. (b) CO_2 sorption isotherms of SIFSIX-2-Cu-i at various temperatures. (c) CO_2 sorption isotherms of SIFSIX-3-Zn at various temperatures. (d) Column breakthrough experiment on SIFSIX-2-Cu-i and SIFSIX-3-Zn with a CO_2/N_2:10/90 gas mixture (298 K, 1 bar). Reprinted with permission from Nugent et al.[165] Copyright 2013, Springer Nature.

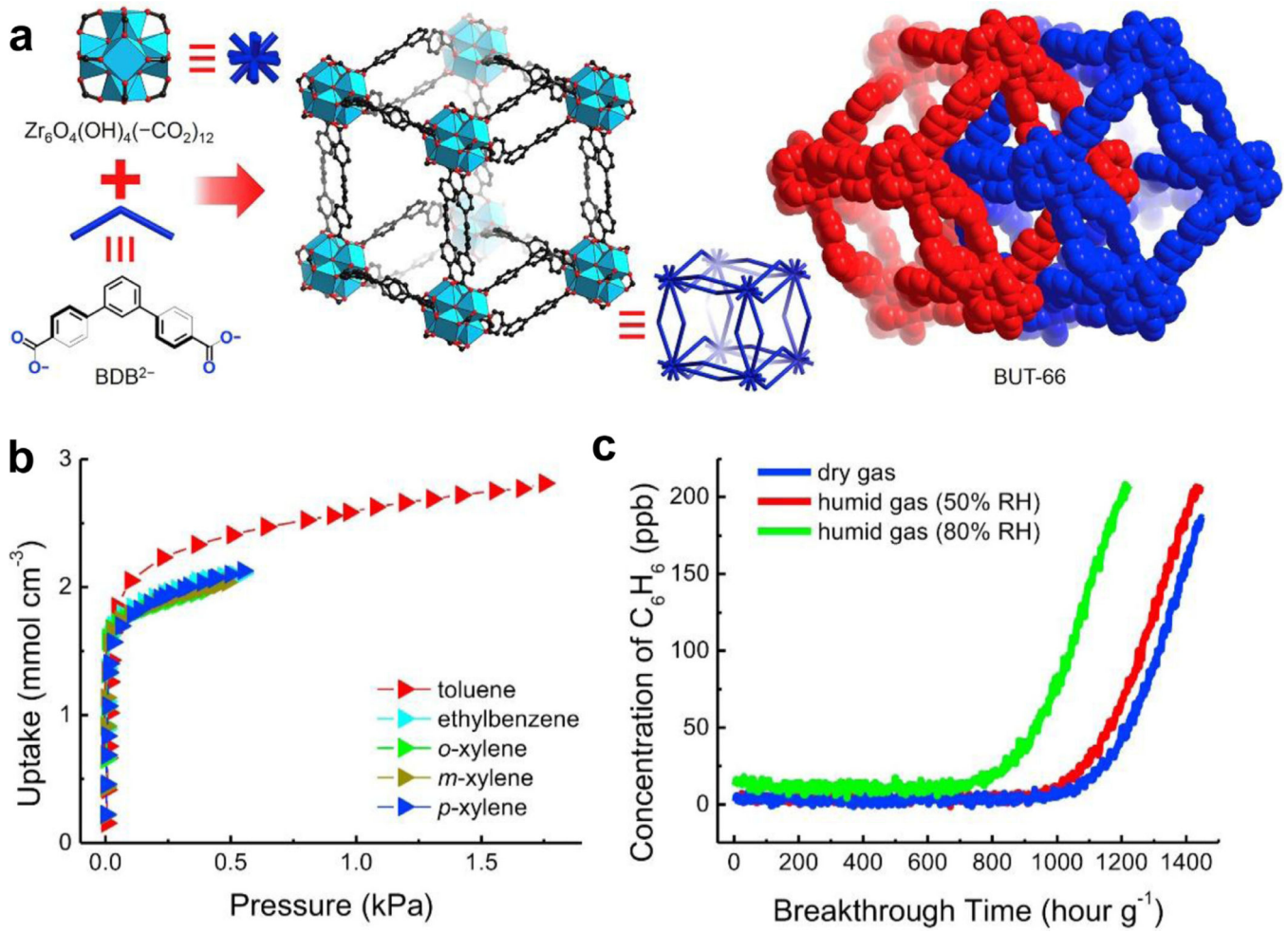

Fig. 17.

(a) BUT-66 structure. (b) Vapor adsorption isotherms of toluene, EB, OX, MX, and PX at 80 °C for BUT-66. (c) Breakthrough curves at 25 °C for dry air and humid air (relative humidity = 50% and 80%, respectively) containing 10 ppm benzene flowed through a column packed with BUT-66. Reprinted with permission from Xie et al.[222] Copyright 2018, Elsevier.

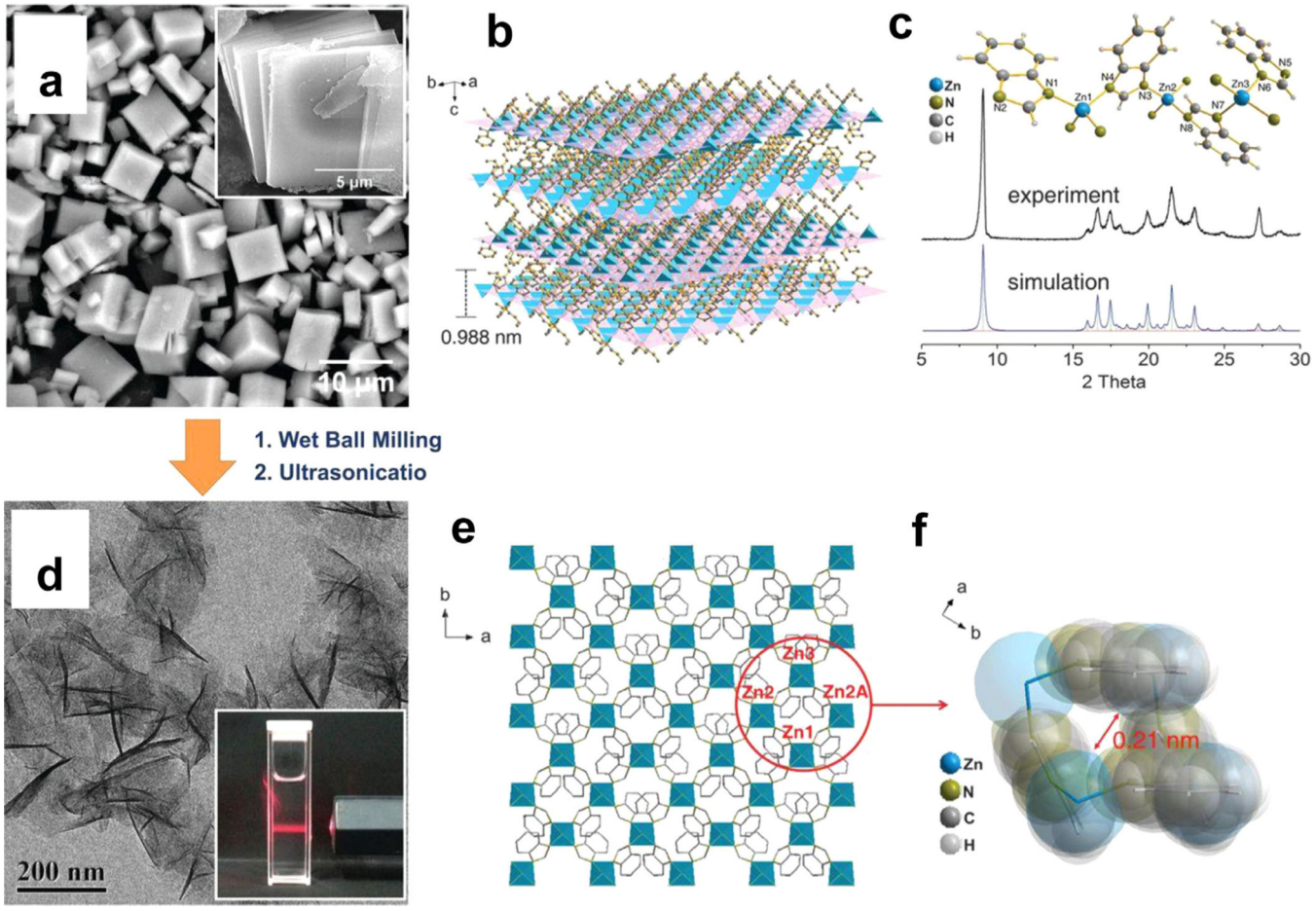

Fig. 18.

(a) Scanning electron microscopy image of as-synthesized $Zn_2(bim)_4$ crystals. (b) Architecture of the layered MOF precursor. (c) Powder X-ray diffraction patterns of $Zn_2(bim)_4$. (d) Transmission electron microscopy image of $Zn_2(bim)_4$ MSNs. (e)Illustration of the grid-like structure of the $Zn_2(bim)_4$ molecular sieving nanosheet. (f) Space-filling representation of a four-membered ring of the $Zn_2(bim)_4$ molecular sieving nanosheet. Reprinted with permission from Peng et al.[241] Copyright 2014, the American Association for the Advancement of Science.

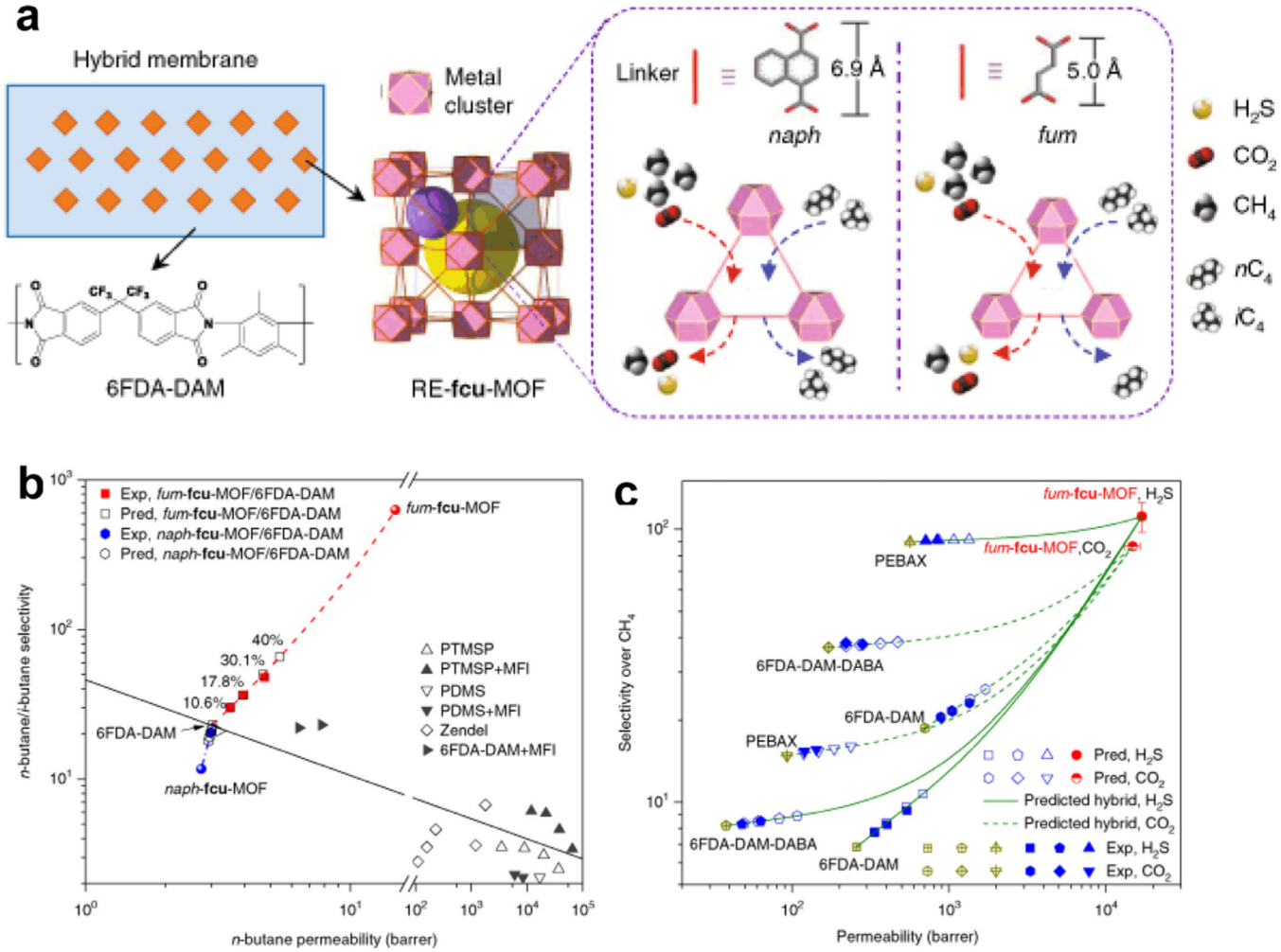

Fig. 19.

(a) Schematic of designing the hybrid membrane based on incorporating RE-fcu-MOF molecular sieve crystals into 6FDA-DAM polymer matrix. (b) nC_4 permeability and nC_4/iC_4 selectivity of Y-fum-fcu-MOF and Eu-naph-fcu-MOF-incorporated 6FDA-DAM hybrid membranes with various MOF loading by wt%. (c) CO_2 or H_2S permeability (*x*-axis), and CO_2/CH_4 or H_2S/CH_4 selectivity (y-axis) of Y-fum-fcu-MOF/polymer hybrid membranes (blue symbols from left to right represent MOF loadings in 6FDA-DAM of 10.6, 17.8, 30.1 and 40 wt%; in 6FDA-DAM-DABA of 9.9, 17.7, 30 and 40 wt%; in PEBAX of 10.1, 20.0, 30 and 40 wt%, respectively). Reprinted with permission from Liu et al.[246] Copyright 2018, Springer Nature. (For interpretation of the references to color in this figure legend, the reader is referred to the web version of this article.)

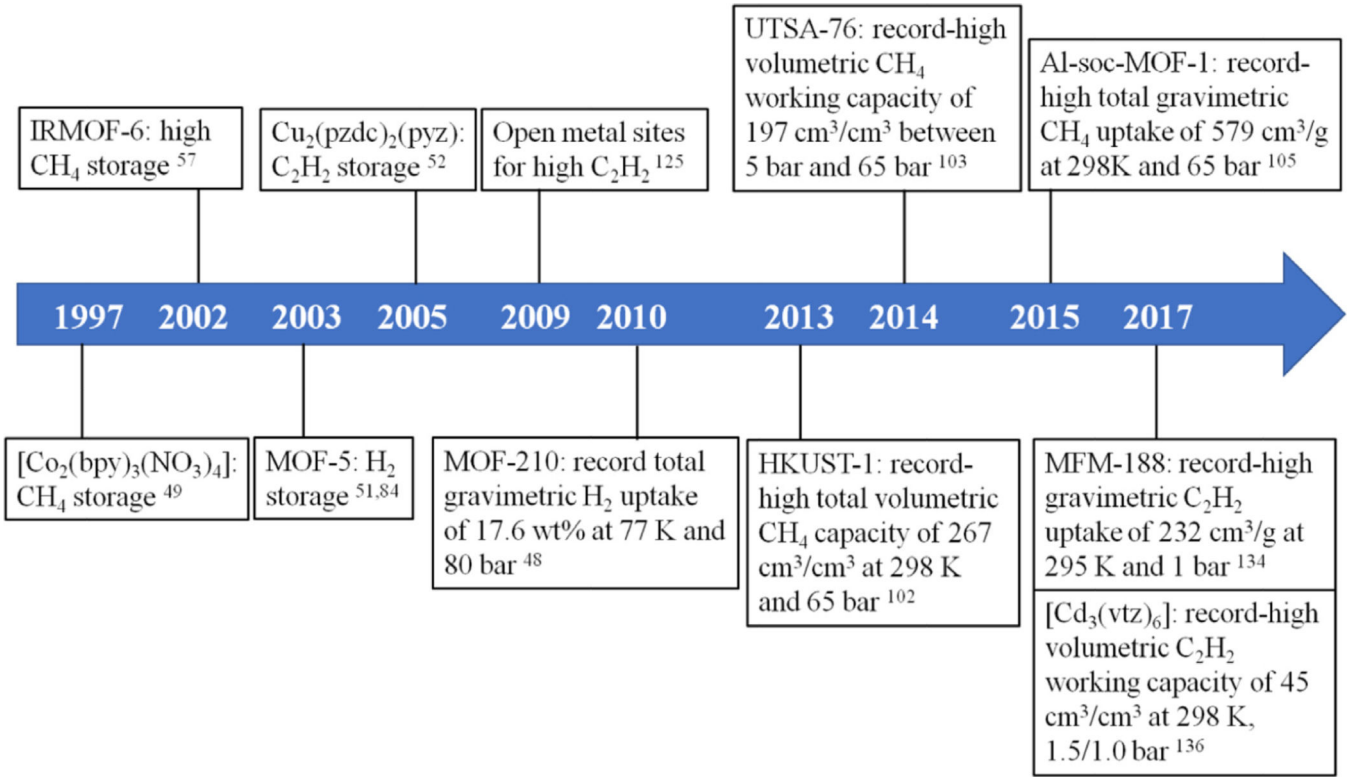

Scheme 1.
Timeline of important breakthroughs in gas storage using MOFs.

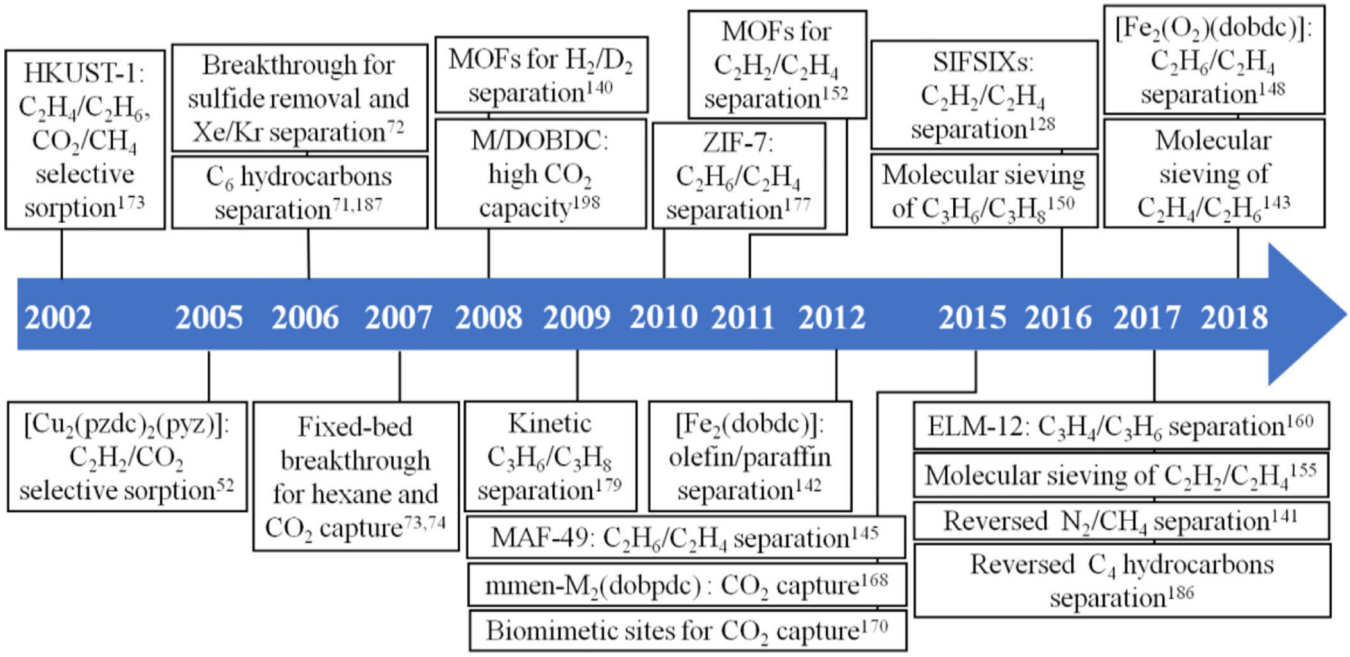

Scheme 2.

Timeline of important breakthroughs in using MOFs for separating representative gases.

Table 1.

Selected examples of MOFs for H_2 storage.

MOFs	BET surface area (m^2/g)	Temperature (K)	Pressure (bar)	Total gravimetric capacity (wt%)	Total volumetric capacity (g/L)	Refs.
MOF-5	3800	77	100	10	66	84
NOTT-112	3800	77	77	10	50.3	91
NU-111	5930	77	70	13.6	–	92
NU-100/PCN-610[94]	6143	77	70	16.4	–	93
MOF-210	6240	77	80	17.6	44	48
IRMOF-20	4073	–	–	9.1[a]	51.0[a]	95
Ni_2 (*m*-dobdc)	1321	298	–	–	11.0[b]	96
SNU-16	2590	77	70	10.0		97
MOF-200	4530	77	80	16.3	36	48
MOF-205	4460	77	80	12.0	46	48
Mg-MOF-74	1510	77	100	4.9	49	98
PCN-46	2500	77	97	6.88	45.7	99
NOTT-115	3394	78	60	7.5	49.3	100
Mn-BTT	2100	77	90	6.9	60	66

[a]Measured usable capacities with a temperature-pressure swing from 77 K and 100 bar to 160 K and 5 bar.

[b]Measured usable volumetric capacity between 100 bar and 5 bar.

Table 2.

Selected examples of MOFs for CH_4 storage.

MOFs	Framework density D_c	BET surface area	Total uptake[a]		Working capacity[b]		Refs.
	(g/cm^3)	(m^2/g)	(cm^3/g)	(cm^3/cm^3)	(cm^3/g)	(cm^3/cm^3)	
HKUST-1	0.883	1850	302 (257)	267 (227)	215 (170)	190 (150)	102
UTSA-76	0.699	2820	363 (302)	257 (211)	282 (216)	197 (151)	103
Co(bdp)	–	2911	–	203 (161)	–	197 (155)[c]	104
Al-soc-MOF-1	0.34	5585	579 (362)	197 (123)	518 (306)	176 (104)	105
MOF-177	0.427	4500	475 (307)	203 (131)	426 (258)	182 (110)	53
UTSA-110	0.600	3241	402 (312)	241 (187)	317 (227)[c]	190 (136)[c]	106
NJU-Bai 43	0.639	3090	396 (315)	254 (202)	308 (228)	198 (146)	107
MOF-905	0.549	3490	377 (264)	207 (145)	331 (219)	182 (120)	108
MAF-38	0.761	2022	346 (297)	263 (226)	246 (197)	187 (150)	109
MFM-115a	0.611	3394	389 (204)	238 (186)	312 (226)	191 (138)	110
LIFM-82	0.922	1624	267 (214)	245 (196)	209 (156)	192 (143)	111
NU-125	0.589	3286	395 (315)	232 (182)	312 (226)	183 (133)	102
NU-111	0.409	4930	503 (337)	206 (138)	437 (271)	179 (111)	102

[a] At room temperature and 65 (35) bar.

[b] Defined as the difference of CH_4 uptake between 65 (35) bar and 5 bar.

[c] Between 65 (35) bar and 5.8 bar.

Table 3.

The C_2H_2 uptake capacity of selected examples of MOFs at ambient temperature and 1 bar.

MOFs	BET surface area (m^2/g)	Temperature (K)	Gravimetric uptake (cm^3/g)	Volumetric uptake (cm^3/cm^3)	Refs.
HKUST-1	1780	295	201	177	125
MOF-505	1694	295	148	137	125
Co-MOF-74	1056[126]	295	197	230	127
Mn-MOF-74	1102[126]	295	168	182	127
Mg-MOF-74	1332[126]	295	184	167	127
NOTT-101	2316	296	184	–	20
SIFSIX-1-Cu	1178	298	190	164	128
ZJU-5	2823	298	193	–	129
ZJU-8	2501	298	195	134	130
ZJU-40	2858	298	216	–	131
NJU-Bai 17	2423	296	222.4	176	132
FJI-H8	2025	295	224	196	133
MFM-188	2568	295	232	–	134
MAF-2	–	298	70	82	135
$[Cd_3(vtz)_6]$	–	298	50	77	136

Table 4.

Selected examples of MOFs for gas separation.

Gas separation	MOF	Adsorption amount[a] (mmol/g)	Temperature (K)	Selectivity[b]	Refs.
C_2H_4/C_2H_6	Fe-MOF-74	6.24[c]/5.19[c]	318	13.6	142
	Fe_2(*m*-dobdc)	6.9[c]/5.9[c]	298	>25	19
	NOTT-300	4.28/0.85	293	48.7	18
	UTSA-280	2.5/0.098	298	Molecular sieving; >10,000[d]	143
	Co-gallate	3.37/0.3[c]	298	52	144
C_2H_6/C_2H_4	MAF-49	1.7[c]/1.6[c]	316	9	145
	$Cu(Qc)_2$	1.85/0.78	298	3.4	146
	PCN-250	5.21/4.22	298	1.9	147
	Fe_2 (O_2)(dobdc)	3.32/2.54[c]	298	4.4	148
C_3H_6/C_3H_8	Co-MOF-74	7.29/5.4[c]	298	46	149
	Fe_2(*m*-dobdc)	7.3[c]/5.9[c]	298	> 55	19
	NbOFFIVE-1-Ni	1.4[c]/0.04[c]	298	Molecular sieving	150
	Y-abtc	2.0[c]/0[c]	298	Molecular sieving	151
C_2H_2/C_2H_4	M'MOF-3a	1.8[c]/0.4[c]	295	24	152
	UTSA-100	4.27/1.66	296	10.72	153
	$[Mn_3(bipy)_3(H_2O)_4][Mn(CN)_6]_2 \cdot 2bpy$	3.2/0.24	283	16*e*	154
	SIFSIX-1-Cu	8.50/4.11	298	10.63	128
	SIFSIX-2-Cu-i	4.02/2.19	298	44.54	128
	SIFSIX-3-Zn	3.64/2.24	298	8.82	128
	SIFSIX-3-Ni	3.30/1.75	298	5.03	128
	UTSA-200	3.65/0.63	298	Molecular sieving; 6320[d]	155
C_2H_2/CO_2	UTSA-74	4.8[c]/3.1[c]	298	9	156
	UTSA-300	3.08/0.14	298	Molecular sieving; 743[d]	157
	TiFSIX-2-Cu-i	2.9[f]/1.6[f]	298	6.5	158

Gas separation	MOF	Adsorption amount[a] (mmol/g)	Temperature (K)	Selectivity[b]	Refs.
CO_2/C_2H_2	Mn(bdc)(dpe)	2.14[c]/0.36[c]	273	8.8	159
	SIFSIX-3-Ni	2.5[f]/2.0[f]	298	7.7	158
C_3H_4/C_3H_6	ELM-12	2.74/1.38[c]	298	84	160
	SIFSIX-1-Cu	8.76/5.9[c]	298	9	161
	SIFSIX-2-Cu-i	3.8[c]/2.6[c]	298	25	161
	SIFSIX-3-Ni	2.98/2.67	298	290[d]	161
	ZU-62	3.6[c]/2.6[c]	298	48	162
	UTSA-200	3.57[c]/1.16[c]	298	Molecular sieving; > 20,000[d]	185
n-C_4H_{10}/iso-C_4H_{10}	Tb_6 (μ_3–OH)$_8$(fum)$_6$(H_2O)$_6$	1.32[c]/0[c]	293	Molecular sieving	163
	Y_6(μ_3–OH)$_8$(fum)$_6$(H_2O)$_6$	1.97[c]/0[c]	293	Molecular sieving	163
n-C_4H_8/iso-C_4H_8	GeFSIX-2-Cu-i	3.3[c]/1.2[c]	298	2.26	164
	NbFSIX-2-Cu-i	2.2[c]/0.5[c]	298	–	164
C_4H_6/iso-C_4H_8[g]	GeFSIX-2-Cu-i	3.6[c]/1.2[c]	298	2.94	164
	NbFSIX-2-Cu-i	2.6[c]/0.5[c]	298	–	164
	GeFSIX-14-Cu-i	2.6[c]/0.4[c]	298	–	164
C_4H_6/n-C_4H_8[g]	GeFSIX-14-Cu-i	2.6[c]/0.6[c]	298	–	164
CO_2/N_2	SIFSIX-2-Cu-i	5.41/0.15	298	140	165
	SIFSIX-3-Zn	2.54/0.23	298	1818	165
	FJI-14H	12.5[c]/–	298	51	166
	Qc-5-Cu-sql-β	2.16/0.01	293	Molecular sieving; 40,000[d]	167
	mmen-Mg_2 (dobpdc)	4.1[c]/–	298	–	168
	[Mg_2 (dobdc)(N_2H_4)$_{1.8}$]	5.51/–	298	–	169
	[$Mn^{II}Mn^{III}$ (OH)Cl_2 (bbta)]	7.1/–	298	250	170
CO_2/CH_4	SIFSIX-2-Cu-i	5.41/0.47	298	33	165
	SIFSIX-3-Zn	2.54/0.79	298	231	165
	Mg2V-DHBDC	10.37/1.7[c]	273	5.15	171

Gas separation	MOF	Adsorption amount[a] (mmol/g)	Temperature (K)	Selectivity[b]	Refs.
	Qc-5-Cu-sql-β	2.16/0.06	293	Molecular sieving; 3300[d]	[172]

[a] Adsorption amount at 1 bar in isotherms.

[b] Calculated by ideal adsorbed solution theory (IAST) at ambient temperature and 1 bar.

[c] Estimated from pure-component adsorption isotherm.

[d] The value is only for qualitative comparison.

[e] The selectivity was calculated at 293 K.

[f] The value is collected from adsorption isotherm of 298 K at 0.1 bar.

[g] C_4H_6 refers to 1,3-butadiene.